ISBN 978-82-326-1666-4 (printed version)
ISBN 978-82-326-1667-1 (electronic version)
ISSN 1503-8181

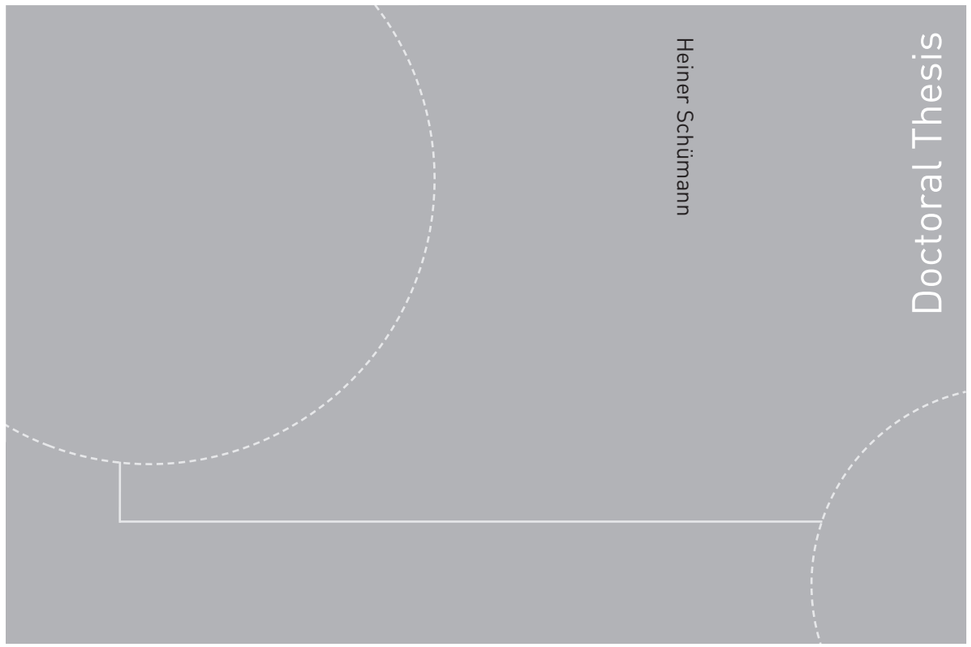

Doctoral theses at NTNU, 2016:164

Heiner Schümann

Experimental investigation of transitional oil-water pipe flow

NTNU
Norwegian University of
Science and Technology

NTNU
Norwegian University of
Science and Technology

NTNU
Norwegian University of
Science and Technology
Faculty of Engineering
Science and Technology
Department of Energy and Process Engineering

Doctoral theses at NTNU, 2016:164

NTNU

Heiner Schümann

Experimental investigation of transitional oil-water pipe flow

Thesis for the degree of Philosophiae Doctor

Trondheim, 06 2016

Norwegian University of Science and Technology
Faculty of Engineering
Science and Technology
Department of Energy and Process Engineering

NTNU
Norwegian University of
Science and Technology

NTNU
Norwegian University of Science and Technology

Thesis for the degree of Philosophiae Doctor

Faculty of Engineering
Science and Technology
Department of Energy and Process Engineering

ISBN 978-82-326-1666-4 (printed version
ISBN 978-82-326-1667-1 (electronic version
ISSN 1503-8181

Doctoral theses at NTNU, 2016:164

Printed by Skipnes Kommunikasjon as

Preface

This thesis is submitted in partial fulfillment of the requirements for the degree of Philosophiae Doctor (PhD) at the Norwegian University of Science and Technology (NTNU).

The work has been performed at the Department of Energy and Process Engineering in the Faculty of Engineering Science and Technology. Professor Ole Jørgen Nydal was the main supervisor, Johan Kristian Sveen and Murat Tutkun were co-supervisors during the work.

The work was carried out in the period of August 2012 to July 2015. The work was part of the PhD program supported by the "Multiphase Flow Assurance Centre" (FACE). FACE was a research cooperation between IFE, NTNU and SINTEF. The center was funded by The Research Council of Norway and by the following industrial partners: Statoil ASA, GE Oil & Gas, SPT Group - A Schlumberger Company, FMC Technologies, CD-adapco, Shell Technology Norway.

Abstract

In this thesis transitional oil-water pipe flow is experimentally studied. Here the word transitional relates to two main topics. First, the study focuses on the investigation of transitional flow patterns and resultant flow phenomena which neither are well described by stratified flow nor by homogeneously dispersed flow. Second, flow development, which can be of extensive length for oil-water flow, is investigated with help of consecutive measurement devices arranged along the test section. The experiments were conducted in two different multiphase flow laboratories. Tap water and different mineral oils with viscosities up to *120mPa*s* were used as test fluids.

The well flow loop at the Institute for Energy Technology (IFE) in Kjeller, Norway, provides a transparent *25m* test section with inner diameter $D = 100mm$, which is equipped with advanced technology for flow visualization. Gamma densitometry and X-ray tomography were used to obtain detailed measurements of local phase fractions and cross-sectional phase fraction distributions. Three FBRM-probes were installed to investigate droplet size evolution. A static inlet mixer was installed to disturb the flow and enable investigating development of premixed flow.

The Multiphase Flow Laboratory at the Norwegian University of Science and Technology (NTNU) provides a transparent test section which is easy to modify. A *50m* long modification with a simple ball valve installed as adjustable inlet mixer was used to investigate flow development in terms of changing flow patterns and pressure gradients.

Onset of dispersion at considerably lower mixture velocities compared to other studies without inlet mixing was found. Settling and inflow separation downstream of the mixing devices was observed. The flow development was further measured in terms of changing droplet sizes and pressure gradients. A rather dense packed droplet layer in the upper part of the pipe was characteristic for higher input water fractions. The occurrence of the dense packed layer always goes along with a significant increase of the pressure gradient.

A simple model for predicting the pressure gradient in dense packed layer flow was proposed. The model considers the dense packed layer as independent phase with its own mixture

properties. Model predictions are in good agreement with the measurements while the two-fluid model for stratified flow and the homogeneous flow model fail.

Furthermore, a tool for the prediction of flow development and development lengths downstream of a mixing device was developed based on simplified settling theory. Applying the tool together with the pressure gradient model allowed for qualitatively reproducing the observed flow development. Locally measured pressure gradient values along the test section could be reproduced with good agreement for low mixture velocities. For higher mixture velocities too fast separation was predicted, as the model does not consider turbulent mixing and droplet break-up.

Acknowledgements

I would like to thank Professor Ole Jørgen Nydal for supporting me as my supervisor and giving me the opportunity to fulfill the PhD study. I enjoyed honest discussions related and not related to work. You were good company during conferences and meetings and an excellent host during Christmas dinners and other occasions.

I also want to thank my co-supervisors Johan Kristian Sveen and Murat Tutkun for critical, but fruitful discussions and help throughout the last years. Without your effort a large part of this work would not have been possible.

Special thanks go to Zhilin Yang, Bjørnar Hauknes Pettersen and Robert Orr from Statoil ASA. Important input and feedback have come from your side.

I want to acknowledge the technicians Martin Bustadmo and Joar Amundsen who were to a main proportion responsible for the success of the experiments.

Thanks go to my colleagues Mariana Diaz, Andrea Shmueli, Andreas Akselsen, Ivar Eskerud Smith and Tor Kindsbekken Kjeldby.

I want to thank the students Milad Kazemihatami, Milad Khatibi and Pankaj Chandra for contributing to the work.

Furthermore I want to acknowledge Roar Skartlien, Martin Foss, Olaf Skjæraasen, Karin Hald, Morten Langsholt and Galina Rodionova for discussions, opinions and support during the PhD time.

Last but not least I want to say thank you to my family, friends and my girlfriend Camilla for supporting and motivating me.

Contents

List of Tables

List of Figures

Nomenclature

Abbreviations

CLD	Chord length distribution
DSD	Droplet size distribution
FBRM	Focused Beam Reflectance Measurement
ID	Inner diameter
IFE	Institute for Energy Technology
NTNU	The Norwegian University of Science and Technology
PVM	Particle Video Microscope

Non-dimensional numbers

Re	Reynolds number

Variables and parameters

γ	Interfacial tension, $[mN/m]$
ε	Local phase fraction, $[-]$
μ	Viscosity, $[Pa*s]$
ρ	Density, $[kg/m^3]$
τ	Shear stress, $[Pa]$
Φ	Dispersed phase fraction, $[-]$
A	Pipe cross sectional area, $[m^2]$
D	Diameter, Inner diameter $[m]$
e	Wall roughness, $[m]$
e	Elemental error, [%]
f	Darcy friction factor, $[-]$
f_w	Input water fraction, $[-]$

L	Length, Test section length, $[m]$
N	Count rate, $[-]$
P , p	Pressure, $[Pa]$
S	Perimeter, $[m]$
U	Velocity, $[m/s]$
z	Space coordinate, $[m]$

Subscripts

c	Continuous
$dense$	Dense packed layer
i	Phase index
mix	Mixture
o	Oil
$o-dense$	Interface between oil and a dense packed layer
ow	Oil-water interface
r	Relative
s	Superficial
w	Water
$w-dense$	Interface between water and a dense packed layer

Chapter 1

Introduction

1.1 Motivation

Simultaneous transport of oil, gas, water and other byproducts in a single pipeline is common practice in oil production systems. Especially water will always be produced along with the desired hydrocarbons. The amount of produced water will vary strongly from well to well and increase with its lifetime (Xu, 2007). When high viscosity oil is produced, water injection into the well is a common technique to increase the recovery rate by reducing the pressure gradient along the pipeline when the oil is transported as dispersion (Nädler and Mewes, 1997).

Even if practiced for several decades, the accurate prediction of multiphase flows is still a challenge. The large number of possible flow patterns, where a flow pattern describes the spatial distribution of the phases within the pipe, and its sensitivity to the fluid properties and the flow line geometry make multiphase flow systems to a complex topic. Along the same flow line, the pipe inclination will typically vary substantially. Fluid properties will not be constant, for example the viscosity of the hydrocarbons increases as the flow cools down in a pipeline surrounded by sea water. Compressors, pumps and valves will influence the flow and rates will change after junctions.

The transition from one to another flow pattern will always go along with a change of the pressure gradient. Pressure gradients and the total pressure drop over a flow line are crucial for the cost effectiveness and feasibility of a production system. Furthermore, for the prediction of scaling and corrosion issues, knowledge about free water as result of the prevailing flow pattern is fundamental (Flores et al., 1999). Therefore, the steady improvement of commercial flow prediction tools is a major concern. Model development is

not possible without data, which is needed for physical understanding and verification. Due to complicated and expensive implementation of field measurement techniques, good field data is rare and model developers are dependent on laboratory data.

Due to the mentioned complexity, a proper understanding of two-phase flow is needed in order to predict three-phase flow based on combining oil-water and liquid-gas models (Oliemans, 2011). While gas-liquid two phase flow has been intensively investigated, knowledge about liquid-liquid flow is still limited (Brauner, 2003). With a considerably smaller density ratio gravitational separation is weak and oil-water flow tends to form dispersions. The range of possible viscosity ratios is larger and interfacial chemistry much more complex compared to gas-liquid flow (Valle, 1998). That makes it difficult, if not impossible, to adapt known relations from liquid-gas to liquid-liquid two phase flow in an easy manner. As current practical examples for liquid dominated flow the Peregrino field in Brazil and the Johan Sverdrup field in the Northern Sea can be mentioned.

Even if the geometry of subsea flow lines covers all inclinations, a trend to long and ultra-long lines (Hedne) and extensive horizontal wells (Elseth, 2001) makes horizontal or near-horizontal flow an important topic.

An experimental investigation of horizontal oil-water flow will be topic of this thesis. With the provision of new experimental data as basis for model development as background, the investigation will focus on four main aspects.

- First, viscous oils will be applied, in order to identify possible viscosity effects. While a lot of data exists for gas-liquid flow with high viscosity oil, only little such data is available for oil-water flow. Commercial flow simulators were mainly developed based on experimental data for oil-water flow with low viscosity oils. From such data important trends might be overseen.
- Secondly, recently developed advanced experimental techniques may provide detailed cross sectional resolution of measurements. This will help to better understand the flow, but also provide data for future model-extensions from one-dimensional to

multi-dimensional models. First approaches were already made in the OLGA HD and LedaFlow Q3D models (Biberg, 2012; Kongsberg Oil & Gas Technologies, 2010).

- Thirdly, repeated measurements along the test section will be used to identify flow development, which can be of extensive length for oil water flow, often exceeding the available test section lengths. Models will predict wrongly, when tuned to data, where fully developed flow was wrongly taken for granted. The development state of the flow is often not reported in the existing literature.
- Fourthly, the better part of available experimental data shows flow development from initially separated flow, where the phases were stratified at the test section inlet and the fluids were subsequently dispersed by turbulence. In real production systems, chokes, pumps, pipe bends and valves will aid to disperse the flow. In some cases, the liquids may already enter the well as a dispersion (emulsion). This is particularly important for viscous oils because turbulence in itself may often be too weak a force to create dispersions. In the extreme case, for example, a highly viscous droplet in a shear flow will simply rotate rather than stretch and subsequently break up. Obviously, this is highly dependent on both the oil viscosity and the type of shear flow (elongational vs simple shear), but serves to illustrate the fourth focus of the present work; the importance of the inlet condition in a laboratory setup with viscous oils.

1.2 Background

A brief introduction to important topics will be given in this section. A more detailed review is given in the introduction of each paper presented in this thesis.

1.2.1 Flow patterns in horizontal liquid-liquid flow

In horizontal flow gravitation acts perpendicular to the flow direction. Therefore, gravity permanently acts as a separating force. At low superficial velocities of the phases (superficial velocity is a hypothetical velocity the fluid would have if it would occupy the cross-section as the only fluid, so the volumetric flow rate divided by the cross-sectional area), oil and water

flow separated with a smooth or wavy interface. At higher mixture velocities droplets are formed at the interface due to shear between the phases. Likely the more turbulent phase, which is water in most cases, entrains droplets of the other phase (Trallero et al., 1997), but also the simultaneous presence of droplets in both layers, dual-continuous flow has been investigated (Lovick, 2004). The dispersion layer at the interface grows with increasing mixture velocity. A three layer flow pattern, oil-dispersion-water, is formed. At sufficiently high mixture velocity turbulent forces overcome the gravity force, which was dominant before. Droplets are spread over the whole cross-section. A more detailed overview of flow patterns and its causing mechanisms is given by for instance Trallero (1995). Figure 1.1 shows a schematic of the most typical flow patterns as observed by Nädler and Mewes (1997).

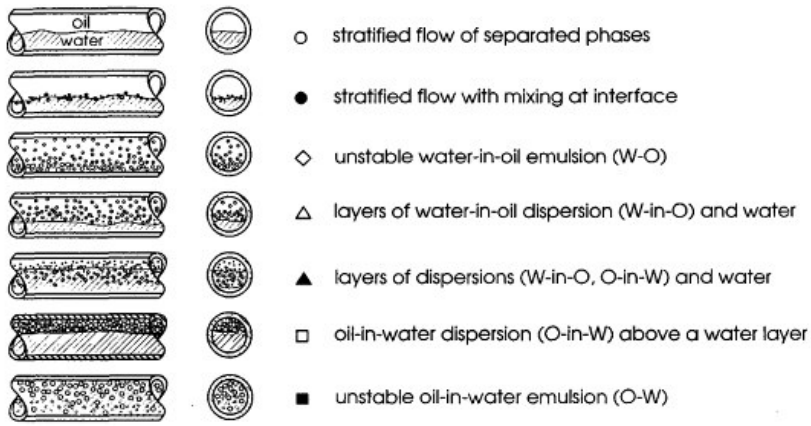

Figure 1.1: Schematic diagram of typical flow patterns in horizontal oil-water pipe flow, from Nädler and Mewes (1997).

A special flow pattern, not shown, is called core-annular flow. Here, an annular ring of one phase surrounds the other phase in the center of the pipe. This flow pattern, which has been common for transporting heavy, high viscosity crude oil, where water forms the annulus, was not observed in the present work and will, therefore, not be part of this study. Reviews are given by Joseph et al. (1997) and Bannwart (2001).

Boundaries between the individual flow patterns depend on a large number of flow and fluid properties.

In dispersed flow the type of dispersion strongly depends on the input water fraction. By increasing the volume fraction of the dispersed phase above a certain limit the dispersion can change its continuity (Nädler and Mewes, 1997). A dispersion of oil droplets in water can suddenly change to a water-in-oil dispersion and the other way around. This phenomenon is called phase inversion. Both total phase inversion, where the flow over the complete cross-section changes its continuity (Arirachakaran et al., 1989; Pal, 1993; Plasencia, 2013; Valle, 2000), as well as partial phase inversion, occurring in a sudden region of the cross section only (Elseth, 2001; Kumara et al., 2010; Nädler and Mewes, 1997; Valle, 2000) have been reported. The input water fraction required for phase inversion varies with the type oil. A reduction of the required input water fraction with increasing viscosity was reported (Arirachakaran et al., 1989; Brooks and Richmond, 1994). Recently Kumara et al. (2010) studied oil-water flow with a low viscosity oil (*1.6mPa*s*). The large difference between the oil viscosity and an effective viscosity of the occurring dispersions led to a distinct peak in the pressure drop curve when partial inversion occurs. The results indicate that partial inversion occurs at lower input water fraction as the mixture velocity increases. A similar trend can be found from the results by Elseth (2001). Observed flow patterns and corresponding pressure drop measurements are shown in Figure 1.2 and Figure 1.3 respectively. A distinct increase of the pressure gradient was found when the continuous oil layer disappeared and a water continuous dense packed droplet layer was formed. This point moved towards lower input water fractions as the mixture velocity increased.

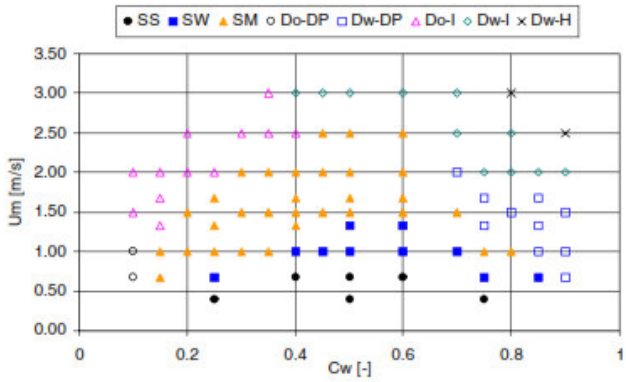

Figure 1.2: Flow pattern map as observed by Elseth (2001). The flow patterns are stratified smooth (SS), stratified wavy (SW), oil continuous dispersion with dense packed layer of water droplets (Do-DP), water continuous dispersion with dense packed layer of oil droplets (Dw-DP), oil continuous dispersion – inhomogeneous (Do-I), water continuous dispersion – inhomogeneous (Dw-I) and water continuous dispersion – homogeneous (Dw-H).

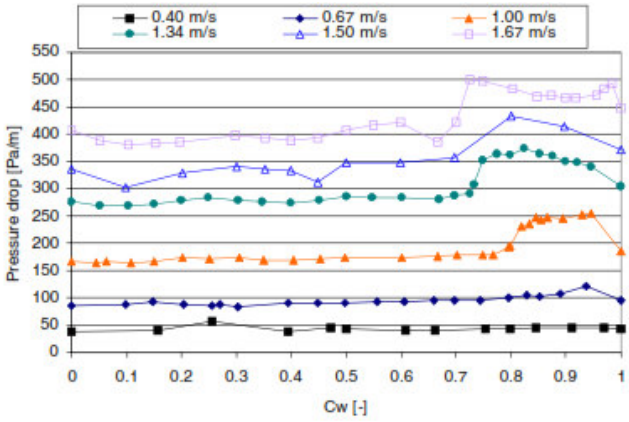

Figure 1.3: Pressure drop measurements for different input water fractions (Cw) and mixture velocities as measured by Elseth (2001).

A large density ratio between the phases stabilizes the stratified flow pattern and leads to faster droplet settling once a dispersion is formed. A study by Charles et al. (1961) with equal density fluids showed a number of new flow patterns, as for instance liquid slug flow. In the present study, however, liquids will have a significant difference in density.

As described by Trallero et al. (1997) viscosity plays a dual role. It helps to dissipate energy of interfacial instabilities on the on hand, while it causes its appearance on the other hand. In most studies no significant viscosity effect on the flow pattern boundaries was reported when the flow was water continuous (Charles et al., 1961; Nädler and Mewes, 1997), while viscosity has an effect in the case of oil continuous flow (Arirachakaran et al., 1989). Vedapuri et al. (1997) reported less intense mixing in dual continuous flow when a high viscosity oil was used compared to low viscosity oil. However, the studies mentioned above did not consider the effect of the initial condition of the flow. Assuming the situation that the dispersion was not produced by instabilities of the flow itself but rather in a pump or valve, once spread over the cross-section, a higher viscosity of the continuous phase will reduce the droplet settling movement, and thus slow down separation. Regarding the viscosity of the dispersed phase, van der Zande and van den Broek (1998), who studied the break-up process occurring in an orifice, explained that a higher viscosity will result in larger droplets. This is due to higher energy dissipation by the internal flow when droplets deform before breaking, leaving less energy for the increase of interfacial area.

Lower interfacial tension promotes dispersion and emulsification of droplets (Kokal, 2005). Comparing the work by Lovick and Angeli (2004b) and (Laflin and Oglesby, 1976) indicates that lower interfacial tension promotes the onset of dispersion at lower mixture velocities. At higher interfacial tension, breakup of droplets is more difficult (Hinze, 1955). Stronger turbulent forces are required for keeping the larger generated droplets dispersed (Torres-Monzón, 2006).

Also the pipe diameter will have an influence on the flow pattern. Mandal et al. (2007), comparing oil-water flow in different pipe diameters, reported that the three layer flow pattern, which is common for larger diameters, did not occur in their small pipe experiments

($D = 0.012m$). An increased effect of the contact angle in narrow pipes was mentioned as a possible reason. Plasencia and Nydal (2010) compared dispersed flow with similar Reynolds number in pipes with different diameters ($D = 16, 32$ and $60mm$). Results indicated that phase inversion occurs at higher input water fractions in small diameter pipes.

A comprehensive overview of liquid-liquid flow models and stability criteria including a summary of experimental data is given by Brauner (2003).

1.2.2 Pressure gradient

The pressure gradient is strongly related to the predominant flow pattern and beyond that a function of mixture velocity, phase fractions and phase viscosities. While the pure phase viscosities are key properties in the case of stratified flow, an effective or apparent viscosity describes the fluid viscosity if dispersion is present. Effective viscosity models were proposed by for instance Pal and Rhodes (1989b), Brinkman (1952) Mooney (1951) or Taylor (1932) and predict higher effective viscosities with increasing dispersed phase fraction. An extensive summary of proposed effective viscosity models is given in Vielma (2006) and Xu (2007). Considering a single characteristic viscosity is, however, only valid for homogeneous dispersions. Otherwise this assumption will fail.

Several experimental studies report a peak in the pressure gradient related to phase inversion, see Figure 1.4, or partial phase inversion when the highest dispersion fractions occur (Angeli and Hewitt, 1999; Arirachakaran et al., 1989; Elseth, 2001; Kumara et al., 2010; Nädler and Mewes, 1997; Pal, 1993; Valle, 2000). Here, a partial phase inversion concerns the transition from dual continuous to fully dispersed flow, where one phase (oil in the reported experiments) is fully entrained, but often with a rather dense dispersion layer.

A higher dispersed phase fraction does not always imply a higher pressure gradient. A drag reduction effect as a result of turbulence modification in the presence of dispersion was described by Pal (1993) who ascribed this effect to dynamic coalescence and breakup processes in unstable dispersions. Similar experimental results were found by Angeli and Hewitt (1999) and Soleimani (1999).

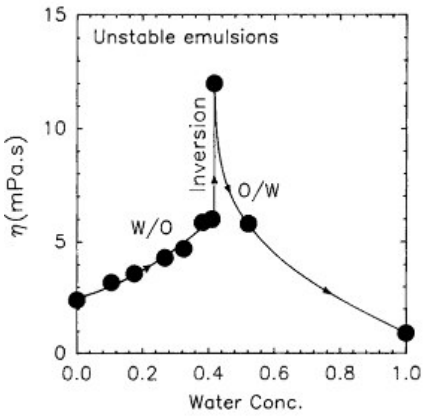

Figure 1.4: Effective viscosity measurements from pipe flow experiments by Pal (1993)

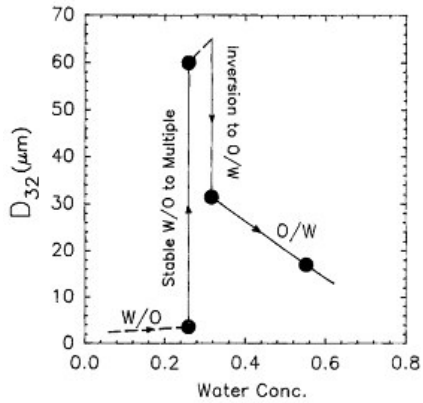

Figure 1.5: Sauter mean diameter (D_{32}) as a function of water concentration. From Pal (1993).

A drag reduction effect as result of increasing input water fraction was also observed for partially dispersed flow (Charles et al., 1961; Nädler and Mewes, 1997). In this case, a water layer at the bottom of the pipe led to a reduced perimeter fraction wetted by the high viscosity oil continuous layer.

A further peak in the pressure gradient versus input water fraction curve was reported as a result of laminar to turbulent transition of the oil phase (Guzhov et al., 1973; Plasencia and Nydal, 2010).

In fully dispersed flow the oil viscosity does not seem to have an important effect on the pressure gradient when the flow is water continuous. In contrast, oil viscosity is crucial when oil is the continuous phase (Arirachakaran et al., 1989). Conducting experiments with different pipe material Angeli and Hewitt identified the wettability characteristics of the pipe as another parameter influencing pressure drop and flow structure (Angeli and Hewitt, 1999, 2000b).

1.2.3 Local phase fractions

The local phase fractions strongly depend on the flow pattern and can differ considerably from the input phase fractions. The velocity or slip ratio S is defined as the ratio between in-situ oil and in-situ water velocity. While S is close to unity in homogeneously dispersed flow, S values smaller or larger than unity are common for other flow patterns. In stratified flow the phase with the higher viscosity tends to accumulate due to higher wall friction. Furthermore, accumulation of the phase forming a thin continuous layer at the bottom or top of the pipe has been reported (Lovick and Angeli, 2004b). In this case, the large wall contact area increases frictional drag. But also pipe wetting properties, affecting the interface shape (curved interface), will be of importance for the resulting slip ratio. As the mixture velocity increases and the flow becomes dispersed, the slip ratio becomes closer to unity (Valle, 2000). However, formation of a dense packed dispersion in the wall region can lead to accumulation of the dispersed phase as a result of a high effective viscosity (Valle, 2000).

1.2.4 Droplet sizes

Droplets, which appear in the flow as droplet size distributions, are influenced by a number of factors, such as interfacial tension, shear, flow properties of oil and water and emulsifying agents or solids which are common in real crude oils (Kokal, 2005). Several studies report

droplet size measurements in pipe flow (Al-Wahaibi and Angeli, 2008; Angeli and Hewitt, 2000a; El-Hamouz and Stewart, 6-9 October 1996; Lovick and Angeli, 2004a; Middleman, 1974; Pal, 1993; Pal and Rhodes, 1989a; Plasencia et al., 2013; Simmons and Azzopardi, 2001; Ward and Knudsen, 1967). In general, droplet sizes increase as a function of the dispersed phase fraction (Pal, 1993), and decrease at higher flow rates with increasing Reynolds numbers. Beside gravitational effects droplet sizes are important for the effective viscosity and thus pressure gradient in dispersed flow. Pal (1993) observed drag reduction effects as the result of dynamic coalescence and breakup. Ward and Knudsen (1967) found anomalous behavior of heavy crude oil emulsions, where viscosity tends to decrease with higher dispersed volume fraction. Droplets were significantly larger compared to droplets observed in experiments with low viscosity oil emulsions. Real crude oils often contain natural components acting in a surface stabilizing way. Droplet sizes in such fluids are reduced and droplets behave more as rigid particles. Surfactants may stabilize emulsions and reduce hydrodynamic particle-particle interactions and thus drag reduction effects by turbulence modification as reported above (Pal, 1993). For such fluids non-Newtonian effects have been reported (Pal, 1987; Zakin et al., 1979). Under certain conditions, when droplets are sufficiently small and dispersions can be considered as stable emulsions single phase flow equations with averaged flow properties can be applied (Pal and Rhodes, 1989a). In many situations, however, when the flow is underdeveloped or at low flow velocities dispersed flow cannot be considered as homogeneous and local variations will occur.

1.2.5 Flow development

In most of the reported experiments the flow develops from initially stratified state at the test section inlet. In this case fully developed flow will be reached relatively fast, because dispersions form as the result of instability and droplet breakup mainly. Developed flow is often taken for granted. A more practical situation, however, is the development of the flow from initially dispersed state, as naturally formed in the reservoir, or downstream of a disturbance by a valve or pump (Cabellos et al., 2009). Plasencia et al. (2013) reported that crude oil emulsions produced in their experiments were typically stable for hours or even

days. This indicates that the flow can have extensive development lengths or even a remaining history of the upstream condition, when coalescence is of importance. Less stable mineral oils, as used in most experiments, will develop faster. Karabelas (1978) assumed that for the reported diluted liquid-liquid dispersions stable droplet sizes were reached 600 pipe diameters downstream of the entrance. This exceeds the test section lengths in many laboratories. History effects of inlet devices have been demonstrated by Angeli (1996), Ngan (2011), Soleimani (1999) and Mandal et al. (2007). Dispersed flow was observed at considerably lower mixture velocities, when inlet mixing was present. Data from Angeli (1996), see Figure 1.6, shows that the measured pressure gradient in premixed flow exceeded the non-premixed data by up to factor three in particular cases.

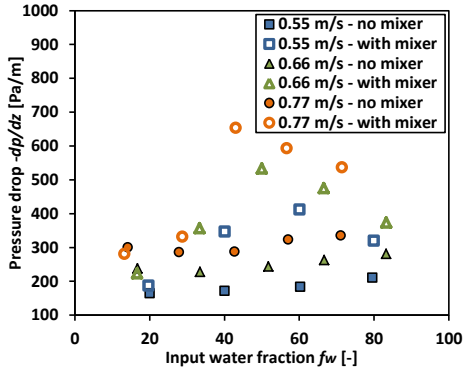

Figure 1.6: Comparison of pressure gradient measurements with and without inlet mixing. Data extracted from Angeli (1996).

1.3 Objectives

The main objective of this thesis is to provide new experimental data for horizontal oil-water pipe flow, which should serve as source for the improvement of models and moreover transport strategies.

In more detail, flow development downstream of a mixing device should be shown for varying superficial velocities and input water fractions. This should help to understand and predict the flow behavior downstream of for instance pumps or valves.

A further objective is the detailed measurement of cross sectional phase distributions in the evolving flow patterns and to understand how this is related to the corresponding pressure gradient. A more detailed differentiation than stratified and homogeneously dispersed flow is needed in order to develop multidimensional models.

Beside flow patterns, pressure gradient and phase fraction measurements also in-situ droplet size measurements should be performed. Changes in the droplet size can indicate a slow development of the flow, which in some situations cannot be measured when changes in for instance the pressure gradient are very small.

As limitation of this work it should be mentioned that the presented experiments were performed with mineral oils or mineral oil mixtures. No complex fluids, such as crude oils or mineral oils with additional surfactant were used. Complex fluids were not used due to limitations set by the test facilities. Furthermore, a much more complex behavior of such fluids is to be expected, which would make it difficult to clearly identify and distinguish different flow effects and to ascribe these to particular flow or fluid properties. Thus, the observed dispersions were of type unstable dispersion.

1.4 Outline of the thesis

The thesis is written in the form of a paper collection with an extended theoretical part. The theoretical part gives an overview of the topic and includes experimental details which were not covered by the papers. The papers are presented at the end of the thesis.

The first chapter ‘Introduction’ introduces to the topic and gives a short overview of oil-water pipe flow in general. Furthermore the objectives of the thesis and a summary of the results, presented in several papers, are given here.

Chapter 2 ‘Experimental techniques’ gives a detailed description of the experimental setups and measurement devices used to produce the results, presented in this thesis. Furthermore, technical difficulties and the approach to solve these problems are pointed out in this chapter.

Liquid properties of the test fluids are presented in chapter 3 ‘Liquid properties’.

In chapter 4 ‘Modeling’ simple theoretical models used for comparison with the experimental results are described. Even if the thesis is of mainly experimental type, a comparison with models was found to be helpful to better explain and understand the measurements and to verify new hypotheses.

A conclusion of the findings is given in chapter 5 ‘Conclusion’. References are listed in chapter 6.

Finally, the papers are collected in chapter 7.

1.5 Summary of papers

Paper 1

FBRM probes (focused beam reflectance measurements) were used in this study for in-situ droplet characterization. The uncertainty of an FBRM instrument was experimentally investigated. Droplets in a beaker-mixer setup were simultaneously measured by FBRM and PVM where the PVM measurements can be considered as very accurate. The same mineral oils as in the pipe flow experiments were used in this study. In addition two different crude oils were tested. An underestimation of droplet sizes by the FBRM of approximately a factor of five was found, which was rather independent of the type of oil and type of phase continuity. Two conversion methods from chord length distribution to droplet size distribution were presented. The uncertainty of the conversion was found to be 50%. This means that compared to the primary underestimation of the FBRM the error could be reduced from a factor of five to a factor of two.

Paper 2

Pipe flow experiments conducted in the well flow loop at IFE are presented. A static inlet mixer was present. Three different oil viscosities were tested. Flow patterns, in situ phase fraction measurements and pressure gradient measurements are presented for a wide range of mixture velocities and input water fractions. Dispersed flow was observed at considerably lower mixture velocities compared to experiments without inlet mixing. A peak in the pressure gradient occurred when the flow pattern changed from the three layer pattern (oil, dispersion and water) to the Do/w&w pattern (dispersion of oil droplets in water and water) with a characteristic dense packed droplet layer. This peak moved towards lower input water fractions as the mixture velocity increased, finally matching the inversion water faction at high mixture velocities. Oil viscosity only had an influence on the oil-dominated flow patterns. Flow development in terms of changing pressure gradients was observed. This could be related to in-flow separation of the phases downstream of the mixing valve.

Paper 3

This paper presents droplet measurements achieved in the experiments reported in paper 2. Traversable FBRM instruments mounted at three different positions along the test section were used. Measurements were performed for $U_{mix} = 0.5m/s$ and $U_{mix} = 1m/s$, Several semi-dispersed and fully-dispersed flow patterns were covered. Cross sectional droplet size profiles in terms of the Sauter mean diameter, D_{32}, are presented. Different flow patterns show different characteristic profiles. This shows the possibility to identify flow patterns based on in-situ droplet size measurements. Probably as a result of inlet mixing, measured droplet sizes were considerably smaller than predicted by models and compared to the literature reporting droplet sizes in non-premixed flow. Comparing the measurements from the three FBRM instruments show droplet growth along the pipe.

Paper 4

A model is developed predicting the pressure gradient in dense packed layer flow. The flow is modelled as stratified flow considering the dense packed layer as an independent phase with

its own mixture density and effective viscosity. The model still depends on knowledge about the local entrainment which would be the challenge of another model. Reproducing data from paper 2 resulted in good agreement while the stratified two-fluid model and the fully dispersed model failed for the semi-dispersed flow patterns.

Paper 5

Experiments performed at NTNU are presented. Flow development downstream of a valve was investigated visually and in terms of changing pressure gradients measured at three different positions along the *50m* transparent test section. First settling was the predominant separation mechanism forming a dense packed layer. Later coalescence led to the reduction of the dense packed layer. Different choking intensities, characterized by the pressure drop over the valve, and three different input water fractions (f_w = *0.1, 0.5* and *0.9*) were tested for mixture velocities of U_{mix} = *0.2m/s* and *0.5m/s*. A complete separation within the test section length was only achieved for the weakest valve choking. A tool was developed predicting the in-flow separation behavior and development length. The tool was able to reproduce the results for U_{mix} = *0.2m/s*. For U_{mix} = *0.5m/s* too fast separation was predicted. Including turbulent mixing and breakup would be necessary in order to model higher mixture velocities.

Paper 6

In this paper flushing operations with complex pipe geometry, with the background in restart or cleaning operations in real offshore production lines, were tested. One liquid initially resting in the test section was replaced by another. This study takes initially completely smooth interfaces as starting point and shows the completely opposite case compared to premixed flow. Further flow development in complex pipe geometries is demonstrated. Dependent on the flushing rates the oil-water interface developed differently which resulted in different. A number of test cases for both flushing scenarios, ‘replacement of oil’ and ‘replacement of water’, were created and compared with the commercial flow simulator LedaFlow. Flushing time and even the residual amount of liquid for low flow rates were

predicted well. Interestingly predictions were worse for the lowest flow rates when the flow was least plug-like.

The paper also addresses the problematic of unwanted mixing of the phases due to for example changing pipe geometry. In many applications sequential single phase transport or at least a limited mixing zone instead of mixture transport is preferred. Mixing always leads to the need for re-processing the fluids.

Paper 7

In this paper follow up experiments of paper 6 are presented. A simpler test section geometry and more detailed measurements allow for better analysis. Oil flushed by water in a horizontal and downward inclined pipe and water flushed by oil in a horizontal and downward inclined pipe were tested. The oil was more viscous (μ_o = *60mPa*s*) as in paper 1 and differences between flushing with oil and with water were expected to be larger. Three conductivity ring probes installed along the test section allowed estimating the flushing front propagation velocity. Again a much more efficient removal was found when the low viscosity liquid was flushed by the high viscosity liquid. In this case the flushing front velocity was equal to the superficial velocity of the flushing liquid, describing a plug flow behavior (still the flushing front was stretched but had stopped developing). The results were compared with predictions by the commercial flow simulator OLGA 7.1. Especially in the case of flushing with water OLGA predicted too low flushing front velocities. Using the recent OLGA HD model, which considers a velocity distribution over the cross section, considerably improved the results. This shows that a cross sectional resolution of the problem can much better predict the correct behavior of a problem where slip between the phases is important.

Chapter 2

Experimental techniques

Two facilities with different setups were used during the experimental campaigns presented in this thesis. This chapter explains experimental details necessary to understand and reproduce the conducted experiments. First, the facilities and the arrangement of the applied measurement devices will be explained. Second, the subsequent sections give more detailed information concerning the main measurement techniques.

2.1 Facilities

2.1.1 The Multiphase Flow Laboratory at NTNU

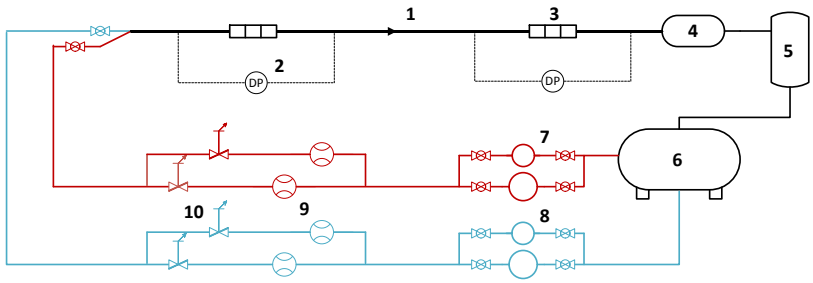

1. Transparent test section
2. Differential pressure transducers
3. Conductance probe
4. Slug catcher
5. Liquid-gas separator
6. Separator tank
7. Centrifugal oil pumps
8. Centrifugal water pumps
9. Flow meters
10. Remote controlled flow valves

Figure 2.1: Schematic of the Horizontal Flow Loop at NTNU. The gas supply is not shown.

The medium scale flow loop at the Multiphase Flow Laboratory at NTNU is a closed loop system. A schematic is shown in Figure 2.1. From a gravity separator in the basement of the building oil and water are pumped through separate flow lines before they merge in a Y

junction at the inlet of the test section. A small and a large centrifugal pump are available for oil and water respectively. In the same way, flow meters with different ranges can be applied. At the end of the test section the fluids enter a slug catcher and thereafter a liquid gas separator. From here the liquids are recycled into the liquid-liquid gravity separator. A pressurized air supply is also available (not shown in Figure 2.1). Experiments with gas phase were, however, not conducted in this thesis. The flow path of the liquids from the separator to the test section inlet is controlled by manual valves. An in-house LabVIEW control program is used to set the rotational speed of the pumps as well as the opening of the automatic valves. Furthermore the LabVIEW program monitors and samples data from the installed measurement devices in real-time.

The test section can be assembled using transparent acrylic pipes which are available with different inner diameters ($D = 32mm, 50mm, 60mm$ *and* $90mm$). For more complex geometries flexible hoses with the same inner diameters are available. Pipe sections and hoses are flange-mounted. In a straight configuration the test section had a total length of $L = 16m$. Measurement devices such as conductivity ring probes or pressure transducers can be mounted along the test section. An overview of measurement devices used in this thesis is given in Table 2.1.

Table 2.1: Overview of measurement devices used at the Multiphase Flow Laboratory at NTNU.

Measured variable	Measurement device	Range	Accuracy
Oil flow rate	Coriolis Flowmeter (MICRO MOTION F025S I 116 SZ)	109 – 1088.4 kg/h	±0.1% of rate
Oil flow rate	Coriolis Flowmeter (MICRO MOTION T150T R 681S1Z)	8700 – 36000 kg/h	±0.15% of rate
		4350 – 8700 kg/h	±0.16% of rate
		871 – 4350 kg/h	±0.31% of rate
		0 – 870 kg/h	±1.6% of rate
Water flow rate	Coriolis Flowmeter (SIEMENS SITRANS F C MASS 2100 Di 15)	0 – 4000 kg/h	±0.15% of rate
Water flow rate	Electromagnetic Flowmeter (FISCHER & PORTER COPA XM 10DX3311 A)	3 – 60 m^3/h	±0.5% of rate
Differential pressure	Fuji Electric (FKCW22V5-AKCYY-AU)	0 – 6 kPa	±0.065% of rate
Local phase fraction / continuity	Conductivity ring probes (in-house)	0 – 100%	

2.1.2 The Well Flow Loop at IFE

Similar to the flow loop at NTNU the Well Flow Loop at IFE is a closed loop system. Figure 2.2 shows a schematic of the loop. From the separator to the test section, the liquids are pumped by centrifugal pumps in separate flow lines. The dense gas SF_6 is used as gas phase and the system can be pressurized up to *10bar*. Heat exchangers for each phase enable to control the temperature within *±0.5°C*. Also for this system the control and sampling program was LabVIEW based.

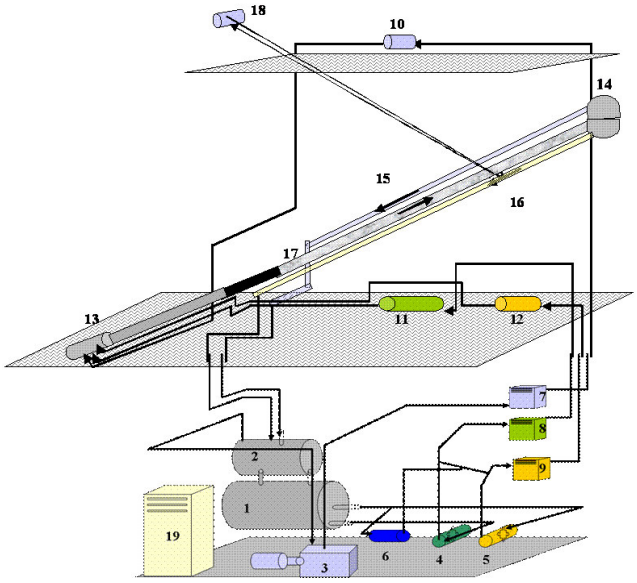

1: Oil-water separator	2: Gas-liquid separator	3: Gas compressor
4: Water pump	5: Oil pump	6: Helical pump
7: Heat exch., gas	8: Heat exch., water	9: Heat exch., oil
10: Gas turbine meter	11: El.Mag.Meter (water)	12: Coriolis meter (oil)
13: Inlet mixing section	14: Slug catcher	15: Return pipe, gas

Figure 2.2: Schematic of the Well Flow Loop at IFE.

The test section has an inner diameter of $D = 100mm$ and a total length of $L = 25m$. Pipe sections in stainless steel 316L or transparent PVC are available. In the reported experiments, the test section was in horizontal alignment. Fast closing valves enable to abruptly stop the flow. Beside differential pressure transducers a broad beam gamma densitometer and an X-ray tomographic system to measure local phase distributions were installed along the test section. Furthermore, several temperature sensors are installed, for instance at the test section inlet. An overview of measurement devices used in this study is given in Table 2.2.

Table 2.2: Overview of measurement devices used at the Well Flow Loop at IFE.

Measured variable	Measurement device	Range	Accuracy
Oil flow rate	Coriolis Flowmeter (Danfoss MASSFLO 1000)	0.025 – 1.5 m/s	±0.3% of range
Water flow rate	Electromagnetic Flowmeter (Fischer & Porter 10 Dx 3311A)	0.01 – 1.5 m/s	±0.5% of range
Temperature	Pt-100 temp sensors	5 - 65°C	
Differential pressure	Fuji Electric (FKKW12V1-AKCYY-AE)	0 – 6 kPa	±0.065% of rate
Local phase fraction	Dual energy (Ba-source) broad beam gamma densitometer (in-house)	2- and 3-phase	
Local phase distribution	X-ray tomography system (Innospexion)	2- and 3-phase	

2.2 Flow pattern characterization

Flow patterns were mainly characterized based on visual observations. Picture and video recordings were taken in order to document the observed flow. An overview is given by Figure 2.3. With increasing degree of dispersion at higher velocities a clear determination of the prevailing flow pattern became difficult and additional methods were needed.

In the fully dispersed flow pattern phase inversion is marked by a distinct peak in the pressure gradient curve (Figure 2.4a). If conductivity ring probes are used, the electrical signal strongly depends on the continuous phase and indicates if water or oil is wetting the pipe wall. A sudden drop of the output voltage marks the transition from water to oil continuous flow (Figure 2.4b).

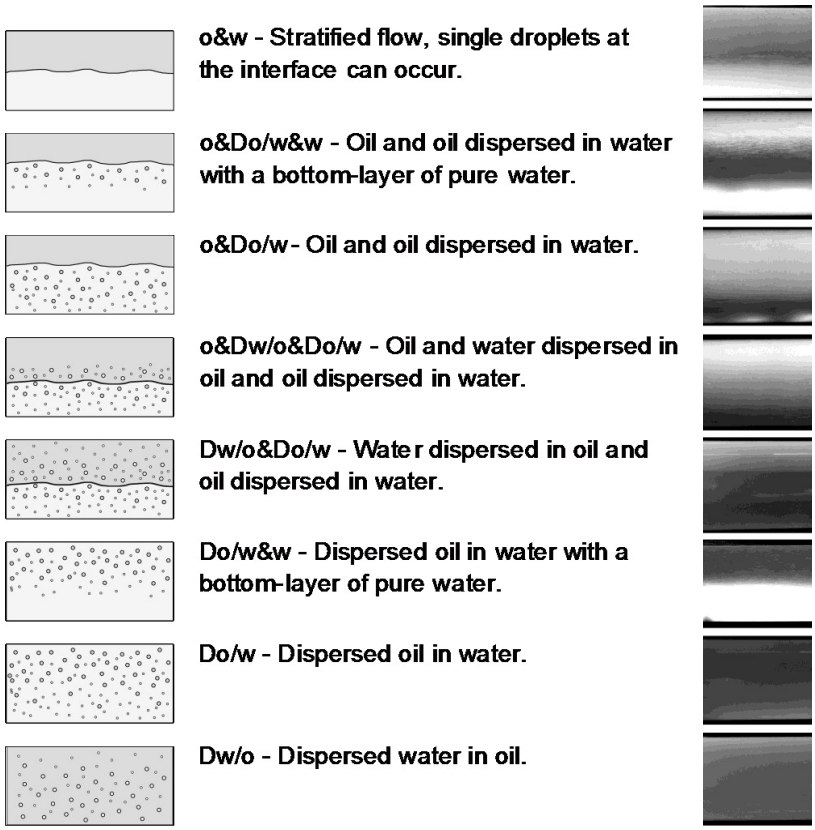

Figure 2.3: Flow patterns as observed in the experiments.

In the semi-dispersed flow pattern line fraction measurements or tomographic reconstructions of the cross section based on x-ray measurements can be used to identify if a droplet free water and/or oil layer is present (Figure 2.4c). If the kind of dispersion is uncertain abruptly stopping the flow by fast closing valves helped to identify the dispersed phase. An oil continuous emulsion can be expected to settle considerably slower than water continuous emulsions. Furthermore, droplets will arrange by size with the largest droplets on top of the emulsion layer if oil is the dispersed phase (Figure 2.4d) and at the bottom if water is the dispersed phase.

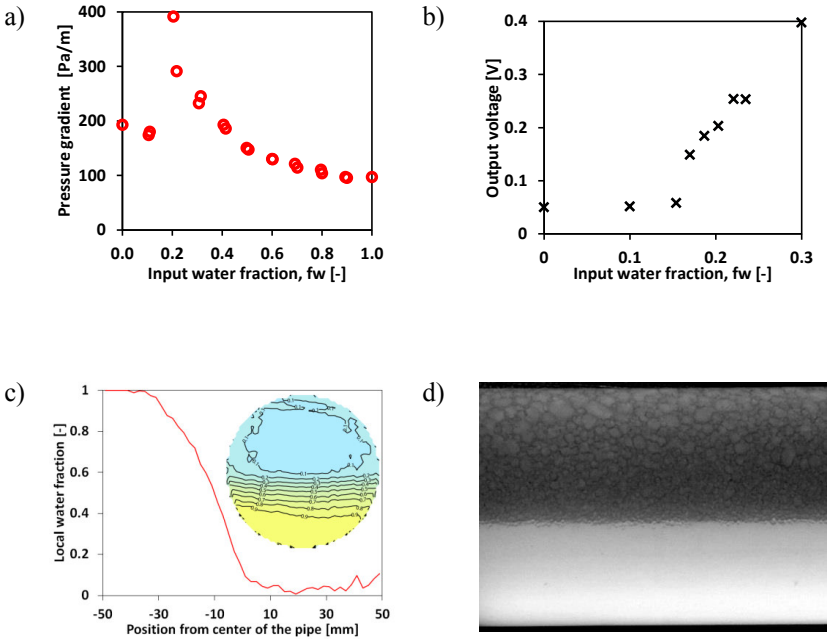

Figure 2.4: Fully dispersed flow: a) Pressure gradient versus input water fraction, f_w. b) Conductivity signal versus input water fraction, f_w. Semi dispersed flow: c) Local phase fraction measurement and tomographic reconstruction. d) Stagnant separation of oil droplets.

2.3 Local phase fraction measurements

2.3.1 Conductivity ring probes

Conductivity ring probes, produced in house, were used at the Multiphase Flow Laboratory at NTNU (see Figure 2.5). These probes can be used to accurately measure phase fractions in stratified two phase flow of two fluids with different electric conductivities. The ring probe is more sensitive to the fluid wetting the pipe wall compared to the fluid in the center of the pipe. Therefore, accurate measurements of the phase fraction are not possible if the flow is dispersed. The continuous phase can still be identified from the measured signal, in this case.

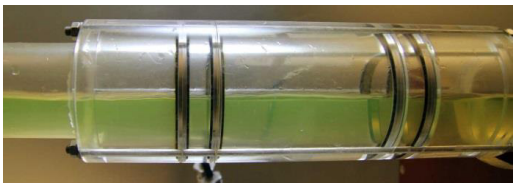

Figure 2.5: Conductivity ring probe.

Each probe consists of two pairs of electrode rings which are flush mounted with the pipe wall. The test section completely filled with water, having the higher electrical conductivity, gives the maximum output signal of approximately *2V*. An oil filled test section resulted in an output signal slightly above *0V*. In between the output voltage of the electronics are proportional to the water holdup. The probes were calibrated for stratified flow by filling a test section with known quantities of water and oil. A calibration curve for a *50mm* probe is shown by Figure 2.6. The relation between output voltage and local phase fraction is not perfectly linear. A best-fit polynomial function of 4th order was found from the calibration curve for each probe. A more detailed description of the electronics is given in Johansen (2006).

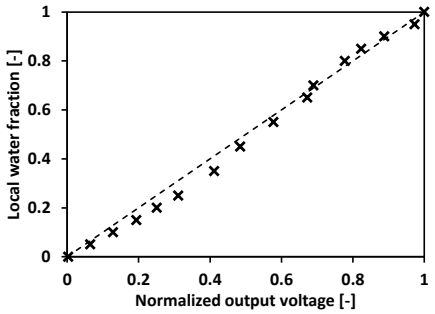

Figure 2.6: Stratified flow - calibration curve for a 50mm conductivity ring probe. The response of the probe differs from a linear relation (dotted line) between water fraction and output signal.

Uncertainty estimate for phase fraction measurements in stratified flow with conductivity ring probes:

Several elemental errors were identified and are listed below:

e_{env} Changing environmental conditions (e.g. temperature) create small fluctuations in the response of the electronics. In order to correct for such fluctuations the offset at $f_w = 0$ and maximum output signal at $f_w = 1$ were measured previous to an experiment. Henceforward, the measured output signals were handled in normalized form. The remaining error is considered to be small and is neglected: $e_{env} = 0\%$.

e_{drift} At steady state conditions signal drift due to saturation of the electronics was observed. This drift was maximum for the maximum output voltage at $f_w = 1$: $e_{drift} = 0.89\%$.

e_{nonlin} As mentioned the response of the probes to the local water fraction is non-linear and 4th order polynomial functions were used to fit the calibration curves. The largest deviation of a function from the corresponding calibration curve was used to define the calibration error: $e_{nonlin} = 2.15\%$.

e_{noise} Noise of the electronics as well as disturbances by single gas bubbles cannot be avoided. This error is expressed as the standard deviation of a steady state flow measurement (saturated signal → no drift) at $f_w = 1$: $e_{noise} = 0.16\%$.

e_{strat} At the end of the stratified flow region droplet formation will disturb the measurements. This cannot be corrected for, but the influence of single droplets is expected to be insignificant: $e_{strat} = 0\%$.

By using the root of the sum of the squares (RSS) a combined systematic uncertainty can be found (Wheeler and Ganji, 2010):

$$R = 2\sqrt{\sum_n e_n^2} = 4.66\% \quad (1)$$

Here, the final uncertainty was multiplied with factor 2 to compensate for elemental errors that could not be measured, e.g. possible droplet formation at the interface.

2.3.2 Broad beam gamma densitometer

At IFE a broad beam gamma densitometer was used to measure phase fractions averaged over the cross-section. The instrument has a Barium 133 (Ba-133) source and operates in a two-energy mode, where the low-energy window covers the energy peaks at *30keV* and *80keV*, and the high-energy window a peak at *350keV* in the energy spectra (see Figure 2.7).

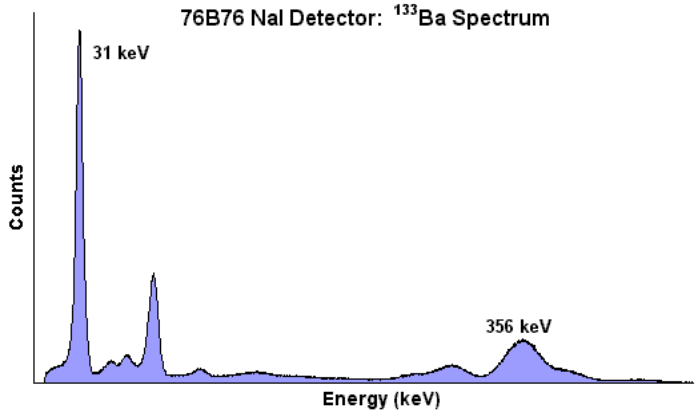

Figure 2.7: Energy spectra for Ba-133. (from http://www.amptek.com/products/gamma-rad5-gamma-ray-detection-system/)

The instrument mounted on the test section and a schematic showing the principle design are shown in Figure 2.8. The distance of the source was chosen in a way that the gamma beam covers the entire pipe. The radiation is damped by the pipe wall and the fluids inside the pipe. Dampening by the pipe wall is unwanted. The thickness of the wall the gamma beams have to travel through changes with the position from the centerline. This is compensated for by a specially shaped collimator between pipe and detector.

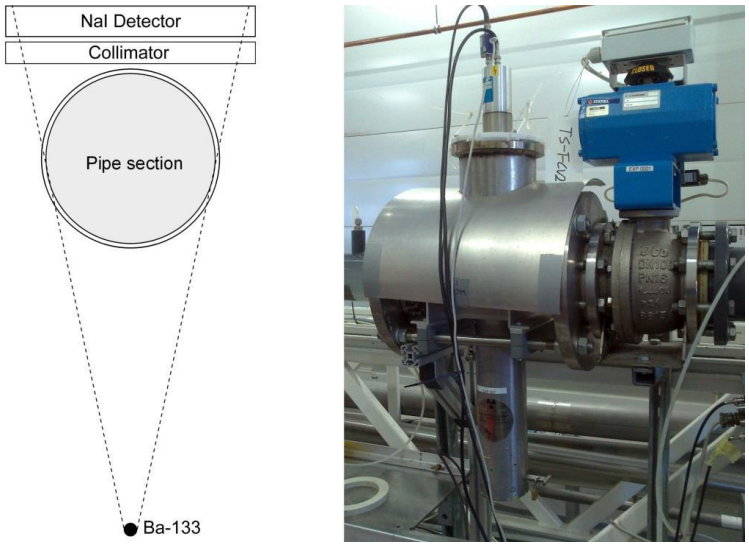

Figure 2.8: Broad beam gamma densitometer at IFE.

A sampling time of *15sec* was used. From the count rates the local water fraction ε_w can be calculated by:

$$\varepsilon_w = \frac{\ln\left(N_{\varepsilon_w} / N_o\right)}{\ln\left(N_w / N_o\right)} \tag{2}$$

where N_{ε_w} is the specific count rate. N_w and N_o are the count rates for single phase water and oil respectively, and were found from a daily calibration routine. The final phase fraction was computed as the average of the phase fractions obtained from the two energy windows respectively.

Uncertainty estimate for phase fraction measurements by the broad beam gamma densitometer.

Several error sources can be listed. The natural fluctuation of the radiation intensity of the source introduces an uncertainty that cannot be corrected for. Also tolerances of the pipe wall thickness cannot be corrected for. However, for a broad beam gamma densitometer, simultaneously measuring the entire cross-section, this error is expected to be small if the instrument is calibrated at the same position. Variations of the flow, e.g. interfacial waves, will also introduce an uncertainty. Furthermore, the electronics will introduce an error. The accuracy and error of every single component was not analyzed in detail. A total error estimate for oil-water measurements of $\pm 3.5\%$ was given by Langsholt (2006). This value is in agreement with the largest measured differences between the phase fractions achieved from the two energy windows.

2.3.3 X-ray tomography system

An X-ray tomography system available at IFE was used to conduct detailed phase fraction measurements that allow for reconstruction of cross-sectional views. The system consists of two source and camera units in vertical and horizontal alignment respectively (see Figure 2.9). The cameras consist of high-resolution, high-sensitivity CdTe-CMOS linear arrays with a pixel size of *0.1mm x 0.1mm*. In the current work the system was operated at *60keV* and *4mA*. A sampling frequency of *40Hz* and a sampling time of *10sec* was used.

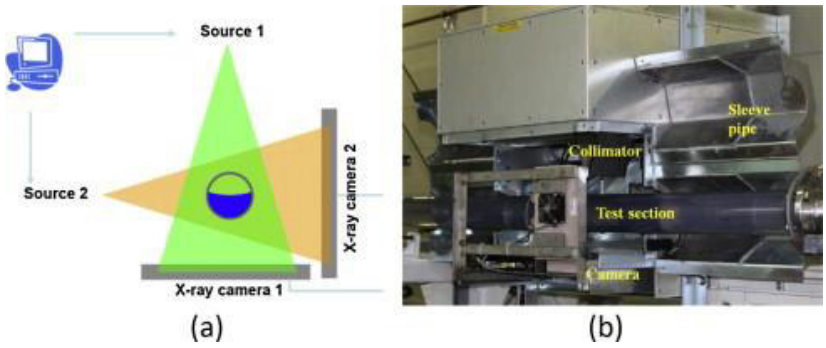

Figure 2.9: a) Schematic drawing of the x-ray system, b) X-ray system installed at the test section. Pictures from Hu et al. (2014).

The instrument was calibrated by measuring single phase water and oil flow. From the measured X-ray intensities the phase fractions can be computed in a similar way as it was done for phase fraction measurements by the gamma densitometer. The stochastic error was reduced by averaging over neighboring groups of pictures. Hence, the final resolution was reduced to *2mm/px*. An algorithm was used to compute cross-sectional reconstructions from the line fraction measurements obtained from each unit respectively. A more detailed description of the algorithm and technical specifications can be found in Hu et al. (2014) and Hu et al. (2005).

Uncertainty estimate for phase fraction measurements by the x-ray tomography system

Absolute errors of mean phase fraction measurements were mentioned to be *5%* for oil and water (Hu et al., 2014). Comparison with mean phase fractions obtained from the broad beam gamma densitometer resulted in a maximum difference of *7%*, which is within the maximum possible difference for these two instruments (*5% + 3.5% = 8.5%*).

2.4 Pressure gradient measurements

Differential pressure transducers by Fuji Electrics, Japan (Type. FKC) with a maximum span of *6kPa* were used in both facilities to measure the pressure gradient. These transducers show a linear characteristic between output signal and differential pressure (see Figure 2.10). l

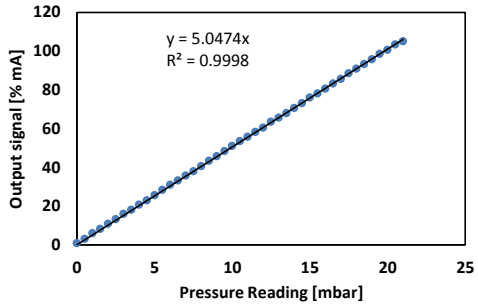

Figure 2.10: Linear characteristic of a differential pressure transducer.

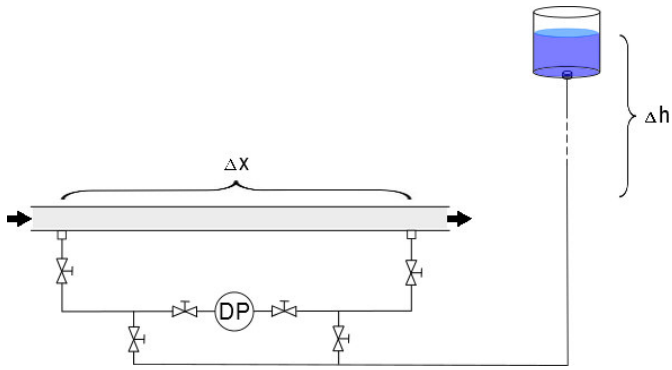

Figure 2.11: Setup for pressure gradient measurements.

The pressure taps (*3mm*) were placed at the bottom of the pipe. The impulse lines from the test section to the pressure chambers were filled and periodically purged with water from a tank placed *5m* above the test section (see Figure 2.11. The distances between the pressure taps were between *1.5m* and *2.5m*. The pressure transducers were calibrated with the test section filled with water at no-flow conditions.

Uncertainty estimate for pressure gradient measurements:

The nominal accuracy of the transducers is better than *0.065%* of rate. The random uncertainty can be kept small by choosing long enough sampling intervals. The absolute

uncertainty, however, is considerably higher and dominated by systematic errors. Possible technical reasons are:

- Imperfect pressure taps (orientation and shape of the orifice, imperfect edge)
- Vibration of the test rig
- Flow disturbances from flanges and probes inside the pipe
- Blocking or entrainment of the impulse lines by oil droplets

It is not possible to separately account for every single error source. The total uncertainty for pressure measurements was determined on the basis of a large number of repeatability tests considering different flow patterns and mixture velocities. In general the difference between repeated measurements was much smaller for single phase experiments compared to oil-water experiments. The maximum absolute difference observed was *20Pa*. The maximum relative difference between independent measurements was *15%*. Based on that an estimate for the uncertainty of the pressure gradient measurements is given by max(*±7.5%, 10Pa*), which is in agreement with previous findings by Langsholt and Liu (2009). Single phase measurements compared with theoretical values agreed well as one can see from Figure 2.12.

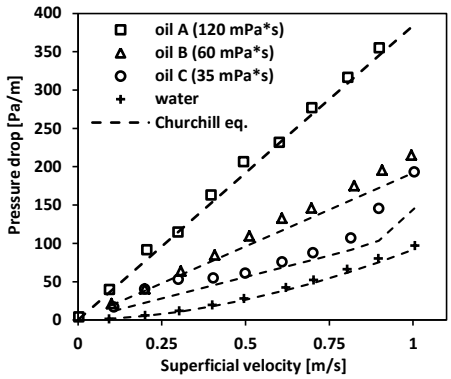

Figure 2.12: Measured pressure gradients for different oils and water compared to theoretical values. Measurements were performed in 100mm pipe. Oil C shows an early transition to turbulent flow.

2.5 Droplet characterization

2.5.1 Focused Beam Reflectance Measurement (FBRM)

The FBRM instrument by Mettler-Toledo Autochem Inc. is an endoscope developed for in situ flow and process control. The measurement principle is based on backscattering of a focused laser beam when it hits a particle in the flow as shown by Figure 2.13. The width of the laser beam is considered negligible. Rotating optics make the laser continuously scan a circle of *8mm* diameter with a constant velocity of *2m/s*. A sensor will measure the backscattered light from particles being traversed by the laser. An algorithm is used to determine chord lengths from the time series of the intensity profile of the backscattered light. Depending on the amount of droplets in the flow thousands of chord lengths will be counted within a few seconds. Based on these counts a chord length distribution (CLD) can be computed.

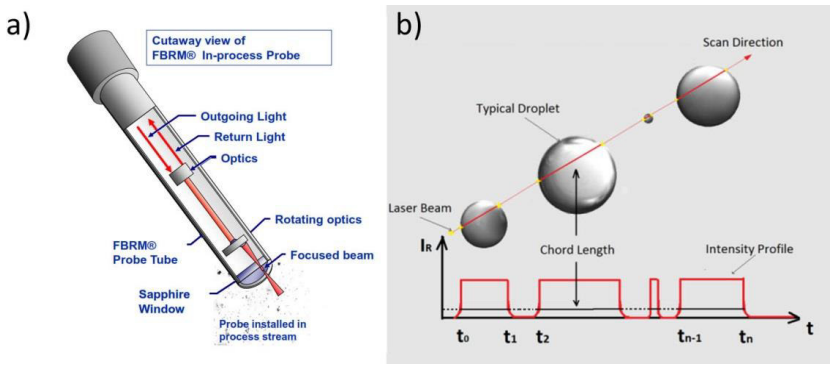

Figure 2.13: FBRM probe: a) Functional sketch (provided by Mettler-Toledo Autochem Inc.), b) Principle of chord length measurements.

FBRM instruments of type D600 were used in this work. A specially designed adapter, that was clued to the test section, made it possible to align the probe by 45° to the flow (see Figure 2.14a). Furthermore, the cross-section of the pipe could be traversed in vertical direction by changing the insertion length. This could be done during an experiment without stopping the

flow. The position was fixated along a bolt with simple screw-nuts as shown by Figure 2.14b. Two O-rings were sufficient to seal the FBRM-adapter combination against leakages.

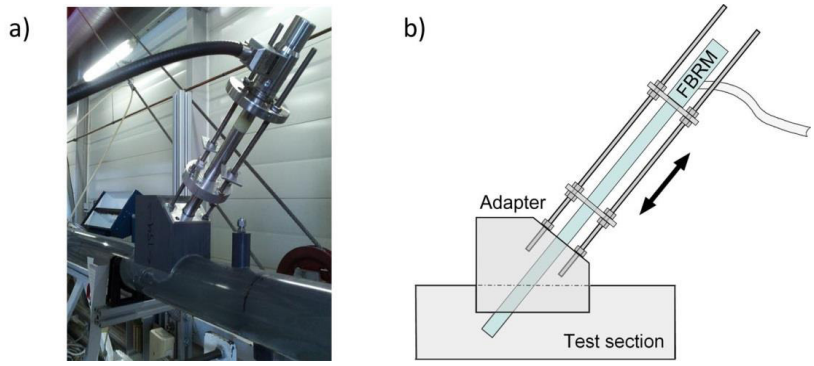

Figure 2.14: a) FBRM mounted at the test section showing the manual traversing mechanism. The alignment was 45° against the flow direction. B) Functional sketch of the adapter.

Even if the probe continuously measures droplets a sampling time has to be defined at the beginning of each experiment and *15s* was used for the reported experiments. Hence a chord length distribution was produced every *15s* based on all counts over the previous *15s*. In this way, changes over time could be monitored and time series of for instance averaged droplet sizes produced. From the available data, counts could still be summarized over several samples in order to reduce the statistical uncertainty. This was done for the steady state period of the experiments. Also chord length distribution curves become smoother when the number of counts increases, as shown for an example in Figure 2.15.

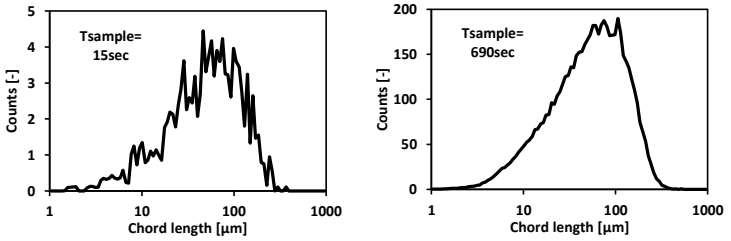

Figure 2.15: CLD: The CLD averaged over 46 samples (right) is much smoother compared to a single sample (left).

Uncertainty estimate for droplet sizes measured by FBRM

As mentioned chord lengths are measured by the FBRM. Chord lengths differ from the real droplet sizes due to several reasons. Important factors are for instance surface roughness or the refractive index of the medium that can influence the scattering of light. A further reason is the geometry factor, meaning that the laser beam traversing a spherical droplet at a random position will create a chord length shorter than the real diameter in most of the cases. Furthermore a statistical error is introduced by measuring single droplets along a line (or circle in this case) in a volume. Bigger droplets have a higher chance of being detected. Another issue can be the blocking of the flow by the probe. The flow will be forced to change direction when it approaches the probe. The different inertia of different droplet sizes can lead to screening of droplets.

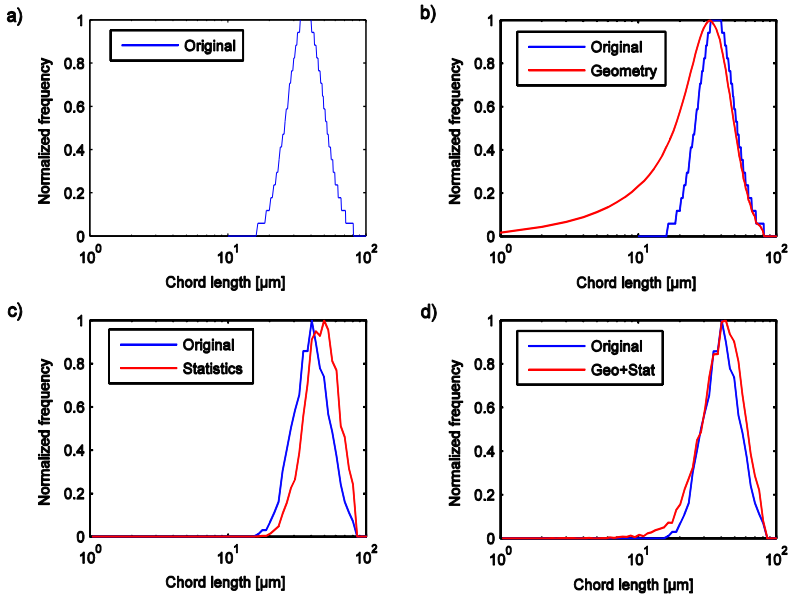

Figure 2.16: Simulating FBRM measurements: a) Original DSD, b) Considering the geometry factor, c) Considering the statistical error, d) Considering both geometry factor and statistical error.

The influences of the geometry factor together with the statistical error were tested in a simple Matlab-model. A given DSD was considered as shown in Figure 2.16a. In the first simulation only the geometry factor was considered. Every droplet of the DSD will be traversed by the laser at all possible positions. Hence, an equal probability for every measurement position is assumed. The result is shown in Figure 2.16b. A considerable number of chord lengths smaller than the actual droplet sizes are counted. In the second simulation only the statistical error is considered. A cubic sample volume with a ring representing the circulating laser beam, fixed in its position, is assumed as test case. In each iteration, the droplets given in the DSD are randomly distributed in the sample volume. Whenever a droplet intercepts with the circle it will be counted. The result in Figure 2.16c shows that larger droplets have a higher chance of being measured than smaller droplets. In a last simulation both models were combined. For every droplet intercepting with the ring a chord length corresponding to its position of interception will be counted. The result is shown in Figure 2.16d. Both error sources will partly cancel each other out.

Weighted and non-weighted mean sizes of the original DSD and modelled CLDs are summarized in Table 2.3. The error predicted for the combined model is small. However, from experience and from the literature, e.g. Boxall et al. (2010), Maaß et al. (2011), Vay et al. (2012), it is known that FBRM measurements can considerably underestimate particle sizes. The geometry factor and the statistical error cannot be the main error sources. It is expected that the FBRM is very sensitive to the surface properties of droplets. Therefore, a detailed study on the uncertainty of FBRM measurements was conducted as described in Paper 1.

Table 2.3: Modeling the FBRM behavior: Mean sizes of the original DSD and the modelled CLDs considering different error sources.

Model	D_{mean}	D_{32}	D_{43}
Original	41.57	48.77	52.35
Geometry factor	35.44 (-14%)	46.24 (-5%)	50.47 (-4%)
Statistical error	48.91 (+18%)	55.86 (+15%)	58.98 (+13%)
Combined model (Geometry+Statistics)	41.58 (0%)	50.69 (+4%)	54.46 (+4%)

2.5.2 Particle Video Microscopy (PVM)

Also the PVM instrument is an endoscope for in-situ particle characterization with equal physical dimensions, see Figure 2.17. A high-resolution CCD camera takes pictures with a size of *1075µm x 850µm* (*680px x 512px*). Internal light sources enhance the picture quality. The PVM allows for particle size and shape characterization. From the sampled pictures droplets have to be counted manually, which is a drawback of the probe. A Matlab-code, based on the Hough-transformation, which automatically identifies, measures and counts droplets in large picture series, was developed in order to simplify the post-processing. In this work the PVM was used as a calibration tool for the FBRM instrument. This enabled to convert chord length data from the FBRM measurements to droplet sizes with a limited amount of post-processing.

Figure 2.17: PVM V819 with processing unit (by Mettler Toledo).

Uncertainty estimate for droplet sizes measured by PVM

The ability to achieve correct droplet sizes from PVM pictures was tested in detail in Paper 1. A restriction is set by the picture size and resolution. Droplets smaller than $5\mu m$ will not appear sharp. Droplets much larger than approximately $600\mu m$ will not fit into a picture. The uncertainty of mean droplet sizes depends on the range of a DSD and will improve with the number of counts. It was found, as one would expect, that the detected maximum droplet size is more sensitive to the number of counts as the mean size. This is simply because the number of the largest droplets is much less than for droplets of average size. At least 500 counts are recommended. If the sample size is very limited a correction-method for the bias introduced by the limited number of counts is described by Gwyn et al. (1965).

2.6 Technical difficulties during experimentation

During experimentation several problems had to be solved. A selection of problems and suggestions how they can be solved are described in this chapter. This should serve as a guide to the reader or simply inform about typical obstacles during oil-water flow experimentation.

2.6.1 Purging the impulse lines

In section "2.4Pressure gradient measurements" a purging system for the impulse lines connecting the pressure-chambers of the differential pressure transducer with the pressure taps is described. It was found that purging the impulse lines is very useful for experiments with high oil fraction and absolutely necessary when an oil continuous layer was wetting the bottom of the pipe or when the pipe was emptied for liquid for a period of time. In Figure 2.18 a pressure tap is shown. One can clearly identify a thin channel drilled through the pipe wall ending in a pocket of larger diameter. Even if the bottom mounted impulse pipes are filled with water penetration of oil droplets or oil droplets blocking the tap are possible. At low velocities oil droplets sitting on top of and blocking the pressure tap were also observed. At the end of the experimental sessions the loop was flushed with air, which could lead to penetration of air.

In Figure 2.19 two measurement series for single phase water flow are shown. For PDT1 the impulse lines were purged with water before the offset of the pressure transducer was calibrated. The trend is in good agreement with the theoretical predictions. The measurement series PDT2 was taken after a standby period, with the pressure transducer calibrated without purging the impulse lines. After the forth measurement inclusion of air was observed in the impulse pipe. Purging with water and removing of the air led to a sudden drop of the differential pressure and a consistent constant deviation of approximately *50Pa/m* from the theoretical pressure gradient. This was a result of the initially wrong offset calibration and equals a water column of *13mm* for our setup.

Figure 2.18: Pressure tap at the pipe bottom.

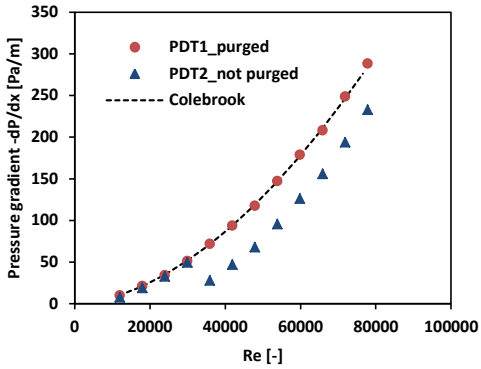

Figure 2.19: Water single phase pipe flow: Measurements with correctly calibrated pressure transducer (PDT1) and with a pressure transducer with blocked impulse line.

2.6.2 The effect of dirty pipe walls

Even if the flow loop is a closed system, a certain amount of unwanted particles will always be present. A common contamination source is microorganisms and algae growth when light and oxygen are present, but also natural degradation of oil and arising byproducts. In other cases the oil can be aggressive and interact with the pipe material. For instance Exxsol oil tends to make hoses stiff and acrylic pipes brittle. Beside the need to empty the pipe for oil and flush it with water after an experimental session it is recommended to clean the pipe walls from time to time. We experienced that some types of oil are sticky and a complete removal of the oil layer on the wall by flushing with water can be time-consuming (up to minutes or even hours!). The wetting of the pipe can influence the flow considerably.

An example is shown below. In Figure 2.20 the pressure gradient measured at three different positions along the pipe is compared for experiments with the same experimental conditions (U_{mix} = *0.5m/s*, f_w = *0.4*) but before and after cleaning of the pipe. Two cases are shown. In the case "no mixing" the liquids were merged in a simple Y-manifold. In the case "inlet

mixing" a partly closed ball valve was installed behind the inlet and mixed the flows. In both cases considerably lower pressure gradients were measured for the cleaned pipe.

Figure 2.21 shows pictures of the test section flushed with water after the experiments presented in Figure 2.20 (inlet mixing). One can see how the test section before cleaning is wetted by oil droplets increasing the effective surface roughness.

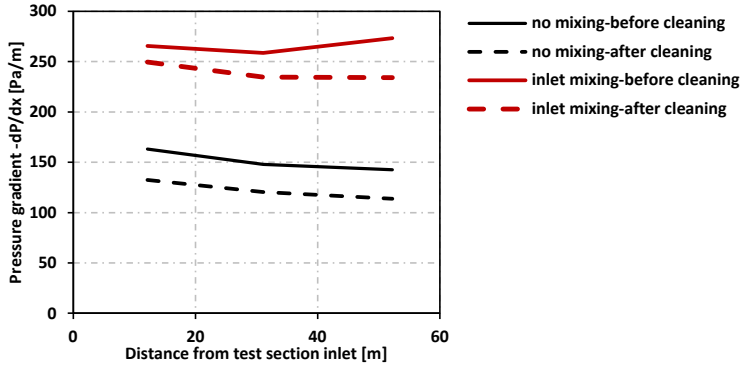

Figure 2.20: Comparison of pressure gradient measurements along the pipe for a cleaned and dirty test section. U_{mix}=0.5 m/s, f_w=40%. For the case with inlet mixing a partly closed ball valve was installed at the inlet.

Figure 2.21: Pipe before (left) and after cleaning (right).

2.6.3 The order of experiments

When experiments with changing input water fraction are to be conducted it is recommended to start with high water fractions. The same applies when oil and water superficial velocities are adjusted independently. One should first increase the water flow rate, before adjusting the oil flow rate. In this way one avoids the possibility of oil penetrating the pressure taps as described above. Also unwanted oil wetting of the pipe, which is difficult to remove, can be avoided.

2.6.4 Preventing gas backflow at the test section end

At low flow rates unwanted backflow of gas from the separator into the test section end can be problematic. If modifications to the loop can be carried out in an easy manner, a flexible hose which is lifted up slightly can be an effective prevention (see Figure 2.22). This can, however, influence the upstream flow by for instance causing a higher water accumulation. A sufficient distance between measurement equipment and the outlet should be considered, even if this will reduce the utilizable length of the test section.

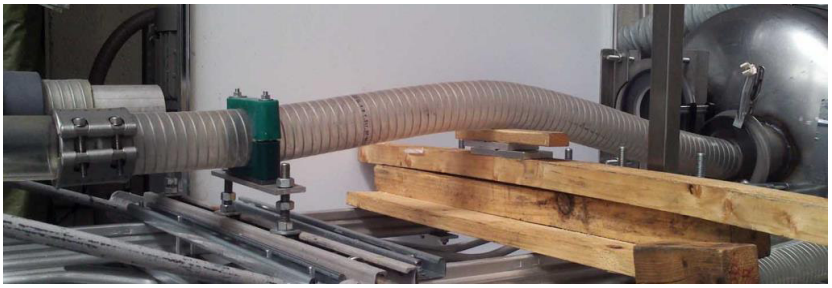

Figure 2.22: Test section end.

2.6.5 Improving droplet measurements by optical probes

Probe coating

A major problem of optical probes used for droplet measurements is probe coating, which happens when single droplets stick on the optics leading to a continuously sampling of those. In the post processing such data will create large peaks in the density distribution curves (see Figure 2.23) and falsify mean sizes. In such cases the sample is in general to be discarded if the peak cannot be corrected for (e.g. identifying and discarding single wrong counts). A water or oil repellent applied to the probe could help to avoid probe coating, as long as the repellent does not change the chemical properties of the liquids.

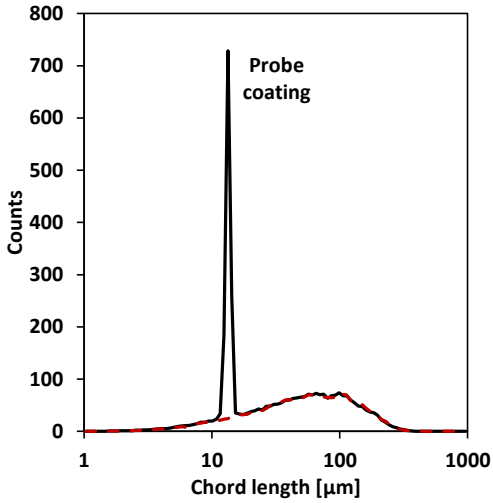

Figure 2.23: Probe coating: CLD for a 5% water-in-oil (Exxsol D80) emulsion.

Improving the contrast

As tested by Maaß et al. (2011) adding small amounts of TiO_2 reduced the underestimation by the FBRM without changing the coalescence behavior of a water-toluene system. The insoluble particles will accumulate at the droplet surface and thus change the light reflection behavior. This was unfortunately not tested in this study but is recommended for future studies. It is imaginable that the changed optical properties also are favorable for other optical measurement methods, such as PVM.

Focal point

Many optical measurement probes, such as FBRM and PVM, provide the possibility to change the focal point. Vay et al. (2012) tested different focal points for the FBRM and found that the measured chord lengths slightly increases as the focal point is changed further into the fluid. In this study, however, the focal point was kept at the recommended factory adjustment, which was *-20µm* inside the lens. In the case of PVM measurements choosing the optimum focal point is not straight forward. One the one hand, it is preferable to focus as much as possible into the fluid. Close to the window droplet measurements can be biased, in the way that the largest droplets avoid the lens. On the other hand, in the case of dense emulsions a focal point too far into the fluid can cause problems as the light has to penetrate other droplets on its way to the lens, which will reduce the picture quality. In this case a compromise has to be found. Figure 2.24 shows droplets of Primol 352 in water. Small droplets close to the lens appear clear while larger droplets in the background are out of focus.

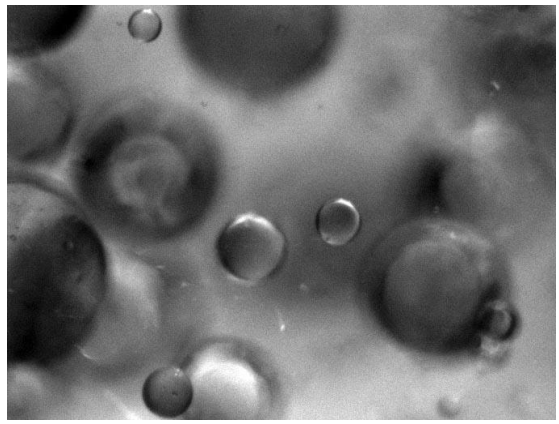

Figure 2.24: Droplets of Primol 352 in water.

Chapter 3

Liquid properties

Tap water was used for all experiments. However, the oil mixtures for the experiments reported in this thesis were changing. The availability of the certain types of oil at the different facilities was one reason. Another reason was the coordination with previous and following experimental campaigns, since replacing the oil in the flow loops implicates a huge amount of work and costs.

Samples for characterization were taken directly from the flow loop. In some cases it was found that the measured oil properties slightly differ from the properties stated in the data sheet provided by the supplier. The most possible reason is that oil mixes with residues from another type of oil used in the loop before. At the Multiphase Flow Laboratory at NTNU a fluorescence powder was added to the water in order to better distinguish between the two liquids. The liquid properties were not changed by the powder. The fluid density was measured by the Coriolis flowmeter. A rheometer was used to measure the fluid viscosity. An Anton Paar – Physica MCR 301 was available at IFE, while a TA Instruments AR-G2 was used at NTNU. In addition, the interfacial tension with water was measured for some oils by the pendant drop method using a CAM 200 (KSV, Instruments Ltd, Finland). An overview of the oil mixtures used in each experimental campaign is given in Table 3.1.

Table 3.1: Overview of oil mixtures used in this thesis.

Name/Composition	**Density, ρ** $\left[kg/m^2\right]$	**Viscosity, μ** $\left[mPa*s\right]$	**Interfacial tension with tap water, γ** $\left[mN/m\right]$
Campaign: Oil-Water Flushing Experiments with Complex Pipe Geometry (NTNU)			
Exxsol D80	800	2	
Campaign: Liquid-liquid displacement in a horizontal and inclined pipe section (NTNU)			
Nexbase 3080	840	60	
Campaign: Dispersed oil-water flow in a horizontal pipe section with enhanced inlet mixing (IFE			
Oil A: Primol 352 / Exxsol D80 (25:1)	866	120	23
Oil B: Primol 352 / Exxsol D80 (6:1)	859	60	23
Oil C: Primol 352 / Exxsol D80 (4:1)	853	35	24
Campaign: Flow development downstream of a choking valve			
Marcol & Nexbase 3080	847	25	

Chapter 4

Modeling

4.1 Introduction

In many of the conducted measurements a dense packed droplet layer formed as a result of gravitational settling of droplets, which were dispersed by an inlet device (mixer or valve). From the pressure drop measurements it became clear that the effective viscosity in such a layer exceeds the viscosity of the continuous phase (which was water in most of the cases) notably. In our observations the dense packed layer was located either between a clear oil and water layer for lower input water fractions or in the upper part of the pipe when oil was fully entrained in the case of higher input water fractions.

The attempt to predict the frictional pressure gradient of such flow regimes by a simple two-fluid stratified model and homogeneous dispersed flow model respectively resulted in unsatisfactory predictions. The question arose if it is possible to make a simple model or rather extend an existing model to include the effect of the dense packed droplet layer on the pressure gradient.

In the following chapters the homogenous dispersed flow and two-fluid stratified model used in this thesis are described. Afterwards a description of a so called “Three layer model” is given. In this approach the two-fluid stratified model was extended including a third phase representing the dense packed droplet layer.

4.2 Homogeneous dispersed flow model

For the homogeneous dispersed flow model it is assumed that the flow is fully dispersed with either oil or water as continuous phase. The dispersion is treated as a single phase occupying

the pipe. In horizontal flow the gravitational pressure gradient disappears. The total pressure gradient is then equal to the frictional pressure gradient (based on the Darcy friction factor, f):

$$-\frac{dp}{dz} = \frac{f_{mix}\rho_{mix}U_{mix}^2}{2D} \tag{3}$$

The mixture velocity and mixture density are obtained from:

$$U_{mix} = U_{sw} + U_{so} \tag{4}$$

$$\rho_{mix} = \varepsilon_w\rho_w + \varepsilon_o\rho_o \tag{5}$$

The mixture viscosity is estimated by a widely used equation by Pal and Rhodes (1989b):

$$\mu_{mix} = \mu_c\left[1+\frac{0.8415\Phi/\Phi_{\mu_r=100}}{1-0.8415\Phi/\Phi_{\mu_r=100}}\right]^{2.5} \tag{6}$$

Φ is the dispersed phase fraction (Φ equals ε_w for oil continuous flow and ε_o for water continuous flow), μ_c is the viscosity of the continuous phase and $\Phi_{\mu_r=100}$ is the dispersed phase fraction when the mixture viscosity exceeds hundred times that of the continuous phase. A constant factor of $\Phi_{\mu_r=100} = 0.765$ is used as proposed by Søntvedt and Valle (1994) in Elseth (2001). Figure 4.1 shows the Pal and Rhodes model for an oil viscosity of $\mu_o = 35mPa*s$.

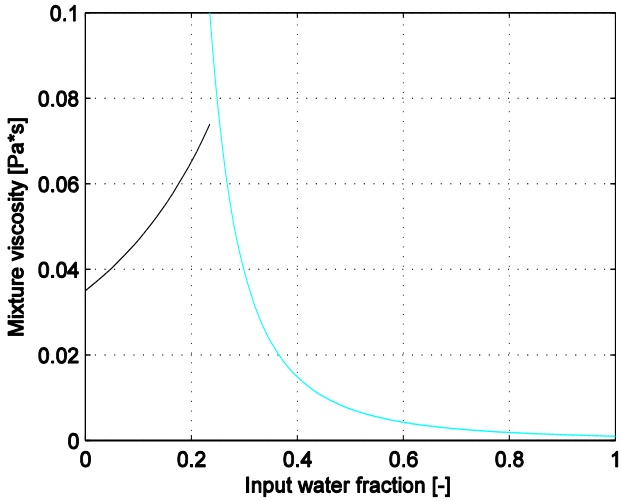

Figure 4.1: Mixture viscosity model by (Pal and Rhodes, 1989b) for an oil viscosity of $\mu_o = 35mPa*s$.

Further, no slip between the phases is assumed. The local phase fractions are equal to the input phase fractions. If oil is the dispersed phase Φ would be equal to (*1-*f_w).

Based on the parameters stated above a mixture Reynolds number is obtained from

$$\mathrm{Re}_{mix} = \frac{\rho_{mix} U_{mix} D}{\mu_{mix}} \tag{7}$$

For laminar flow the friction factor is calculated by the Hagen-Poiseuille equation:

$$f = \frac{64}{\mathrm{Re}} \tag{8}$$

If the flow is turbulent the friction factor can be obtained by solving the Colebrook equation:

$$\frac{1}{\sqrt{f}} = -2\log_{10}\left(\frac{e}{3.7D} + \frac{2.51}{\mathrm{Re}\sqrt{f}}\right) \tag{9}$$

Here e is the wall roughness in $[m]$. In the literature different critical Reynolds numbers for the end of the laminar region can be found, e.g. $Re_{crit} = 1500$ by Arirachakaran et al. (1989) or $Re_{crit} = 2100$ by Brauner (2003). In this work the Churchill equation valid for both turbulent and laminar flow, predicting a smooth transition, is applied to solve directly for the friction factor (Churchill, 1977):

$$f = 8\left[\left(\frac{8}{\mathrm{Re}}\right)^{12} + \frac{1}{\left(\Theta_1 + \Theta_2\right)^{1.5}}\right]^{\frac{1}{12}} \tag{10}$$

where

$$\Theta_1 = \left[-2.457\ln\left[\left(\frac{7}{\mathrm{Re}}\right)^{0.9} + 0.27\frac{e}{D}\right]\right]^{16} \tag{11}$$

and

$$\Theta_2 = \left(\frac{37530}{\mathrm{Re}}\right)^{16} \tag{12}$$

The Colebrook equation is shown together with the Hagen-Poiseuille equation for laminar flow and Colebrook equation for turbulent flow in Figure 4.2.

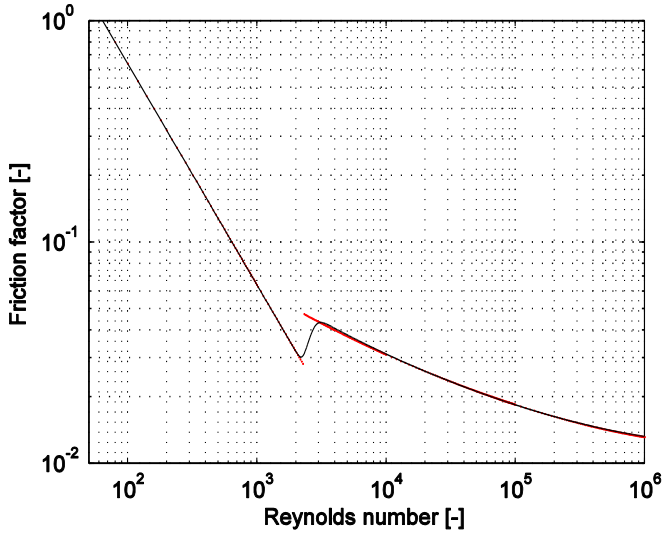

Figure 4.2: Churchill equation (black line) compared to solving the Hagen-Poiseuille equation and Colebrook equation (red dots).

4.3 Two-fluid stratified flow model

For the horizontal case the momentum equations for fully developed stratified flow for oil and water respectively can be written as (Brauner, 2003):

$$-A_o\left(\frac{dp}{dz}\right)+\tau_o S_o-\tau_{ow}S_{ow}=0 \tag{13}$$

$$-A_w\left(\frac{dp}{dz}\right)+\tau_w S_w+\tau_{ow}S_{ow}=0 \tag{14}$$

A_o and A_w are the cross sectional pipe areas occupied by oil and water respectively. S_o and S_w are the oil and water wetted pipe perimeters respectively. The oil-water interface is described by S_{ow}. τ_o, τ_w and τ_{ow} are the shear stresses to the corresponding perimeters/interfaces. Equation (13) and (14) can be combined by eliminating the pressure drop $\left(\frac{dp}{dz}\right)$ and introducing local phase fractions $\varepsilon_w = \frac{A_w}{A}$ and $\varepsilon_o = \frac{A_o}{A}$ which results in:

$$\tau_o S_o \varepsilon_w - \tau_w S_w \varepsilon_o - \tau_{ow} S_{ow} \left(\varepsilon_o + \varepsilon_w\right) = 0 \tag{15}$$

From our experiments the local phase fractions, $\varepsilon_w = 1 - \varepsilon_o$, are known. Since we are only interested in the applicability of the two-fluid stratified model to predict the pressure gradient in semi-dispersed flow, the measured local phase fractions are used directly, which simplifies the computation. A modified model described by Arirachakaran et al. (1989) was applied. In this model the pressure gradient for each phase is computed as if the phase would occupy the entire cross section. The total frictional pressure gradient is then computed as the sum of the single phase pressure gradients multiplied with the perimeter fractions wetted by the respective phase:

$$\left(\frac{dp}{dz}\right)_{2\,fluid} = \frac{S_o}{S}\left(\frac{dp}{dz}\right)_o^{'} + \frac{S_w}{S}\left(\frac{dp}{dz}\right)_w^{'} \tag{16}$$

In equation (16) the single phase pressure gradients are calculated as

$$\left(\frac{dp}{dz}\right)_o = \frac{f_o \rho_o U_o^2}{2D} \tag{17}$$

and

$$\left(\frac{dp}{dz}\right)_w = \frac{f_w \rho_w U_w^2}{2D} \tag{18}$$

with the local velocities of each phase obtained from

$$U_o = \frac{U_{so}}{\varepsilon_o} \tag{19}$$

and

$$U_w = \frac{U_{sw}}{\varepsilon_w} \tag{20}$$

The friction factors for each phase in equation (17) and (18) were again calculated by the Churchill equation based on the pipe diameter.

In a second approach the model was modified by applying hydraulic diameters as described by Brauner (2003). This did, however, not improve the simulation results.

4.4 Three layer model

In order to cover the impact of a dense packed droplet layer in the flow a third layer is added to the two-fluid stratified model. To keep this model as simple as possible a couple of assumptions are needed. Even if the experimental results in this thesis indicate that the dense packed layer mainly consists of oil droplets in water, it is not entirely sure whether a water-in-oil emulsion can exist in the upper part. The experiments show that the local water fraction in

the dense packed layer is very low and close to that needed for phase inversion. Based on this observation a constant water fraction of $\varepsilon_{w\_dense} = 0.2$ is assumed for the entire dense packed layer. Therewith the dense packed layer becomes independent of the possibility of two regions of oil and water continuous flow respectively. The mixture density of the dense packed layer can then be calculated as follows:

$$\rho_{dense} = (1-\varepsilon_{w\_dense})\rho_{oil} + \varepsilon_{w\_dense}\rho_w \tag{21}$$

The mixture viscosity is again calculated by Pal and Rhodes (1989b), equation (6) with $\Phi_{dense} = \left(1-\varepsilon_{w\_dense}\right)$ where water is the continuous phase.

In order to make a complete model the local phase fractions and amount of dispersed phase would have to be predicted as well. A separate entrainment and separation model would be required. However, here it is only the objective to investigate if an additional layer, handled as a third phase and representing the dense packed layer, is sufficient to achieve the correct pressure gradient. The height, h_i, and position of each layer is therefore found from video observations and line fraction measurements (X-ray). As shown in Figure 4.3 the cross sectional areas and perimeters for each phase can be found by:

$$A_o = \left(\frac{D}{2}\right)^2 \cdot \arccos\left(1-\frac{2h_o}{D}\right) - \left(\frac{D}{2}-h_o\right)\cdot\sqrt{Dh_o - h_o^2} \tag{22}$$

$$A_w = \left(\frac{D}{2}\right)^2 \cdot \arccos\left(1-\frac{2h_w}{D}\right) - \left(\frac{D}{2}-h_w\right)\cdot\sqrt{Dh_w - h_w^2} \tag{23}$$

$$A_{dense} = A - (A_o + A_w) \tag{24}$$

and

$$S_w = \alpha_w \frac{D}{2} \tag{25}$$

$$S_o = \alpha_o \frac{D}{2} \tag{26}$$

$$S_{dense} = \pi D - \left(S_o + S_w\right) \tag{27}$$

$$S_{o-dense} = D \cdot \sin\left(\frac{\alpha_o}{2}\right) \tag{28}$$

$$S_{w-dense} = D \cdot \sin\left(\frac{\alpha_w}{2}\right) \tag{29}$$

The central angle α_i can be found by solving:

$$A_i = \frac{D^2}{8} \cdot \left(\alpha_i - \sin\alpha_i\right) \tag{30}$$

where i indicates the phase (either oil or water).

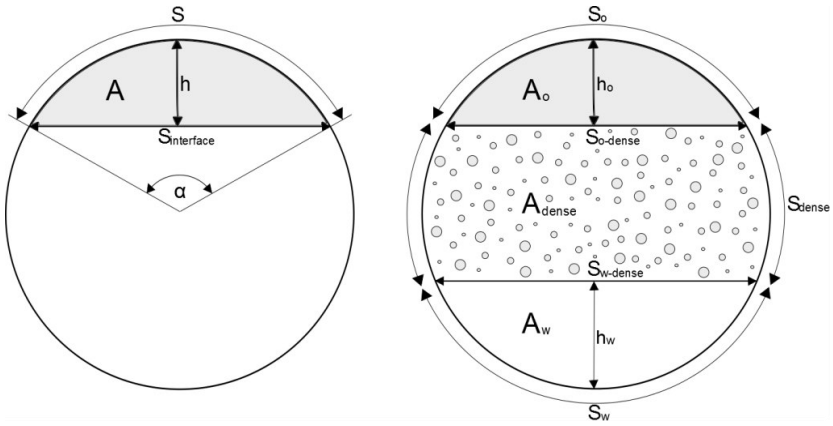

Figure 4.3: Geometry of a segment of a circle (left), Three-layer geometry (right).

The measured local phase fractions showed good agreement with the phase fractions achieved by this method:

$$\varepsilon_w = \frac{A_w + A_{dense}\varepsilon_{w\_dense}}{A} \tag{31}$$

The phase velocities are coupled via U_{dense}:

$$U_w = \frac{Q_w - U_{dense}A_{dense}\varepsilon_{w\_dense}}{A_w} \tag{32}$$

$$U_o = \frac{Q_o - U_{dense}A_{dense}\left(1-\varepsilon_{w\_dense}\right)}{A_o} \tag{33}$$

In order to obtain a unique solution it was further assumed that

$$U_{dense} = \frac{U_o + U_w}{2} \tag{34}$$

In theory U_{dense} can have any value. For oil with a very low viscosity it is even thinkable that U_{dense} exceeds U_o. With equation (34), however, good simulation results were achieved. Also from our experiments it was observed that $U_o \le U_{dense} \le U_w$.

The Reynolds numbers, friction factors and single phase pressure gradients can then be computed as shown for the two-fluid stratified model. The total pressure gradient reads

$$\left(\frac{dp}{dz}\right)_{3layer} = \frac{S_o}{S}\left(\frac{dp}{dz}\right)_o' + \frac{S_{dense}}{S}\left(\frac{dp}{dz}\right)_{dense}' + \frac{S_w}{S}\left(\frac{dp}{dz}\right)_w' \tag{35}$$

Chapter 5

Conclusion

A large number of oil-water pipe flow experiments with inlet mixing have been presented in this work. Results show that the flow development length in this case can be of extensive length. Droplet settling and coalescence were the main mechanisms in this study leading to in-flow separation. The results can be related to real situations in a flow line, were pumps and valves force mixing of the phases or the flow enters the well as dispersion.

This shows the importance of considering the upstream history of the flow. In the presented work dispersed flow was observed at lower mixture velocities compared to non-premixed flow. Formation of a dense packed layer resulted in considerably higher pressure gradients, which would be undesirable in a real system. With further flushing experiments it was demonstrated that flow development can be an issue for other operational situations also.

Better understanding of flow development will help to improve the design of transport processes. Separation design will further benefit from better knowledge about the separator inlet conditions.

Future model improvements should enable to predict flow development and consider upstream conditions of the flow. This work has shown that improvements can be achieved by extending models from 1D to multi-dimensional state including a more detailed resolution of the cross-section.

It can be questioned if many of the experiments reported in the literature can be considered as fully developed. Test sections in laboratory facilities are very restricted in length. In most of the literature prove of the flow development state is missing. This can be an issue especially when used for model tuning and comparison. A better documentation of flow development is

recommended for future studies. In this context longer test sections and different inlet section designs could be alternatives to field measurements. Also, real fluids instead of model fluids should be considered. In real crude oils the presence of surface active components often influences the stability of dispersions and, thus, flow development.

Further achievements in the present work are as follows:

- An FBRM instrument used for in-flow droplet characterization was calibrated against a PVM in-flow particle video microscope. It was also demonstrated that FBRM can be used for flow pattern characterization based on measurements traversing the cross section.
- A Matlab code for automatic droplet identification, sizing and counting from pictures measured by a PVM instrument was written.
- Characteristic cross-sectional droplet size profiles were found for several flow patterns.
- A pressure gradient model for flow patterns involving dense packed layer flow was developed. The model showed good agreement with measurements and enabled to explain the high pressure gradient related to the appearance of the dense packed layer.
- A tool for the prediction of the flow development length downstream of a valve was developed. The tool performs well for low mixture velocities.

Chapter 6

References

Al-Wahaibi, T., Angeli, P., 2008. Droplet size and velocity in dual continuous horizontal oil-water flows. Chemical Engineering Research and Design 86, 83-93. http://dx.doi.org/10.1016/j.cherd.2007.10.012

Angeli, P., 1996. Liquid-liquid dispersed flows in horizontal pipes. Ph.D. Thesis. Imperial College of Science, Technology and Medicine, London

Angeli, P., Hewitt, G.F., 1999. Pressure gradient in horizontal liquid-liquid flows. Int J Multiphas Flow 24, 1183-1203. http://dx.doi.org/10.1016/S0301-9322(98)00006-8

Angeli, P., Hewitt, G.F., 2000a. Drop size distributions in horizontal oil-water dispersed flows. Chemical Engineering Science 55, 3133-3143. http://dx.doi.org/10.1016/S0009-2509(99)00585-0

Angeli, P., Hewitt, G.F., 2000b. Flow structure in horizontal oil-water flow. Int J Multiphas Flow 26, 1117-1140. http://dx.doi.org/10.1016/S0301-9322(99)00081-6

Arirachakaran, S., Oglesby, K.D., Malinowsky, M.S., Shoham, O., Brill, J.P., 1989. An Analysis of Oil/Water Flow Phenomena in Horizontal Pipes. SPE Production Operations Symposium, Oklahoma City. Society of Petroleum Engineers. http://dx.doi.org/10.2118/18836-MS

Bannwart, A.C., 2001. Modeling aspects of oil-water core-annular flows. Journal of Petroleum Science and Engineering 32, 127-143. DOI: 10.1016/S0920-4105(01)00155-3

Biberg, D., 2012. The HD Stratified Flow Model. Design og drift flerfasesystemer for olje og gass, Oslo.

Boxall, J.A., Koh, C.A., Sloan, E.D., Sum, A.K., Wu, D.T., 2010. Measurement and Calibration of Droplet Size Distributions in Water-in-Oil Emulsions by Particle Video Microscope and a Focused Beam Reflectance Method. Industrial & Engineering Chemistry Research 49, 1412-1418. DOI: 10.1021/ie901228e

Brauner, N., 2003. Liquid-Liquid Two-Phase Flow Systems, Modelling and Experimentation in Two-Phase Flow. Springer Vienna, pp. 221-279.

Brinkman, H.C., 1952. The viscosity of concentrated suspensions and solutions. J. Chem. Phys. 20, 571-581. http://dx.doi.org/10.1063/1.1700493

Brooks, B.W., Richmond, H.N., 1994. Phase inversion in non-ionic surfactant-oil-water systems - III. The effect of the oil-phase viscosity on catastrophic inversion and the

relationship between drop sizes present before and after catastrophic inversion. Chemical Engineering Science 49, 1843-1853. doi:10.1016/0009-2509(94)80069-3

Cabellos, E.M., Carvalho, M.S., Ponce, R.V., 2009. Oil-in-water emulsion formation in laminar flow through capillaries. 20th International Congress of Mechanical Engineering, Gramado.

Charles, M.E., Govier, G.W., Hodgson, G.W., 1961. The horizontal pipeline flow of equal density oil-water mixtures. The Canadian Journal of Chemical Engineering 39, 27-36. DOI: 10.1002/cjce.5450390106

Churchill, S.W., 1977. Friction-factor equation spans all fluid-flow regimes. Chemical Engineering 84, 91-92.

El-Hamouz, A.M., Stewart, A.C., 6-9 October 1996. On-line measurement of oil-water dispersion using a Par-Tec M300 laser backscatter instrument. SPE Annual Technical Conference, Denver.

Elseth, G., 2001. An Experimental Study of Oil / Water Flow in Horizontal Pipes. Ph.D. Thesis. Telemark University College, Porsgrunn

Flores, J.G., Chen, X.T., Sarica, C., Brill, J.P., 1999. Characterization of Oil-Water Flow Patterns in Vertical and Deviated Wells. SPE Production & Facilities 14, 94-101. http://dx.doi.org/10.2118/56108-PA

Guzhov, A.I., Grishin, A.D., Medvedev, V.F., Meved-eva, O.P., 1973. Emulsion Formation During the Flow of Two Liquids in a Pipe. Neftianoe Khoziastvo Oil Industry 8, 58-61.

Gwyn, J.E., Crosby, E.J., Jr., W.R.M., 1965. Bias in particle-size analyses by the count method. Ind. Eng. Chem. Fundamen. 4, 204-208.

Hedne, P., Key Technology Challenges - Flow Assurance and Subsea processing. Statoil.

Hinze, J., 1955. Fundamentals of the hydrodynamic mechanism of splitting in dispersion processes. AIChE Journal 1, 289-295. DOI: 10.1002/aic.690010303

Hu, B., Langsholt, M., Liu, L., Andersson, P., Lawrence, C., 2014. Flow structure and phase distribution in stratified and slug flows measured by X-ray tomography. Int J Multiphas Flow 67, 162-179. http://dx.doi.org/10.1016/j.ijmultiphaseflow.2014.06.011

Hu, B., Stewart, C., Hale, C.P., Lawrence, C.J., Hall, A.R.W., Zwiens, H., Hewitt, G.F., 2005. Development of an X-ray computed tomography (CT) system with sparse sources: application to three-phase pipe flow visualization. Experiments in Fluids 39, 667-678. DOI 10.1007/s00348-005-1008-2

Johansen, M., 2006. An experimental study of the bubble propagation velocity in 3-phase slug flow. Ph.D. Thesis. Norwegian University of Science and Technology, Trondheim

Joseph, D.D., Bai, R., Chen, K.P., Renardy, Y.Y., 1997. Core-annular flow. Annual Review of Fluid Mechchanics 29.

Karabelas, A.J., 1978. Droplet size spectra generated in turbulent pipe flow of dilute liquid/liquid dispersions. AIChE Journal 24, 170-180. DOI: 10.1002/aic.690240203

Kokal, S., 2005. Crude-Oil Emulsions: A State-Of-The-Art Review. SPE Production & Facilities 20, 5-13. http://dx.doi.org/10.2118/77497-PA

Kongsberg Oil & Gas Technologies, 2010. LedaFlow - Flow Assurance for 21st Century Oil & Gas Production.

Kumara, W.A.S., Halvorsen, B.M., Melaaen, M.C., 2010. Single-beam gamma densitometry measurements of oil-water flow in horizontal and slightly inclined pipes. Int J Multiphas Flow 36, 467-480. http://dx.doi.org/10.1016/j.ijmultiphaseflow.2010.02.003

Laflin, G.C., Oglesby, K.D., 1976. An experimental study on the effects of flow rate, water fraction and gas-liquid ratio on air-oil-water flow in horizontal pipes. B.Sc. Thesis. The University of Tulsa,

Langsholt, M., 2006. Onset of liquid accumulation in multiphase flow pipelines with low liquid loading, IFE internal report IFE/KR/F-2006/232.

Langsholt, M., Liu, L., 2009. Internal report, Multiphase pipe flow experiments on viscous newtonian and non-newtonian oils and oil-water emulsions. Institute for Energy Technology, Kjeller, Norway.

Lovick, J., 2004. Horizontal, Oil-Water Flows in the Dual Continuous Flow Regime. Ph.D. Thesis. University College London,

Lovick, J., Angeli, P., 2004a. Droplet size and velocity profiles in liquid-liquid horizontal flows. Chemical Engineering Science 59, 3105-3115. DOI:10.1016/j.ces.2004.04.035

Lovick, J., Angeli, P., 2004b. Experimental studies on the dual continuous flow pattern in oil-water flows. Int J Multiphas Flow 30, 139-157. http://dx.doi.org/10.1016/j.ijmultiphaseflow.2003.11.011

Maaß, S., Wollny, S., A.Voigt, Kraume, M., 2011. Experimental comparison of measurement techniques for drop size distributions in liquid/liquid dispersions. Experiments in Fluids 50, 259-269. DOI: 10.1007/s00348-010-0918-9

Mandal, T.K., Chakrabarti, D.P., Das, G., 2007. Oil Water Flow Through Different Diameter Pipes: Similarities and Differences. Chemical Engineering Research and Design 85, 1123-1128. http://dx.doi.org/10.1205/cherd06036

Middleman, S., 1974. Drop Size Distributions Produced by Turbulent Pipe Flow of Immiscible Fluids through a Static Mixer. Ind. Eng. Chem. Process Des. Dev. 13, 78-83. DOI: 10.1021/i260049a015

Mooney, M., 1951. The viscosity of a concentrated suspension of spherical particles. Journal of Colloid Science 6, 162-170. doi:10.1016/0095-8522(51)90036-0

Ngan, K.H., 2011. Phase inversion in dispersed liquid-liquid pipe flow. Ph.D. Thesis. Unviversity College London, London

Nädler, M., Mewes, D., 1997. Flow induced emulsification in the flow of two immiscible liquids in horizontal pipes. Int J Multiphas Flow 23, 55-68. http://dx.doi.org/10.1016/S0301-9322(96)00055-9

Oliemans, R., 2011. Oil-Water Liquid Flow Rate Determined from Measured Pressure Drop and Water Hold-up in Horizontal Pipes. J. of the Braz. Soc. of Mech. Sci. & Eng. 33, 259-264. http://dx.doi.org/10.1590/S1678-58782011000500008

Pal, R., 1987. Emulsions: Pipeline Flow Behaviour, Viscosity Equations and Flow Measurement. PhD Thesis. University of Waterloo, Ontario

Pal, R., 1993. Pipeline Flow of Unstable and Surfactant-Stabilized Emulsions. AIChE Journal 39, 1754-1764. DOI: 10.1002/aic.690391103

Pal, R., Rhodes, E., 1989a. Emulsion Flow in Pipelines. Int J Multiphas Flow 15, 1011 - 1017. DOI: 10.1016/0301-9322(89)90028-1

Pal, R., Rhodes, E., 1989b. Viscosity/Concentration Relationships for Emulsions. Journal of Rheology 33, 1021-1045. http://dx.doi.org/10.1122/1.550044

Plasencia, J., 2013. Experimental study on two phase oil-water dispersed flow. Ph.D. Thesis. Norwegian University of Science and Technology, Trondheim

Plasencia, J., Nydal, O.J., 2010. Influence of the pipe diameter in dispersed oil-water flows. 7th International Conference on Multiphase Flow, Tampa.

Plasencia, J., Pettersen, B., Nydal, O.J., 2013. Pipe flow of water-in-crude oil emulsions: Effective viscosity, inversion point and droplet size distribution. Journal of Petroleum Science and Engineering 101, 35-43. DOI: 10.1016/j.petrol.2012.11.009

Simmons, M.J.H., Azzopardi, B.J., 2001. Drop size distributions in dispersed liquid-liquid pipe flow. Int J Multiphas Flow 27, 843-859. Doi 10.1016/S0301-9322(00)00055-0

Soleimani, A., 1999. Phase distribution and associated phenomena in oil-water flows in horizontal tubes. Ph.D. Thesis. Imperical College Lodon, London

Søntvedt, T., Valle, A., 1994. Capacities of Troll Oil Flow Lines wit High Water Cuts. Predictions based upon Recorded Pipe Flow Friction Factors for Stable Troll Oil Dispersions, Report no. R-068557, Norsk Hydro ASA, Norway.

Taylor, G.I., 1932. The Viscosity of a Fluid Containing Small Drops of Another Fluid. Proceedings of the Royal Society of London. Series A, Containing Papers of a Mathematical and Physical Character, DOI: 10.1098/rspa.1932.0169

Torres-Monzón, C.F., 2006. Modeling of oil-water flow in horizontal and near horizontal pipes. Ph.D. Thesis. The University of Tulsa,

Trallero, J.L., 1995. Oil-Water Flow Patterns in Horizontal Pipes. The University of Tulsa, Tulsa

Trallero, J.L., Sarica, C., Brill, J.P., 1997. A Study of Oil/Water Flow Patterns in Horizontal Pipes. SPE Production & Facilities 12, 165-172. http://dx.doi.org/10.2118/36609-PA

Valle, A., 1998. Multiphase pipeline Flows in hydrocarbon recovery. Multiphase Science and Technology 10, 1-139. DOI: 10.1615/MultScienTechn.v10.i1.10

Valle, A., 2000. Three Phase Gas-Oil-Water Pipe Flow. Ph.D. Thesis. Imperial College of Science, Technology and Medicine, London

van der Zande, M.J., van den Broek, W.M.G.T., 1998. Break-up of oil droplets in the production system. Proceedings of ASME Energy Sources Technology Conference and Exhibition, Housten.

Vay, K., Friess, W., Scheler, S., 2012. Understanding reflection behavior as a key for interpreting complex signals in FBRM monitoring of microparticle preparation processes. International Journal of Pharmaceutics 437, 1-10. http://dx.doi.org/10.1016/j.ijpharm.2012.07.072

Vedapuri, D., Bessette, D., Jepson, W.P., 1997. A segregated flow model to predict water layer thickness in oil-water flows in horizontal and slightly inclined pipelines. 8th International Conference on Multiphase Production, Cannes.

Vielma, J.C., 2006. Rheological behavior of oil-water dispersion flow in horizontal pipes. M.Sc. Thesis. The University of Tulsa,

Ward, J.P., Knudsen, J.G., 1967. Turbulent Flow of Unstable Liquid-Liquid Dispersions: Drop Sizes and Velocity Distributions. AIChE Journal 13, 356-365. DOI: 10.1002/aic.690130229

Wheeler, A.J., Ganji, A.R., 2010. Experimental Uncertainty Analysis, Introduction to Engineering Experimentation, 3rd ed. Pearson, pp. 209-253.

Xu, X.-X., 2007. Study on oil-water two-phase flow in horizontal pipelines. Journal of Petroleum Science and Engineering 59, 43-58. http://dx.doi.org/10.1016/j.petrol.2007.03.002

Zakin, J.L., Pinaire, R., Borgmeyer, M.E., 1979. Transportation of Oils as Oil-in-Water Emulsions. Journal of Fluids Engineering 101. DOI: 10.1115/1.3448717

Chapter 7

Papers

Paper 1

Droplet Size Measurements in Oil–Water Dispersions: A Comparison Study Using FBRM and PVM

Heiner Schümann, Milad Khatibi, Murat Tutkun, Bjørnar H. Pettersen, Zhilin Yang and Ole Jørgen Nydal

Journal of Dispersion Science and Technology, 36:10, 1432-1443,
DOI: 10.1080/01932691.2014.989569

Is not included due to copyright

Paper 2

Experimental study of dispersed oil-water flow in a horizontal pipe with enhanced inlet mixing,
Part 1: Flow patterns, phase distributions and pressure gradients

---

Heiner Schümann, Murat Tutkun, Zhilin Yang and Ole Jørgen Nydal

Submitted to the
Journal of Petroleum Science and Engineering

Experimental study of dispersed oil-water flow in a horizontal pipe with enhanced inlet mixing, Part 1: Flow patterns, phase distributions and pressure gradients

Heiner Schümann[1,2]*, Murat Tutkun[3,4], Zhilin Yang[1,5], Ole Jørgen Nydal[1]

[1]Department of Energy and Process Engineering, Norwegian University of Science and Technology, NTNU, Trondheim, Norway
[2]Multiphase Flow Laboratory, SINTEF Petroleum AS, Trondheim, Norway
[3]Department of Fluid Flow Technology, Institute for Energy Technology, Kjeller, Norway
[4]Department of Mathematics, University of Oslo, Oslo, Norway
[5]Statoil ASA, Research, Development and Innovation, Trondheim, Norway

*Corresponding author, Email: heiner.schumann@ntnu.no

Abstract

The study demonstrates how a disturbance of the flow can affect the pressure gradient and further needs a considerable development length to recover. This is of importance for experimental studies as well as industrial applications. Oil-water experiments were conducted in the Well Flow Loop at the Institute for Energy Technology, Norway. Three different mineral oils (*120 mPa*s*, *60 mPa*s* and *35 mPa*s*) and tap water were used. Input water fractions from *0* to *100%* and mixture velocities up to *1.1 m/s* were tested. A static mixer was installed at the test section inlet to introduce mixing. Comparison with non-premixed data showed that onset of dispersion shifts towards lower mixture velocities when the inlet disturbs the flow. This will also have an impact on the pressure gradient. At low mixture velocities when the flow was semi-dispersed, the influence seems to be most serious. Formation of a dense packed droplet layer is assumed to be a major reason for an increasing pressure gradient. Comparing pressure gradient measurements along the pipe it was found that the development length of the flow was still not reached 200 diameters downstream of the inlet mixer.

1. Introduction

Simultaneous transport of oil and water is common practice in petroleum production systems. Initially stratified flow at sufficiently high flow rate can cause instabilities in the oil-water interface leading to droplet formation and transition to flow dispersion. In a production line, however, an emulsion forms already in the reservoir and disturbances due to processing units such as valves and pumps sustain the dispersion process (Cabellos et al., 2009).

Most experimental work, which can be found in the literature, takes separated flow as a starting point were oil and water are merged using Y- or T-manifolds or something similar (Elseth, 2001; Lovick and Angeli, 2004; Nädler and Mewes, 1997; Plasencia and Nydal, 2010; Trallero et al., 1997). Such inlet devices are expected to not considerably contribute to, or force, the dispersion process. Inlet devices are not standardized.

One might hypothesize that the flow becomes independent of the inlet device sufficiently far downstream of the pipe inlet. Unfortunately the flow development is not documented well in many experimental studies. Nädler and Mewes (1997) and Karabelas (1978) assume developed flow after approximately *600* inner pipe diameter (*D*), based on pressure gradient and droplet size measurements respectively. This is considerably longer than most of the reported data which are taken in shorter test sections. Depending on the situation, the development length might be even longer than *600 D*. Therefore, the history of the flow is crucial and the effect of inlet conditions has to be considered. Inlet history effects were found by for instance Angeli (1996), Ngan (2011), Soleimani (1999) and Mandal et al. (2007). In their studies both flow patterns and pressure gradients were influenced by the inlet.

The main objective of this work is to demonstrate the influence of the inlet device on oil-water flow in multiphase laboratories. This was tested by installing a static mixer at the inlet of the test section. Flow patterns, local phase distributions and pressure gradients were then measured for a range of mixture velocities, U_{mix}, and input water fractions, f_w, and compared with data with comparable experimental conditions but without inlet mixer. Three pressure measurements along the test section help to make a statement on the development of the flow.

Particular focus of this paper should be on a peak in the pressure gradient curve when plotted versus the input water fraction which was observed in several previous studies in the case of semi-dispersed flow (Angeli, 1996; Elseth, 2001; Kumara et al., 2009; Nädler and Mewes, 1997). The authors assumed a partial inversion from oil to water continuous flow in the upper part of the pipe to be the reason for this sudden increase of the pressure gradient, typically occurring for input water fractions $f_w > 0.3$. Such a behavior was also found in our laboratory. We were surprised as a smooth pressure gradient curve was expected for low mixture velocities. The question arose if this jump was caused by flow mixing created in the inlet.

In this study a static mixer was chosen as inlet device as it has a fixed geometry as most manifolds used in experimental studies. The flow disturbance is therewith dependent on the mixture velocity. At the same time the mixer will create a strong inlet mixing effect which is easy to identify.

The study focuses on laboratory conditions and does not try to achieve most realistic field conditions. Therefore a straight horizontal test section and tap water instead of brine were chosen which simplifies the requirements to the infrastructure. This choice also enables to compare the results with previous work by Trallero et al. (1997), Angeli (1996) and Nädler and Mewes (1997) who had similar test conditions.

Trallero et al. (1997) experimentally studied oil-water flow pattern transition, local phase fraction and pressure drop in a *15.54 m* long, *5 cm* inner diameter horizontal pipe. An oil-water system, similar to the one used in this study, with a viscosity ratio of $\mu_o / \mu_w = 29.6$ and density ratio of $\rho_o / \rho_w = 0.85$ was tested. A flow pattern classification with six flow patterns, namely segregated flow (stratified flow without and with mixing at the interface, ST and ST&MI), water dominated dispersed flow (dispersion of oil-in-water and water, Do/w&w, and oil-in-water emulsion, o/w) and oil dominated dispersed flow (dispersion of water-in-oil and oil-in-water, Dw/o, Do/w, and water-in-oil emulsion, w/o), was proposed.

Experiments with and without inlet mixing were documented by Angeli (1996). A low viscosity oil was used in her experiments ($\mu = 1.6$ *mPa*s*), and the pipe inner diameter was rather small ($D = 24$ *mm*). The difference in the pressure gradient between the two cases was significant.

The results by Nädler and Mewes (1997) are of interest for comparison because the entrance nozzle was specially designed to prevent the formation of emulsion and the test section length ($L = 48$ *m*, $D = 59$ *mm*) was long enough to reach fully developed flow.

2. Experimental details

2.1 Well Flow Loop

The experiments were performed in the Well Flow Loop of the Institute for Energy Technology (IFE) in Kjeller, Norway. The closed flow loop has a *25 m* long test section with an inner diameter of $D = 100$ *mm*. The pipe sections are made of transparent PVC. From a gravity oil-water separator in the basement of the building the liquids are pumped separately before mixed at the test section inlet. Centrifugal pumps are used to circulate the liquids. At the end of the test section, the liquids enter a pre-separator before returning to the main oil-water separator. A manual choke valve at the bottom of the pre-separator is used to control the liquid level in the vessel. In this way, backflow of gas in the test section can be prevented. The temperature of the liquids are monitored and regulated by a heat exchanger system. The system can be pressurized up to *10 bar(g)*.

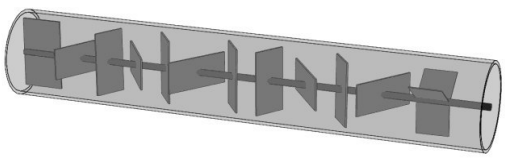

Figure 1: Static mixer at the test section inlet. The flow direction is from left to right.

A detailed sketch of the test section is shown by Figure 2. The test section was horizontally aligned at $0 \pm 0.1°$. A simple static mixer was installed at the test section inlet, as seen in Figure 1. Crosswise baffles enhanced mixing and promoted an early transition to dispersed flow. The transparent pipe allowed for visual observation of the flow. Video recordings at

approximately *20 m* downstream of the inlet were taken. Differential pressure cells were used to measure the pressure drop over three different sections. A broad beam gamma densitometer, measuring the local phase fractions, was installed *18.88 m* downstream of the inlet. Phase fraction and pressure measurements were averaged over a sampling time of *15 sec*. Further shown in Figure 2 are three traversable FBRM probes (focused beam reflection measurement). These probes were used for in-situ droplet characterization. In order to not disturb the flow, the probes, however, were extracted when measurements, presented in this paper, were performed. FBRM results are presented by another study (Schümann et al.).

2.2 Liquid properties

To investigate the effect of the viscosity on the measured parameters we used three different mineral oil mixtures with different viscosities. All oils were mixtures of Exxsol D80 (μ *= 1.7 mPa*s*) and Primol 352 (μ *= 165 mPa*s)* and mainly varied in the viscosity. The liquids were mixed by circulating in the flow loop for several hours until property readings were constant as demonstrated in Table 1. Viscosity measurements were completed using an Anton Paar – Physica MCR 301 rheometer. Sample oil was extracted directly from the separator before and after the experiments. The viscosity measurements showed Newtonian behavior. During the experiments the oil density was continuously monitored by Coriolis flow meters. Interfacial tension measurements between water and oil were done with a CAM 200 (KSV Instruments Ltd., Finland) using the pendant drop method.

Table 1: Properties of the tested mineral oil mixtures.

Oil	Composition Primol 352/ Exxsol D80	Density [kg/m^3] (measured at 20°C)	Viscosity [mPa*s] (measured at 20°C)	Interfacial tension with tap water [mN/m] (short/long term)
Oil A	25:1	866 (±0.2%)	120 (±3%)	23/14 (±10%)
Oil B	6:1	859 (±0.2%)	60 (±2%)	23/14 (±10%)
Oil C	4:1	853 (±0.2%)	35 (±2%)	24/15 (±10%)

The temperature of the Well Flow Loop was constantly controlled during the experiments and kept at *20°C* with an accuracy of *±0.5°C*. Arising viscosity changes are considered in the uncertainties given in Table 1.

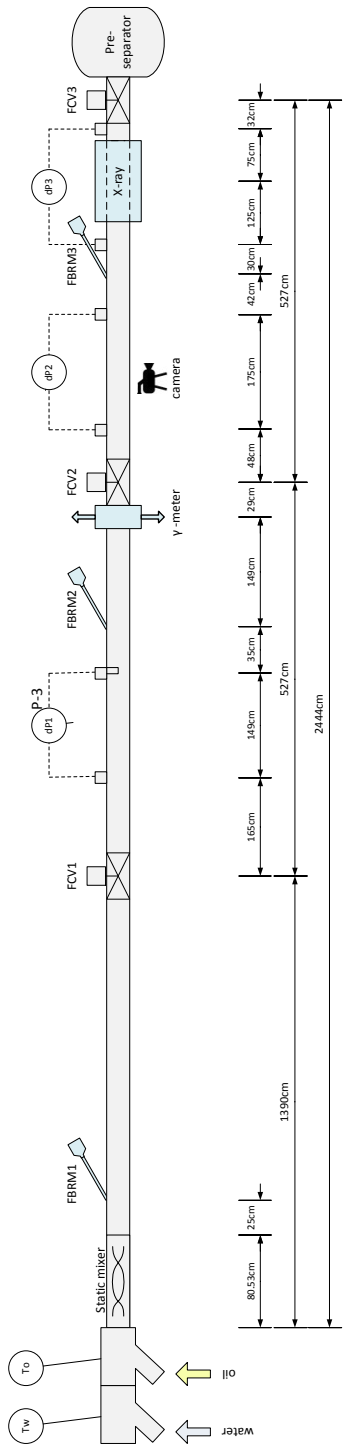

Figure 2: Test section.

2.3 Measurement techniques

An electromagnetic flow meter was used to measure the water flow rate. The oil flow rate, however, was measured by Coriolis flow meters. The Coriolis flow meter simultaneously measured the density of the oil as well. When the flow rate is high the retention time of the liquids in the separator could be shorter than the time needed for complete liquid separation. In particular cases we observed that the pumps started to pump an emulsion at high flow rates ($U_{mix} \geq 0.5$ *m/s*). In such cases the permanent monitoring of the density was helpful to identify the water content in the oil. When the water content was distinctively increasing or higher than *2%*, the experiment was stopped. The final input water fraction, f_w, computed from the flow rate measurements, was corrected for the water content in the oil.

Three differential pressure transducers by Fuji Electric (model: FKKW12V1-AKCYY-AE) were positioned along the test section as shown in Figure 2. The *3 mm* diameter pressure tap holes were located at the bottom of the pipe. The impulse pipes from the pressure taps to the DP-cells were filled with water. Before every experiment the impulse pipes and pressure cells were flushed with water to replace possible oil entrainments. The zero point was set at no-flow conditions.

A broad beam gamma densitometer was installed 18.88 m downstream of the test section inlet. It was able to measure 3-phase gas-oil-water flow. In our setup the instrument was used in a 2-phase mode and calibrated once a day. A single value for the overall phase fractions of the scanned cross section was measured.

In addition an X-ray tomography system, that provided more detailed phase fraction data, was installed at the end of the test section, *23 m* from the inlet. With two sources and two detectors in horizontal and vertical alignment respectively, the X-ray tomography system is able to scan the complete cross section of the pipe. The detector-cameras give a resolution better than *1 mm* per pixel. In order to reduce noise groups of neighboring pixels were averaged. The final resolution was *2 mm/pixel*. A sampling frequency of *40 Hz* and sampling times between *10* and *25 sec* were chosen for the experiments. More details on the system can be found in Hu et al. (2014).

Flow patterns were primarily based on visual observations approximately *20 m* (*L/D = 200)* downstream of the mixer. While stratified flow was easy to identify visually the flow became more and more opaque with increasing amount of dispersion. In these cases observations were supplemented by other measurement techniques. Cross sectional reconstructions by the x-ray instrument were useful to investigate the phase distribution inside the pipe. Especially regions free of dispersion could be identified in this way. In fully dispersed flow pressure gradient measurements indicated flow inversion and therewith helped to identify the type of continuity. As described in more detail below, the pressure gradient reaches its maximum at phase inversion which occurs at a specific input water fraction. Water fractions required for phase inversion were found to be in the range between 18% and 30% for the tested oils. Dual continuous flow, where a region of water-in-oil and a region of oil-in-water are present simultaneously could be well identified by a different shading of these regions. The oil-in-water region was typically the darker one.

A major problem was the identification of the type of dispersion in semi dispersed flows for intermediate flow rates. For such flow single droplets were identifiable visually; a distinct interface between an oil and a water continuous region within the dispersion layer, however, as it was the case for dual continuous flow, was only present for the lowest input water fractions and less clear. For higher input water fractions, $f_w > 0.3$, no such a line was observed. We believe that for input water fractions larger than $f_w \approx 0.3$ the dispersion was of type oil-in-water only while for lower input water fractions both types were present. However, in order to not to confuse with speculations we will not further specify the type of dispersion when it was not clear.

2.4 Measurement uncertainties

Uncertainty estimates for pressure gradient and phase fraction measurements following a common root of the sum of the squares method are difficult to perform due to several elemental errors which cannot be tested separately. Uncertainty estimates given here are based on experience and are in good agreement with uncertainties from a simple upper-lower bound method for independent repeatability experiments covering both, single phase and two phase flow. Differences between measurements of equivalent experiments were all within the estimates. All uncertainties are given as absolute uncertainties.

The uncertainty of the pressure measurements is in general much higher than the accuracy of the pressure transducers (*<0.1%*). Typical error sources are drops blocking the impulse pipes, vibrations of the test rig, flow disturbances or an imperfect pressure tap geometry. An upper limit estimate for the uncertainty of two-phase measurements is given by *max(±7.5%, ±10 Pa/m)*. Also, single phase measurements were compared with theoretical values showing good agreement.

The uncertainty for oil and water phase fraction measurements was *±0.035* using the gamma densitometer.

For X-ray tomography measurements it is more difficult to give an uncertainty estimate. The upper-lower bound method was not applied for this instrument. Comparing the total local phase fractions measured by the gamma densitometer with the x-ray system reveals an agreement more than *93%* between these two instruments. Also, we noticed a difference in the total phase fractions when data from the horizontal and vertical collimators of the x-ray system were compared. Cross sectional information provided by the x-ray system have a high spatial resolution; therefore it gives important qualitative insight into the flow behavior, even though the total phase fraction readings from the broad beam gamma densitometer provide the most accurate data.

3. Test matrix

Mixture velocities up to $U_{mix} = 1.1$ *m/s* and input water fractions, f_w, varying from *0 – 100 %* (with increments of *10%*) were tested. The mixture velocity was limited by the pumps. Video recordings, pressure drop and local phase fraction measurements were performed for all test cases. We repeated the same test matrix for each oil mixture. A summary is listed in Table 2.

Table 2: Test matrix.

Property	Tested range
Oil viscosity, μ:	35, 60 and 120 mPa*s
U_{mix}:	0.1 – 1.1 m/s
f_w:	0 – 100%

4. Results

4.1 Flow pattern observations

The flow patterns found in this study are in good agreement with flow patterns proposed by Trallero et al. (1997). We chose, however, a further division to better understand the changes in the flow. Figure 3 gives an overview of the observed flow patterns.

Flow pattern maps for oil A, B and C are shown in Figure 4, Figure 5 and Figure 6 respectively. At the lowest mixture velocities the flow was stratified (o&w). Single droplets at the interface could occur. Increasing the mixture velocity resulted in a larger number of droplets. The droplets were still located close to the interface forming a dense packed layer. Turbulence was not strong enough to keep droplets spread over the pipe cross section. A flow pattern sometimes referred to as three-layer pattern, 3L (oil – dispersion – water) occurred (Angeli, 1996; Brauner, 2003; Mandal et al., 2007). The transition criterion from stratified to semi-dispersed flow was a closed droplet layer along the interface. At even higher mixture velocities the droplet layer continued to grow and single droplets were also distributed further away from the interface.

For higher inlet water fractions oil was completely dispersed and the continuous oil phase disappeared. Depending on the mixture velocity, oil droplets were mainly distributed in the upper part (Do/w&w) or spread over the whole pipe cross section for the highest mixture velocities (Do/w). The criterion for the Do/w pattern was based on x-ray measurements showing dispersion present in the whole cross section. In general, as the mixture velocity increases turbulence gains importance compared to the gravitational force. This, in turn, leads to a more uniform distribution of droplets over the cross section. In our case, i.e., premixed flow, this means that turbulence keeps the flow in a dispersed state over a long distance downstream of the mixer. Separation of the phases due to gravitational settling and coalescence is slowed down as the mixture velocity increases.

On the other hand, when the inlet water fraction was low, the free water layer at the bottom of the pipe disappeared. The flow pattern was oil and dispersion (o&D). We observed a stream of fast moving dispersion at the bottom of the pipe and single slower moving droplets in the region above. This could indicate that the dispersion was divided into an oil continuous region and the fast moving water continuous region below. Again, for the highest mixture velocities the phases were not able to separate and the flow was fully dispersed, but this time of the type oil continuous flow (Dw/o).

In fully dispersed state the flow can suddenly transform from oil-in-water to a water-in-oil dispersion and opposite when a certain input water fraction is reached. This is also known as phase inversion and happened for oil A and B when the input water fraction was changed from one to the next measurement point keeping U_{mix} constant. The input water fraction at phase inversion was approximately $f_w = 0.18$ for oil A and approximately $f_w = 0.28$ for oil B. According to Arirachakaran et al. (1989) the input water fraction at phase inversion decreases with increasing oil viscosity. This is in agreement with our results.

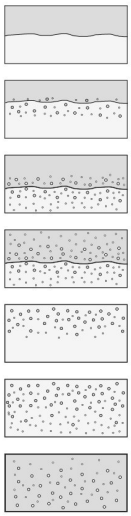

o&w - Stratified flow, single droplets at the interface can occur.

3L (o&D&w) - Three-layer flow: Pure oil and dispersion with a bottom-layer of pure water.

o&D - Oil on top and dispersion in the lower part of the pipe.

Dw/o&Do/w - Dual continuous flow: Water dispersed in oil and oil dispersed in water.

Do/w&w - Dispersed oil in water with a bottom-layer of pure water.

Do/w - Dispersed oil in water.

Dw/o - Dispersed water in oil.

Figure 3: Observed flow patterns.

Phase inversion goes along with a sudden increase of the pressure gradient and was visually observable in the transparent test section. Depending on the initially continuous phase, phase inversion happened in different ways. When the initial flow pattern was Dw/o, we observed a continuous build-up of a Do/w layer (dark shading) from the bottom of the pipe until the complete flow was inverted. The dual-continuous flow pattern was present during the inversion period. On the other side, when the initial flow pattern was Do/w, the flow seemed to collapse and the phases alternately occupied the pipe (fast alternating dark/bright shading), which was described as intermittent flow by Arirachakaran et al. (1989). After a while the Dw/o pattern stabilized. Phase inversion did not occur for oil C. A stable region of dual continuous flow (Dw/o&Do/w) divided the regions of Dw/o and Do/w.

The proposed flow pattern boundaries assembled using the data shown in figures Figure 4, Figure 5 and Figure 6 for oil A, B and C respectively are plotted together in Figure 7. The boundaries move towards higher input water fractions for lower oil viscosities, similar to the input water fractions needed for phase inversion. This can be due to a partly inversion of the dispersed layer also occurring at higher input water fractions. Furthermore, for oil B and C fully dispersed flow of oil-in-water, Do/w, was observed at slightly lower mixture velocities as for oil A. A possible explanation can be found in the work of van der Zande and van den Broek (1998) who measured oil droplets in water in turbulent pipe flow and flow through an orifice. This was attributed to the fact that the viscous oil results in larger energy dissipation during droplet deformation, which leaves less energy for the break-up process, hence the increase of interfacial area of the drops is reduced. Droplets remain large. In our experiments, larger droplets produced in the inlet mixer led to a faster separation of the flow.

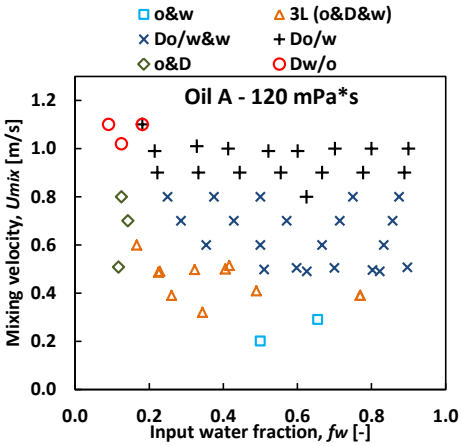

Figure 4: Observed flow pattern map for Oil A - 120 mPa*s.

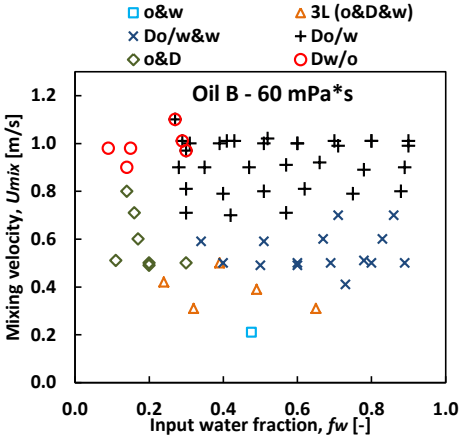

Figure 5: Observed flow pattern map for Oil B - 60 mPa*s.

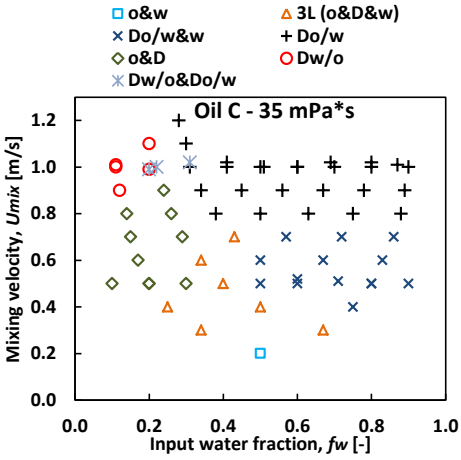

Figure 6: Observed flow pattern map for Oil C - 35 mPa*s.

In general, the minimum mixture velocity needed for the emergence of fully dispersed flow was slightly higher for the oil continuous flow compared to water continuous flow. An even stronger difference was found by Guzhov et al. (1973).

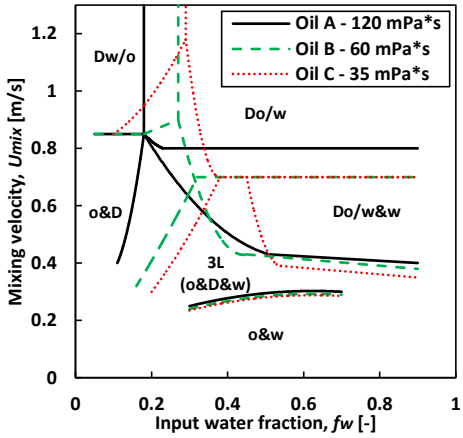

Figure 7: Comparison of observed flow pattern boundaries.

The succession of the observed flow patterns is in good agreement with the flow patterns reported by Trallero et al. (1997) who tested a similar oil-water system. Some discrepancy was found at the boundaries between individual flow patterns. The main difference is the boundary of the stratified region and dispersed flow that appeared at lower mixture velocities in our study. This can be attributed to two main reasons as we compare the experimental conditions: First, the larger pipe diameter in the presented work will lead to larger Reynolds numbers at equal superficial velocities. Second, the inlet static mixer promotes dispersion even at lower flow rates. As mentioned earlier. The inlet used in the present work differed from the simple Y-junction, which was used by Trallero et al. (1997) to mix the phases. Similar, Angeli (1996) documented that the use of an in-line mixer results in dispersed flow patterns at much lower mixture velocities compared to the same setup without.

Another reason which might be causing the difference between the current work and Trallero et al. (1997) is the interfacial tension. As can be seen in Table 1 the interfacial tension in our work is about *24 mN/m* whereas Trallero et al. reported a value of *36 mN/m*, which is *50%* higher than for our oil.

4.2 Local water fractions

Total local water fractions, measured using the broad beam gamma densitometer, are shown in Figure 8. When U_{mix} = *1 m/s*, the flow was fully dispersed, and resulting local water fractions are in good agreement with the input water fractions for both oil and water continuous flow. In contrast, at U_{mix} = *0.5 m/s*, the flow was partly dispersed and local water fractions are below the corresponding input water fractions. Especially for input water fractions larger than *0.4* the oil accumulated distinctively. From f_w = *0.4* to *0.5* a flow pattern transition was observed. At low input water fraction oil was wetting the upper wall of the pipe. At approximately f_w = *0.4* a partial inversion (Kumara et al., 2009) of this layer, thus complete dispersion of the oil occurred. At higher input water

fractions the flow pattern was a dense packed layer of oil droplets in water on top of a free water layer, Do/w&w. The dispersed oil-in-water layer visually moved considerably slower than the free water, which explains the higher oil accumulation for input water fractions larger than *0.4.*

The measurements were similar for the three tested mineral oils. No significant influence of the viscosity on the total local water fractions was found.

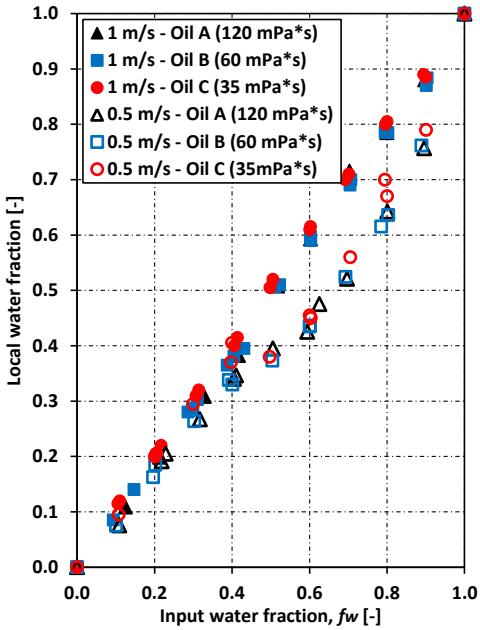

Figure 8: Local water fraction versus input water fraction, f_w, for different mixture velocities.

X-ray data was summarized in line fraction measurements giving the local phase fraction within the pipe (bottom-to-top). Such measurements are shown for oil C (*35 mPa*s*) and the mixture velocities U_{mix} = 1 m/s and U_{mix} = 0.5 m/s in Figure 9 and Figure 10 respectively. Tomographic reconstructions of the total cross sections showing the spatial distribution of the phases are presented in Figure 11 for characteristic cases.

For fully dispersed oil continuous flow (U_{mix} = 1 m/s, f_w = *0.11* and f_w = *0.20*) water droplets are rather uniformly distributed over the cross section. In water continuous flow, f_w > *0.31*, the amount of dispersed oil is continuously increasing towards the top of the pipe. This indicates a faster separation behavior downstream of the inlet mixer when the flow is water continuous. In oil continuous flow the viscosity of the oil will slow down this process. For f_w = *0.31* the line fraction curve shows a bend in the lower part of the pipe section. This could indicate the interface between the water and oil continuous layer in a dual continuous flow pattern.

For U_{mix} = 0.5 m/s, regions of water, oil and dispersed flow can be clearly distinguished using both the line fraction and cross sectional measurements. In agreement with the visual observations, a pure oil layer was only found for input water fractions of f_w = *0.4* and below. At f_w = *0.5*, the line fraction measurements show a dispersed layer of relatively constant water fraction in the upper part of the pipe. This supports the assumption of partial inversion in this region forming a dense packed dispersion layer.

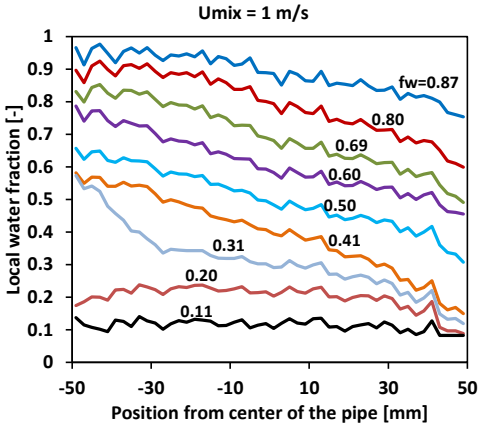

Figure 9: Water line fraction measurements for Oil C (35 mPa*s) at U_{mix} = *1m/s*. The input water fractions, f_w, are shown in the figure.

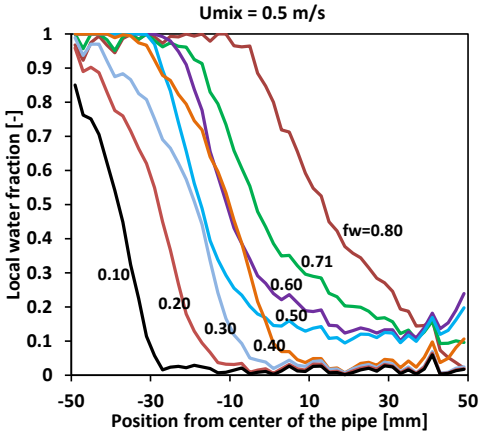

Figure 10: Water line fraction measurements for Oil C (35 mPa*s) at U_{mix} = *0.5m/s*. The input water fractions, f_w, are shown in the figure.

.

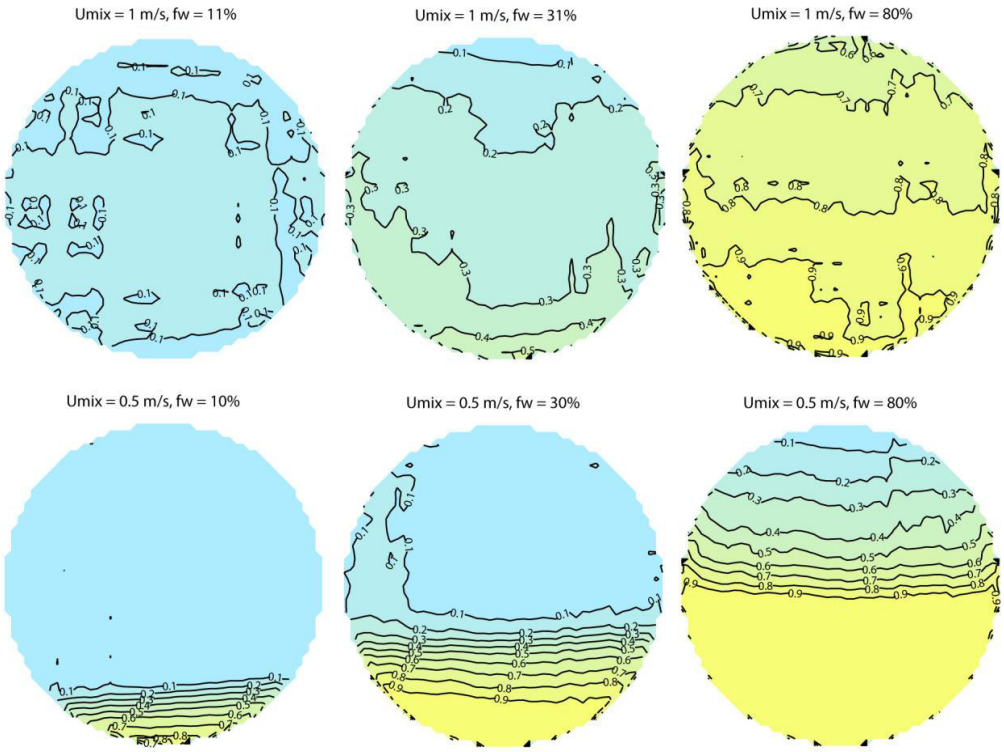

Figure 11: Tomographic reconstruction of the cross sectional water distribution for oil C (35 mPa*s). Contour lines show the local water fraction in steps of 0.1.

From the cross sectional plot, Figure 11 (U_{mix} *= 0.5 m/s*, f_w *= 80%*), we find a region in the upper part of the dense packed droplet layer where the local water fraction falls below that at phase inversion. We tried to better identify the type of dispersion by suddenly stopping the flow, using fast closing valves, and observing the stagnant separation behavior. Droplets started to arrange by size developing a gradient in droplet size with the largest droplets on top. From visual observations of the flow and the separation behavior we got the impression of the dispersion being of type oil droplets in water.

Also droplet deformation was observed in this dense packed layer which would allow for closer packing. The pipe wall blocks further upward movement. As explained in Merchuk et al. (1998) droplets in this situation queue up and wait for coalescence to take place

4.3 Oil-water pressure drop

Figure 12 shows pressure gradients for U_{mix} *= 1 m/s* and U_{mix} *= 0.5 m/s* measured using the second pressure transducer at *200 D* downstream of the inlet.

At U_{mix} *= 1 m/s* the pressure gradient increases toward a peak in the phase inversion region, which is well documented in the literature (Angeli and Hewitt, 1999; Arirachakaran et al., 1989; Nädler and Mewes, 1997; Pal, 1993). As mentioned earlier, oil C does not show a direct phase inversion. Instead, the flow crosses a dual-continuous flow region, Dw/o&Do/w. Also in this case a peak is shown.

Comparing the different oils, we found that the pressure gradient for oil-continuous flow increases with increasing oil viscosity. In contrast, the water-continuous flow does not show a dependency on the oil viscosity. This is in agreement with measurements by Arirachakaran et al. (1989).

Lovick and Angeli (2004) reported a drag reduction effect for both oil and water continuous flow. This was attributed to dynamic coalescence and breakup processes reducing turbulence in unstable dispersions as explained by Pal (1993). According to our results it, however, is clear that a higher dispersed phase concentration increased the pressure drop. Only for oil C, the lowest viscosity case, a drag reduction effect was found when the flow is oil continuous. Single phase flow of oil C at Umix = 1m/s provides a Reynolds number of Re= 2429. This indicates that the flow is in a transitional regime which can be sensitive to drag reduction effects.

The viscosity dependency of the pressure gradient shows a similar behavior for U_{mix} *= 0.5 m/s*. For input water fractions less than *0.4* when an oil continuous layer was present, the flow was sensitive to the oil viscosity. Here a drag reduction was found when a higher water fraction increased the water wetted perimeter. This effect was stronger for higher oil viscosities.

The flow pattern transition to Do/w&w between f_w *= 0.4* and f_w *= 0.5* goes along with a sudden increase in the pressure gradient as the oil continuous layer disappears. The dense packed layer forming in the upper region of the pipe seems to have a higher effective viscosity than that of the pure oil, which causes the peak. With a further increase in f_w the

observed dense packed droplet layer becomes thinner and, in turn, the pressure gradient decreases. Again, no significant influence of the oil viscosity was found, which would be expected assuming that oil was completely dispersed. A peak at partial inversion was documented in the literature for both non-premixed flow (Angeli, 1996; Elseth, 2001; Kumara et al., 2009; Nädler and Mewes, 1997), and premixed flow (Angeli, 1996). The increase in the pressure gradient from $f_w = 0.4$ to $f_w = 0.5$ is in accordance with the oil accumulation found in section 4.3.

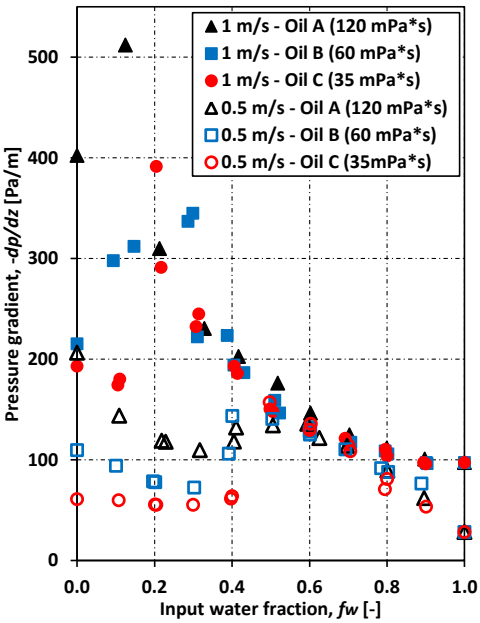

Figure 12: Pressure gradient versus input water fraction, f_w.

Interestingly, for $0.5 < f_w < 0.8$ the pressure gradient reached similar values for $U_{mix} = 0.5$ *m/s* as for $U_{mix} = 1$ *m/s*. At $U_{mix} = 1$ *m/s*, inlet mixing creates a relatively homogeneous droplet distribution over the cross section which prevails downstream the pipe. At $U_{mix} = 0.5$ *m/s*, the weak dynamics of the flow allow fast droplet settling and form the dense packed droplet layer with a very high effective viscosity, probably exceeding this of homogenous flow strongly. This is an interesting result as the practical meaning would be a larger amount of transported liquid without increasing the pumping power in this case. The same result was found when further mixture velocities were considered (Figure 13). The reason behind this observation is not entirely clear. Further experiments with different inlet mixing rates would be necessary to understand if the coinciding lines are characteristic for inlet mixing or just coincidence. However, from Figure 13 we can further investigate that the partial inversion and thus the peak in the pressure gradient moves towards lower input water fractions for higher U_{mix}.

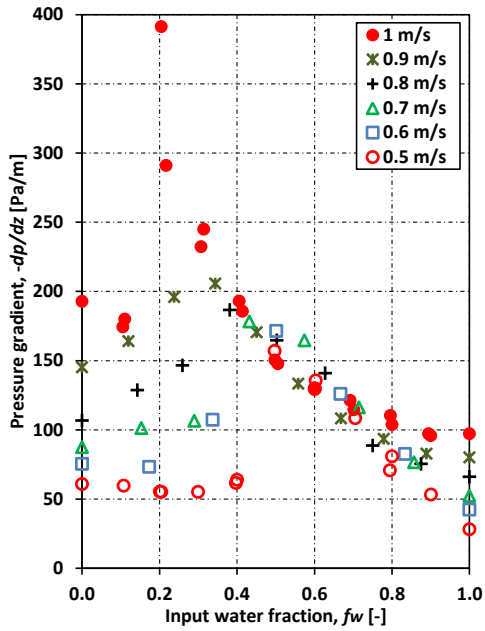

Figure 13: Pressure gradient versus input water fraction, f_w, for oil C and different U_{mix}.

5. Comparison with non-premixed data

Results for oil B (*60 mPa*s*) were compared with experimental data (*69 mPa*s*) from a previous measurement campaign conducted at the same facility, but without the static mixer installed at the inlet. Both oils are mixtures of the same base oils. The viscosities differ to some degree which introduces an uncertainty in the comparison. However, we will allow for a qualitative comparison of the data, as we have shown before that the influence of the viscosity is limited and the relative viscosity difference is small. Similar to the presented experiments, also in the previous measurement campaign different oil viscosities, covering a range from *69* to *153 mPa*s* were tested. Again, measurements repeated for different oil viscosities were collapsing when oil was dispersed (e.g. Do/w and Do/w&w). Differences due to viscosity were only observed when oil formed a continuous layer, but were small compared to differences when the flow pattern was changed as a result of inlet mixing, which will be shown below.

Line fraction measurements for the non-premixed experiments at $U_{mix} = 1$ *m/s* and *0.5 m/s* are shown in Figure 14 and Figure 16. Pressure gradient measurements for both cases are compared in Figure 15 and Figure 17.

From Figure 14 we observe that for measurements of $f_w > 0.3$ the local water fraction shows a steep gradient from pure water at the bottom of the pipe to an approximately constant low value in the upper part of the pipe, which is significant for a dense packed dispersion. The flow pattern is Do/w&w. Premixed flow at $U_{mix} = 1$*m/s* was more homogeneous with a weak gradient in the water line fraction. Comparing the pressure gradient measurements (Figure 15), with inlet mixer the more homogeneous dispersion resulted in lower pressure gradients when the flow was water continuous. It was further found that phase inversion, identified by a peak in the pressure gradient, takes place at slightly higher input water

fractions when a mixer was installed. Alteration of the phase inversion point as result of inlet mixing was also found by Soleimani (1999).

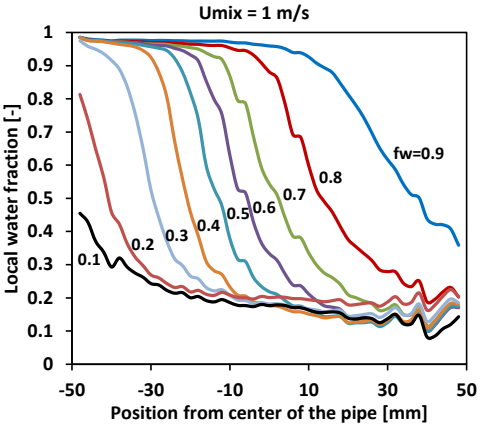

Figure 14: Water line fraction measurements at U_{mix} = *1m/s* without inlet mixing (69 mPa*s). The input water fractions, f_w, are shown in the figure.

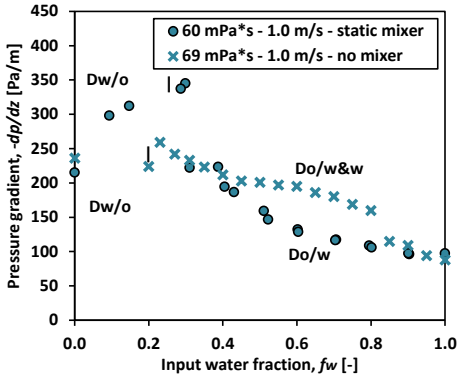

Figure 15: Comparison of pressure gradient measurements with and without inlet mixing at U_{mix} = *1 m/s*. The X-axis shows the input water fraction, f_w.

At U_{mix} = *0.5 m/s* the same flow patterns were found with and without mixer. As before, the line fraction gradient is steeper for the non-premixed case. This indicates a thin dispersion layer in the 3L flow pattern. Also the input water fraction required for flow pattern transition (partial phase inversion) was different. For input water fractions smaller than *0.4* the pressure gradient is almost identical. At f_w = *0.4* the 3L flow pattern (oil-dispersion-water) changes to Do/w&w in the premixed case and the pressure gradient rises dramatically. This transition happens at much higher input water fraction, f_w = *0.8* without the inlet mixer. Also in this case, the partial inversion goes along with a jump in the pressure gradient, but less dramatic as with the mixer.

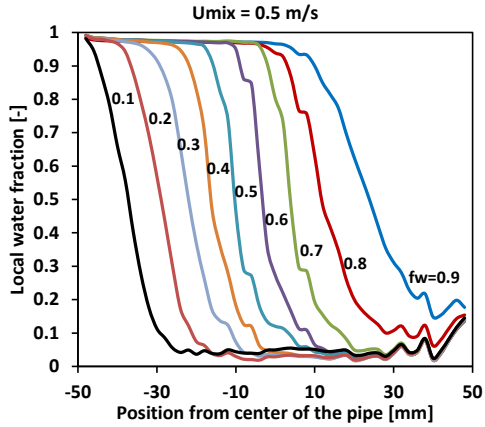

Figure 16: Water line fraction measurements at U_{mix} = *0.5m/s* without inlet mixing (69 mPa*s). The input water fractions, f_w, are shown in the figure.

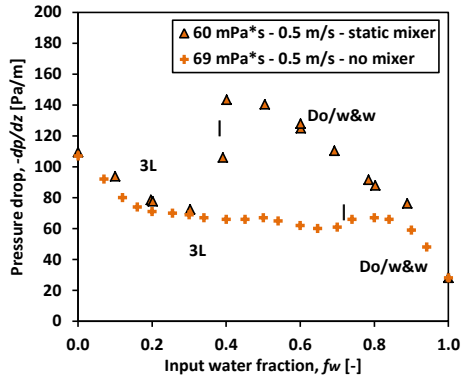

Figure 17: Comparison of pressure gradient measurements with and without inlet mixing at U_{mix} = *0.5 m/s*. The X-axis shows the input water fraction, f_w.

Our measurements agree with findings of Soleimani (1999), who measured a substantial pressure increase for water dominated flow, while the measurements for oil dominated flow stayed constant when a mixer was used.

Similar results were found when pressure gradient data with and without inlet mixing of Angeli (1996) were plotted together in Figure 18. The mixer used was a STATIFLOW in-line static mixer. The data shows that the effect of inlet mixing also applies when low viscosity oil is used.

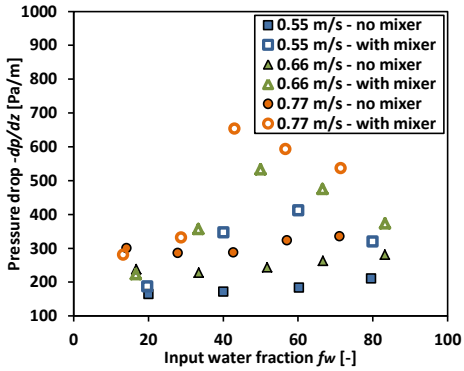

Figure 18: Comparison of pressure gradient measurements with and without inlet mixing. The X-axis shows the input water fraction, f_w. Data extracted from (Angeli, 1996). $\mu = 1.6$ mPa*s, ID = 24 mm.

6. Flow development

Flow development along the pipe was found by comparing pressure gradient measurements at three different positions. Figure 19 displays these measurements for oil B (*60 mPa*s*) at $U_{mix} = 1$ *m/s*. The trend is not clear in the case of oil continuous flow ($f_w < 0.29$.) The local pressure gradient increases from the first to the second pressure transducer and decreases from the second to the third pressure transducer. For water continuous flow the pressure gradient was gradually decreasing further downstream the pipe. This trend is clear, even considering the measurement uncertainty, *max(±7.5%, ±10 Pa/m)*. Trends were similar for oil A and C (not shown). Also for $U_{mix} = 0.5$ *m/s* the trend was decreasing for the major part of the cases.

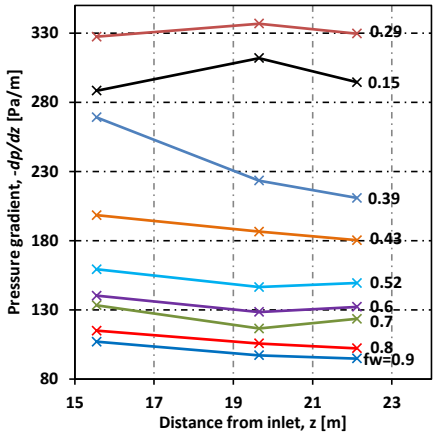

Figure 19: Pressure gradient along the pipe for oil B (60 mPa*s) at $U_{mix} = 1$ m/s. Different lines represent different input water fractions, f_w.

The development length of the flow will depend on the velocity and initial mixing. In premixed flow three main mechanisms, namely turbulence decay, droplet settling and droplet coalescence will be important where coalescence most likely has the longest time scale. Especially in water continuous flow the low viscosity of the water is not expected to restrict droplet settling considerably when droplets overcome turbulent diffusion or the flow is laminar. As mentioned before several experiments were abruptly stopped in order to investigate the stagnant separation behavior. The stagnant separation behavior cannot be adopted to flow development not considering the dynamics of the flow. However, here we can consider it for the simplest estimate. As an example the separation time for the flow pattern Do/w&w at $U_{mix} = 0.5$ *m/s* and $f_w = 0.7$ after stopping was over four minutes. Considering $U_{mix} = 0.5$ *m/s* this would correspond to a developing length of over *120 m* or *L/D = 1200* which is considerably longer than the test section. Separation experiments in separate beaker-mixer tests showed that the total separation time is one order of magnitude higher than the settling time. This would explain the formation of a thick dense packed layer in premixed flow as it was observed for semi dispersed flow in this study. Pal (1996) found that droplet growth reduces the emulsion viscosity which is in agreement with the decreasing pressure gradient measurements.

7. Conclusion

Horizontal oil-water pipe flow experiments using different oil viscosities (*120 mPa*s*, *60 mPa*s* and *35 mPa*s*) were presented. With help of a static inlet mixer the phases were premixed and developed further downstream toward a less mixed or separated flow pattern. Comparison with experimental studies using a simple Y- or T-junction as inlet manifold showed that the flow is sensitive to the inlet. If the inlet device promotes mixing of the flow, transition to dispersed flow was observed at lower mixture velocities. This has an impact on the frictional pressure gradient. In the case of low mixture velocities, when the flow was semi dispersed, higher pressure gradients were measured with inlet mixing. Especially a pressure gradient peak appearing at the transition from 3L-flow to Do/w&w when the inlet water fraction was increased was amplified. Furthermore, this transition shifted towards lower input water fractions. At higher mixture velocities when the flow is fully dispersed mixing provides more homogenous flow. Higher pressure gradients were measured at low input water fractions and lower pressure gradients at higher input water fractions compared to non-premixed flow.

Changing pressure gradient measurements along the pipe showed that fully developed flow was not yet reached after L/D = 200. Also for non-premixed experiments the literature reports considerable developing lengths (L/D = 600) (Nädler and Mewes, 1997).

As consequence of limited test section lengths in experimental studies the inlet section should be chosen carefully. Possible influence on the flow has to be considered. Also the state of flow development should be investigated and reported. This has further impact on model development and comparison. Data from several studies is probably not suitable for evaluating point models predicting developed steady state flow.

Even if the presented experiments have been conducted under simplified laboratory conditions some conclusions can be drawn regarding practical problems of oil production. In real crude oils natural or added emulsifiers can be present (Kokal, 2005). Enhanced mixing of the flow caused by for instance pumps and valves can be expected to persist considerably longer than for mineral oils without surface active agents. Depending on the infrastructure the impact of a

resulting higher pressure gradient over the development length of the flow for example would be limited if the total transport length is long (many kilometers). However, additional mixing of the flow can be problematic at the end of a production line. When a choke valve is installed shortly before the flow enters a separator more dispersion or a finer droplet size could influence the subsequent separation of the fluids. A larger required volume or even different type of the separator can be consequences (Lim et al., 2015; van der Zande and van den Broek, 1998).

8. Acknowledgements

The authors acknowledge the financial support from The Multiphase Flow Assurance Innovation Centre (FACE). FACE is a research cooperation between IFE, NTNU and SINTEF. The center is funded by The Research Council of Norway and by the following industrial partners: Statoil ASA, GE Oil & Gas, SPT Group - A Schlumberger Company, FMC Technologies, CD-adapco, Shell Technology Norway.

9. References

Angeli, P., 1996. Liquid-liquid dispersed flows in horizontal pipes. Ph.D. Thesis. Imperial College of Science, Technology and Medicine, London

Angeli, P., Hewitt, G.F., 1999. Pressure gradient in horizontal liquid-liquid flows. Int J Multiphas Flow 24, 1183-1203. http://dx.doi.org/10.1016/S0301-9322(98)00006-8

Arirachakaran, S., Oglesby, K.D., Malinowsky, M.S., Shoham, O., Brill, J.P., 1989. An Analysis of Oil/Water Flow Phenomena in Horizontal Pipes. SPE Production Operations Symposium, Oklahoma City. Society of Petroleum Engineers. http://dx.doi.org/10.2118/18836-MS

Brauner, N., 2003. Liquid-Liquid Two-Phase Flow Systems, Modelling and Experimentation in Two-Phase Flow. Springer Vienna, pp. 221-279.

Cabellos, E.M., Carvalho, M.S., Ponce, R.V., 2009. Oil-in-water emulsion formation in laminar flow through capillaries. 20th International Congress of Mechanical Engineering, Gramado.

Elseth, G., 2001. An Experimental Study of Oil / Water Flow in Horizontal Pipes. Ph.D. Thesis. Telemark University College, Porsgrunn

Guzhov, A.I., Grishin, A.D., Medvedev, V.F., Meved-eva, O.P., 1973. Emulsion Formation During the Flow of Two Liquids in a Pipe. Neftianoe Khoziastvo Oil Industry 8, 58-61.

Hu, B., Langsholt, M., Liu, L., Andersson, P., Lawrence, C., 2014. Flow structure and phase distribution in stratified and slug flows measured by X-ray tomography. Int J Multiphas Flow 67, 162-179. http://dx.doi.org/10.1016/j.ijmultiphaseflow.2014.06.011

Karabelas, A.J., 1978. Droplet size spectra generated in turbulent pipe flow of dilute liquid/liquid dispersions. AIChE Journal 24, 170-180. DOI: 10.1002/aic.690240203

Kokal, S., 2005. Crude-Oil Emulsions: A State-Of-The-Art Review. SPE Production & Facilities 20, 5-13.

Kumara, W.A.S., Halvorsen, B.M., Melaaen, M.C., 2009. Pressure drop, flow pattern and local water volume fraction measurements of oil-water flow in pipes. Measurement Science and Technology 20, 1-18. http://dx.doi.org/10.1088/0957-0233/20/11/114004

Lim, J.S., Wong, S.F., Law, M.C., Samyudia, Y., Dol, S.S., 2015. A review on the effects of emulsions on flow behaviours and common factors affecting the stability of emulsions. Journal of Applied Sciences 15, 167-172. 10.3923/jas.2015.167.172

Lovick, J., Angeli, P., 2004. Experimental studies on the dual continuous flow pattern in oil-water flows. Int J Multiphas Flow 30, 139-157. http://dx.doi.org/10.1016/j.ijmultiphaseflow.2003.11.011

Mandal, T.K., Chakrabarti, D.P., Das, G., 2007. Oil Water Flow Through Different Diameter Pipes: Similarities and Differences. Chemical Engineering Research and Design 85, 1123-1128. http://dx.doi.org/10.1205/cherd06036

Merchuk, J.C., Andrews, B.A., Asenjo, J.A., 1998. Aqueous two-phase systems for protein separation, Studies on phase inversion. Journal of Chromatopraphy B: Biomedical Sciences and Applications 711, 285-293. http://dx.doi.org/10.1016/S0378-4347(97)00594-X

Ngan, K.H., 2011. Phase inversion in dispersed liquid-liquid pipe flow. Ph.D. Thesis. Unviversity College London, London

Nädler, M., Mewes, D., 1997. Flow induced emulsification in the flow of two immiscible liquids in horizontal pipes. Int J Multiphas Flow 23, 55-68. http://dx.doi.org/10.1016/S0301-9322(96)00055-9

Pal, R., 1993. Pipeline Flow of Unstable and Surfactant-Stabilized Emulsions. AIChE Journal 39, 1754-1764. DOI: 10.1002/aic.690391103

Pal, R., 1996. Effect of Droplet Size on Rheology of Emulsions. AIChE Journal 42, 3181-3190. DOI: 10.1002/aic.690421119

Plasencia, J., Nydal, O.J., 2010. Influence of the pipe diameter in dispersed oil-water flows. 7th International Conference on Multiphase Flow, Tampa.

Schümann, H., Tutkun, M., Nydal, O.J., Experimental study of dispersed oil-water flow in a horizontal pipe with enhanced inlet mixing, Part 2: In-situ droplet measurements. submitted to the Journal of Petroleum Science and Engineering.

Soleimani, A., 1999. Phase distribution and associated phenomena in oil-water flows in horizontal tubes. Ph.D. Thesis. Imperical College Lodon, London

Trallero, J.L., Sarica, C., Brill, J.P., 1997. A Study of Oil/Water Flow Patterns in Horizontal Pipes. SPE Production & Facilities 12, 165-172. http://dx.doi.org/10.2118/36609-PA

van der Zande, M.J., van den Broek, W.M.G.T., 1998. Break-up of oil droplets in the production system. Proceedings of ASME Energy Sources Technology Conference and Exhibition, Housten.

Paper 3

Experimental study of dispersed oil-water flow in a horizontal pipe with enhanced inlet mixing,
Part 2: In-situ droplet measurements

Heiner Schümann, Murat Tutkun and Ole Jørgen Nydal

Submitted to the
Journal of Petroleum Science and Engineering

Experimental study of dispersed oil-water flow in a horizontal pipe with enhanced inlet mixing,
Part 2: In-situ droplet measurements

Heiner Schümann[1,2]*, Murat Tutkun[3,4], Ole Jørgen Nydal[1]

[1]Department of Energy and Process Engineering, Norwegian University of Science and Technology, NTNU, Trondheim, Norway
[2]Multiphase Flow Laboratory, SINTEF Petroleum AS, Trondheim, Norway
[3]Department of Fluid Flow Technology, Institute for Energy Technology, Kjeller, Norway
[4]Department of Mathematics, University of Oslo, Oslo, Norway

*Corresponding author, Email: heiner.schumann@ntnu.no

Abstract

Droplet size measurements in premixed oil-water flow are presented. Three traversable focused beam reflectance measurement probes (FBRM) positioned along the test section allowed for measuring averaged droplet size profiles over the cross section. Measurements for two mixture velocities, U_{mix} = 0.5 m/s and U_{mix} = 1 m/s, and the complete range of input water fractions were performed with tap water and medium viscosity mineral oil. The flow facility provided a *10 cm* inner diameter test section of *24 m* total length. Flow development in terms of droplet growth was documented. Averaged droplet sizes showed to be a function of the dispersed phase fraction with sizes increasing towards a maximum at phase inversion. Different flow patterns show characteristic droplet size profiles over the cross-section. Common models over-predict the presented droplet size data, most probably as a result of enhanced inlet mixing and underdeveloped flow.

1. Introduction

Pipe flow of liquid-liquid dispersions is common in the process industry. Transport of oil-water dispersions in oil production systems is difficult to predict and often requires special attention. Formation of emulsion affects not only individual components like separators, pumps or pipelines, but also overall flow assurance (Lim et al., 2015). One of the key issues in oil-water dispersed flow is size and dynamics of droplets. Detailed in-situ measurements of droplets, therefore, are necessary to gain more insight into dispersed flows. This, in turn, will help us to improve simulation tools as well as our predicting capacity and flow control strategies. These eventually lead to cost reduction and increased safety.

It is a known fact that any change in droplet size distribution within the flow is always accompanied by change in rheology of emulsion (Pal, 1996). A reduction in droplet size was found to increase the effective viscosity. In some cases the presence of droplets can lead to drag reduction as result of turbulence modification in the flow (Angeli and Hewitt, 1999; Pal, 1993). In a similar manner, droplet size reacts on changes in the flow. Higher mixture velocities for instance will reduce droplet sizes as a consequence of enhanced break-up. At higher dispersed phase fractions coalescence becomes more active and droplet sizes increase (Ioannou, 2006; Ward and Knudsen, 1967). Droplets can further be influenced by adding stabilizing agents, the so-called surfactants, to the flow.

Droplets arise from instabilities at the liquid-liquid interface at sufficiently high flow rates. In more realistic oil-water transport systems, however, a dispersion usually forms in the reservoir (Cabellos et al., 2009). Flow control units like mixers, pumps and valves add additional droplets as the flow passes through them (Middleman, 1974; Morales et al., 2013; Noïk et al., 2005; van der Zande and van den Broek, 1998). Eventually this develops towards a final droplet size distribution which is controlled by simultaneous break-up and coalescence in the system.

Droplet size distributions in horizontal oil-water dispersed flow with a low viscosity oil ($1.6\ mPa*s$) were measured by Angeli and Hewitt (2000) using an endoscope camera. A T-junction and low dispersed phase inlet velocities ensured break-up in the test section and not at the inlet. At equal mixture velocities and dispersed phase fractions, droplets were found to be smaller in oil continuous flow compared to water continuous flow. In the tested range ($3.4 - 9\%$) the dispersed phase fraction did not seem to influence the droplet size.

Simmons and Azzopardi (2001) found droplet size stratification at low velocities in a horizontal pipe section, using kerosene as continuous phase and potassium carbonate solution as dispersed phase. Hinze (1955) theory agreed well with droplet size measurements for low dispersed phase

fractions only. A special inlet device in this case prevented dispersion formation due to the merging of the phases.

El-Hamouz and Stewart (6-9 October 1996) used a Par-Tec M300 laser backscatter instrument to investigate droplet sizes in oil-water flow through different pipe fittings and geometries. Even if the oil-water volumetric ratio was low (i.e., 1:50) droplet growth downstream of the inlet was measured.

Middleman (1974) measured water continuous dispersions formed in pipe flow through a static mixer. A positive effect of dispersed phase fraction and viscosity on the mean droplet size was found.

Droplets in dual-continuous flow were measured by Lovick and Angeli (2004) with help of a dual sensor impedance probe. This study mainly concerned the chord lengths instead of actual droplet size and showed that chord size was largest at the interphase. Furthermore, high shear in the pipe wall region was found to reduce droplet sizes.

In a study by Ioannou (2006) droplet sizes of oil and water continuous flow at high mixture velocities ($U_{mix} = 3.0$, 3.5 and $4.0\ m/s$) before and after phase inversion are presented. Cross sectional averaged means peaked at phase inversion point.

This paper focuses on the development of unstable dispersions downstream of a static mixer. We present new experimental data which are also compared to existing droplet size models. We utilized a focused beam reflectance measurement (FBRM) system and further investigate the applicability of the FBRM as a tool for in-situ droplet measurements in liquid-liquid pipe flow. Of particular interest is the possibility to distinguish certain flow regimes based on droplet size measurements.

2. Experimental setup

Experimental facility is the Well Flow Loop of the Institute for Energy Technology (IFE) in Kjeller, Norway. The transparent PVC test section has a total length (L) of 25 m and inner diameter (D) of 100 mm. Oil and water were mixed at the inlet of the test section. Enhanced mixing was ensured by a static mixer installed right after the section where oil and water were injected into the pipe. The flow therefore was initiated in a premixed state.

The test section was horizontally aligned (0°±0.1°). Figure 1 shows a schematic of the test section. The pressure gradient was measured over three separate sections along the pipe. A broad beam gamma densitometer and an X-ray tomography instrument provided local phase fraction measurements. Video recordings and visual observations were used to identify flow patterns. Three traversable FBRM probes collected data at three different downstream locations for in-situ droplet characterization. A more detailed experimental description as well as flow pattern, pressure drop and phase fraction measurements were presented in (Schümann et al.).

Droplets were measured at two different mixing velocities: $U_{mix} = 0.5\ m/s$ and $1\ m/s$. These measurement were carried out for input water fractions changing from 0% to 100 % with 10% intervals.

2.1 Fluid properties

Tap water and mineral oil mixtures were the test fluids. The experiments were repeated for three different oil viscosities as summarized in Table 1. The flow loop was temperature controlled and a liquid temperature of 20± 0.5°C was kept for all experiments. Input water fractions needed for phase inversion were typically in the range of $20\% < f_{w\_inv} < 30\%$ for these oil mixtures. f_{w_inv} was smallest for oil A and largest for oil C.

Table 1: Properties of the tested mineral oil mixtures.

Oil	Composition Primol 352: Exxsol D80	Density [kg/m^3]*	Viscosity [mPa*s]*	Interf. tension [mN/m]** (short/long term)
Oil A	25:1	866 (±0.2%)	120 (±3%)	23/14 (±10%)
Oil B	6:1	859 (±0.2%)	60 (±2%)	23/14 (±10%)
Oil C	4:1	853 (±0.2%)	35 (±2%)	24/15 (±10%)
Tap water	-	999	1	-

*Viscosity was measured at 20 C. Viscosity uncertainties due to temperature fluctuations are considered in the uncertainties.
** With tap water

2.2 FBRM (Focused beam reflectance measurement)

The FBRM is a widely used in-situ particle characterization tool. A focused laser beam with negligible width rotates at high speed and scans the flow. Whenever the laser crosses a particle or a droplet, backscattered light is measured by a sensor. An algorithm distinguishes between different chord lengths corresponding to the scanned particles. In this way the FBRM automatically counts thousands of droplets within a short period of time. After a predefined sampling interval (15 sec in our case) a chord length distribution is computed and stored. 15 sec was found to be long enough to give sufficient numbers of counts to produce smooth size distributions. At the same time it was short enough to identify eventual fluctuations and changes of the flow. The scanned circle has a diameter of $8\ mm$. The size limit, however, is smaller. The software allows measuring chord lengths up to $4\ mm$. For chord lengths larger then $1\ mm$ one can expect the influence of the curvature of the circle to become important. More technical details regarding the instrument and principles of operation are documented in Schümann et al. (2015).

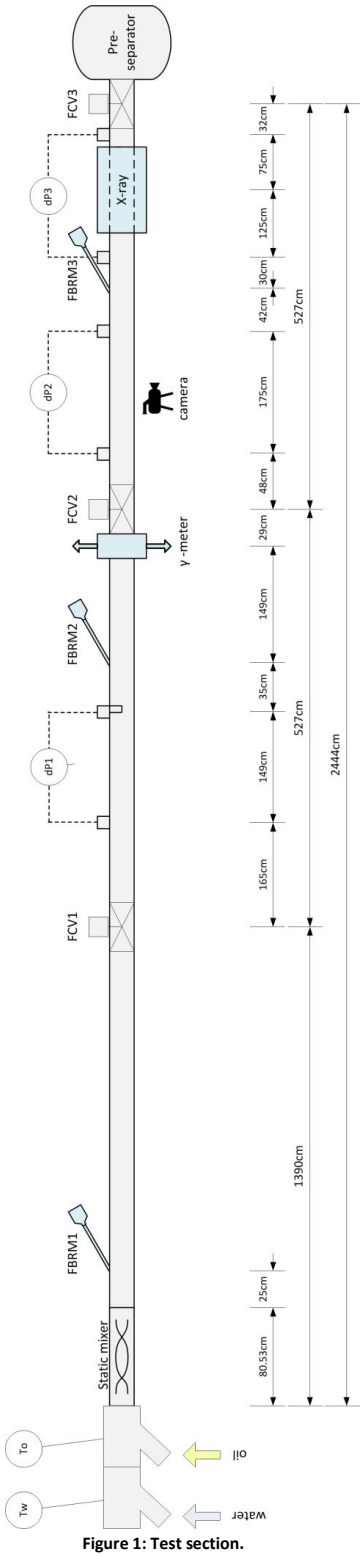

Figure 1: Test section.

Three FBRM probes (by Mettler Toledo) of type D600 were mounted in adapters as shown in Figure 2. The probes were aligned 45° against the flow. The adapters were specially designed to allow traversing into the pipe to measure different position in vertical direction. Five measurements were chosen as measurement locations and they were distributed symmetrically around the center point; e.g. +/- 4 cm, +/- 2cm and 0. In this way we were also able to obtain a coarse vertical droplet size profile over the cross section of the pipe.

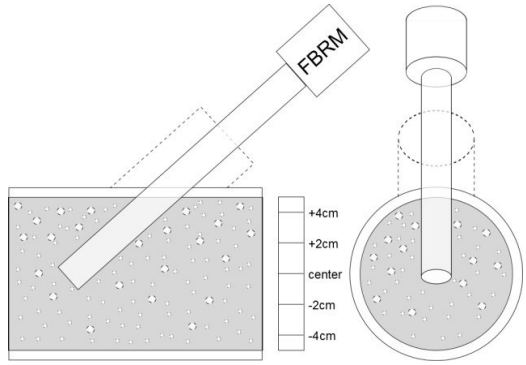

Figure 2: Sketch of the traversable FBRM mounted in an adapter. The flow direction was from left to right for the figure showing the side view.

Every measurement probe inserted into the pipe is intrusive. A strict procedure was followed in order to minimize flow disturbances by the probe. Local phase fractions and pressure gradients were measured with the probes extracted to its maximum at the beginning of an experiment. Afterwards, the probes were traversed through the cross section starting with the probe at the end of the test section. When all measurements at the five vertical sample positions were obtained, this procedure was repeated by with middle probe and finally the last probe. In this way, upstream probes did not disturb the downstream measurements.

Another issue is the influence of the flow field upstream of the probe. Unfortunately, the upstream blockage introduced by the probe cannot be avoided. While the small droplets are influenced by the probe, the large droplets will follow their trajectory due to their larger inertia. This would also be dependent on the flow velocity and water fraction. This means that the droplet size distribution measured by the FBRM would be most affected at the lower end of the spectrum, representing the smallest droplets, because these droplets follows the modified streamlines of the flow. We would therefore expect to see the effect of probe in the pipe in the lower end of droplet size distribution spectrum. Comparing the data between the measurement points located close to the top wall, which represents minimum intrusiveness, and close to the bottom wall, which represents the maximum intrusiveness, is useful in order to see the effect. A distinct difference was, however, not found from our measurements. Also, the Sauter mean diameter, D32, mainly

presented in this paper, is little sensitive to the smallest droplets.

2.3 Data processing

The chord length distribution measured by the FBRM differs from the real droplet size distribution due to several reasons: (i) The laser beam does not necessarily cross a droplet in the center every time the laser hits the droplet, which would automatically lead to the correct diameter. The laser beam crossing the droplet through off-center points introduces an underestimation of the droplet size. (ii) In dense emulsions scattering of light by other droplets can lead to a misinterpretation of the measured signal. (iii) Differences in the refractive index of the liquids as well as rough droplet surfaces on the micro scale can further influence the backscattering.

In order to reduce the underestimation of droplet size, we developed a methodology of calibrating the FBRM using an optical in-situ measurement technique (Particle Video Microscopy – PVM) (Schümann et al., 2015). This methodology was able to provide real droplet sizes with an uncertainty of 50%. This conversion was applied to the measurements presented in this study. Therefore, we will present our results in terms of droplet size, meaning the diameters of individual droplets, instead of chord lengths, which is what one can get from the FBRM.

A main problem of the FBRM, called probe coating, occurs if single droplets stick to the probe window. In this case a continuous sampling of the same droplets creates large peaks in the chord length distribution. Furthermore, such peaks affect mean sizes derived from the distribution curves. We noticed that probe coating in this study occurred for single samples only and stuck droplets were washed away again automatically. The software which we used in our measurement monitors the samples real time and it was easy to catch probe coating problem immediately. Throughout the experimental campaign several samples were taken for every data point. In a manual screening, later, samples where probe coating occurred were rejected. The accepted samples were then averaged in order to reach final and actual chord length distributions.

3. Results

3.1 *Cross sectional droplet size distribution*

In this section we investigate cross sectional characteristics of the droplet size and try to identify specific flow regimes. Considering the measurement uncertainty results were similar for the different oils. Here we will focus on oil C. With the lowest viscosity of the three tested oils, probe coating was least problematic and results most clear. Also, unless otherwise specified the presented results are based on measurements by FBRM probe 3, where the flow is most developed.

In order to better understand the following results we will recall the cross sectional water line-measurements, Figure 3 and Figure 4, as presented in Schümann et al. (). At $U_{mix} = 0.5\ m/s$ the flow was semi-dispersed. For input water fractions less than 50%, the flow was three-layered with a layer of pure oil on top, a dispersed layer in the middle, and a pure water layer at the bottom. A pure water layer was not present for the lowest input water fraction. Higher input water fractions resulted in a water continuous flow with a dense packed layer of oil droplets in the upper part of the pipe. Here, the pure oil layer disappeared. At $U_{mix} = 1\ m/s$ the flow was fully dispersed, either water continuous or oil continuous. We observed a dual continuous flow pattern only for oil C around the inversion point, $f_w = 0.31$.

Cross sectional water fraction measurements are presented together with Sauter mean diameters, D_{32} at the particular measurement positions in Figure 5 and Figure 6. The presented water fraction measurements and tomographic reconstructions were obtained from X-ray measurements described in detail in Schümann et al. (). The Sauter mean diameter is calculated as

$$D_{32} = \sum_{i=1}^{k} n_i D_i^3 \Big/ \sum_{i=1}^{k} n_i D_i^2 \qquad (1)$$

where D_i is the median of a particular bin i with the number of counts n_i. For a volumetric dispersed phase fraction Φ the D_{32} allows for directly obtaining the interfacial area per unit volume (Middleman, 1974):

$$A_v = 6\Phi / D_{32} \qquad (2)$$

Figure 5 shows the three typical cases for $U_{mix} = 0.5\ m/s$ with different positions of the dispersion layer.

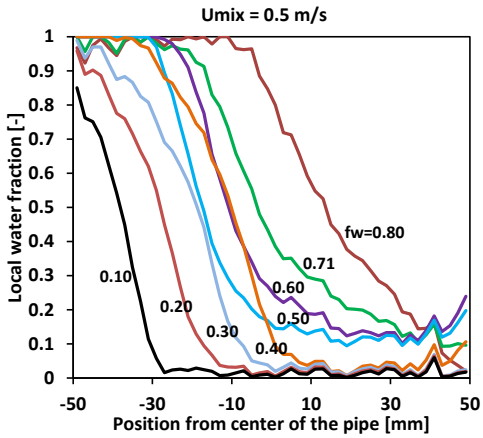

Figure 3: Water line fraction measurements for Oil C (*35 mPa*s*) at $U_{mix} = 0.5 m/s$. The input water fractions, f_w, are shown in the figure. Results from Schümann et al. ().

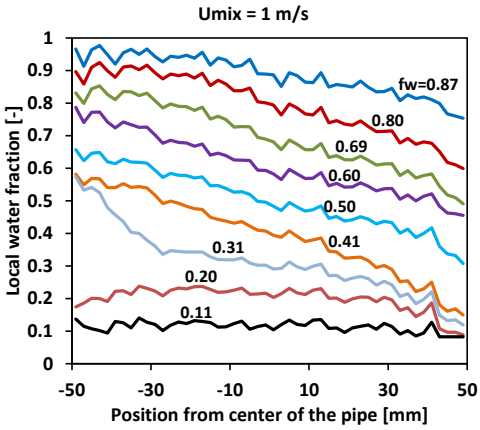

Figure 4: Water line fraction measurements for Oil C (*35 mPa*s*) at U_{mix} = *1m/s*. The input water fractions, f_w, are shown in the figure. Results from Schümann et al. ().

Comparison of the D_{32} values in the upper and lower part of the dispersed layer indicates some distinct features of a three-layered flow pattern. This means that the dispersed layer was divided into a region of dispersed water droplets in oil, which formed the upper part, and a region of oil droplets in water, which formed the lower part. In the upper layer, water droplets (D_{32}) typically were less than $0.5\,mm$. Oil droplets in the lower layer were in the range of *1 mm* to *2.5 mm*. When f_w *> 50%,* droplet sizes were more uniform. This essentially confirms the assumption that the dispersion is of oil-in-water type for these input water fractions.

Figure 6 shows measurements for oil continuous flow ($f_w = 20\%$), dual continuous flow ($f_w = 31\%$), and water continuous flow ($f_w = 80\%$).

For oil continuous flow (f_w *= 20%)* the dispersed phase was homogeneously distributed over the cross section. A slightly lower concentration of dispersed phase close to the pipe wall can be attributed to the near wall effect which essentially leads to a reduced mixing due to the substantial drop of velocity. Droplet size measurements demonstrate that the largest droplets are mainly in the center of the pipe with a decreasing size towards the wall. Even if detailed local velocity and turbulence measurements are missing, one can assume the following: Considering the presence of a inlet mixer and a Reynolds number of *Re = 2400* based on oil properties, the flow might be turbulent. The shear around the pipe centerline is very low compared to the shear one observes near the wall. The level of turbulence also drops significantly around the centerline. Due to these effects, the level of break-up process around the centerline is not very high, which eventually results in larger droplets. High shear near the wall together with large turbulent fluctuations enhance the break-up process and droplet size drops accordingly.

For water continuous flow (f_w *= 80%*) the dispersed oil fraction and droplet size increase simultaneously with the height. As the oil blends into the water, then the local viscosity increases. This leads to lower turbulence intensity, hence larger droplets. In addition, larger droplets will settle faster towards the top of the pipe and increasing dispersed phase fraction promotes coalescence.

The dual-continuous case is presented by f_w *= 31%*. Even though the boundary between oil continuous and water continuous regions is difficult to identify, we expect it to be around -25 mm from the centerline where we observe the slope change in water fraction profile.

Sauter mean diameters over the cross section for all measured input water fractions at $U_{mix} = 1\ m/s$ are shown in Figure 7. Droplet sizes increase as the dispersed phase fraction does, which is the case for both water and oil-continuous flow. A stratification of the droplet size, with increasing mean sizes towards the pipe top, is observed for high input water fractions, f_w *= 0.87, 0.8 and 0.69*. A similar stratification for oil continuous flow is also documented in Simmons and Azzopardi (2001). For lower input water fractions, fw = 0.6, 0.5 and 0.41, a size reduction also towards the upper pipe wall was measured. Thus, the largest droplets were measured in the center of the pipe. Again, high shear close to the wall enhances the break-up process and leads to a decreasing droplet size profile toward the wall. This has also been observed by Lovick and Angeli (2004) as droplet measurements close to the interface in dual continuous flow showed a profile of smaller droplets toward the wall. . The interface close to the pipe wall did have no large droplets.

We found following relation between mean and maximum droplet size:

$$D_{32} = cD_{\max} \tag{3}$$

This is in agreement with our previous findings as documented in Schümann et al. (2015). This relation was first mentioned in Sprow (1967) regardless of the shape of a DSD and of the mixing intensity. A value of $c = 0.61$ with a standard deviation (std(c)) of 0.03 was obtained from the converted DSD. Similar c values have already been documented by others: for gas bubbles 0.62 by Hesketh et al. (1987), 0.48 by Angeli and Hewitt (2000). The latter was due to the method of calculation since Angeli and Hewitt (2000) used the 95th percentile per volume, D_{95_vol}, as a measure for D_{max}. It was also reported by the authors that only 0.3% of the numbers of drops were larger than the D_{max}. In our work, however, the 99th percentile per number, D_{99_num}, was used. This naturally results in a larger value for c. Note that range of c values reported in literature in mixer experiments is from 0.38 to 0.7 (Brown and Pitt, 1972; Calabrese et al., 1986; Coulaloglou and Tavlarides, 1976; Giapos et al., 2005; Sprow, 1967; Zhou and Kresta, 1998).

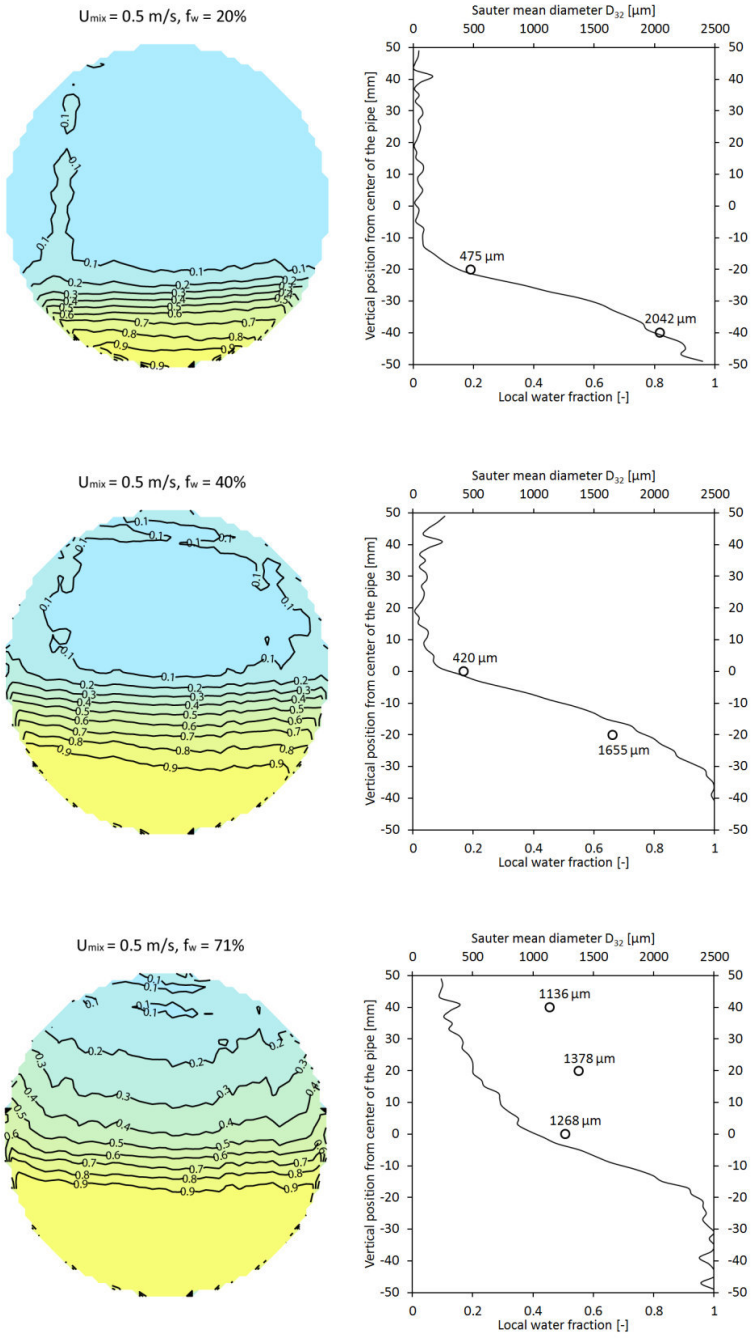

Figure 5: Selected measurements for U_{mix} = 0.5 m/s. Left column: Cross sectional water distribution. Contour lines show the local water fraction with an increment of 0.1. Right column: Water line fraction measurements and droplet sizes across the pipe. The uncertainty of the droplet sizes is approximately 50%. The respective flow patterns are, from top to bottom: oil & dispersion; oil, dispersion & water; dispersion of oil in water & water.

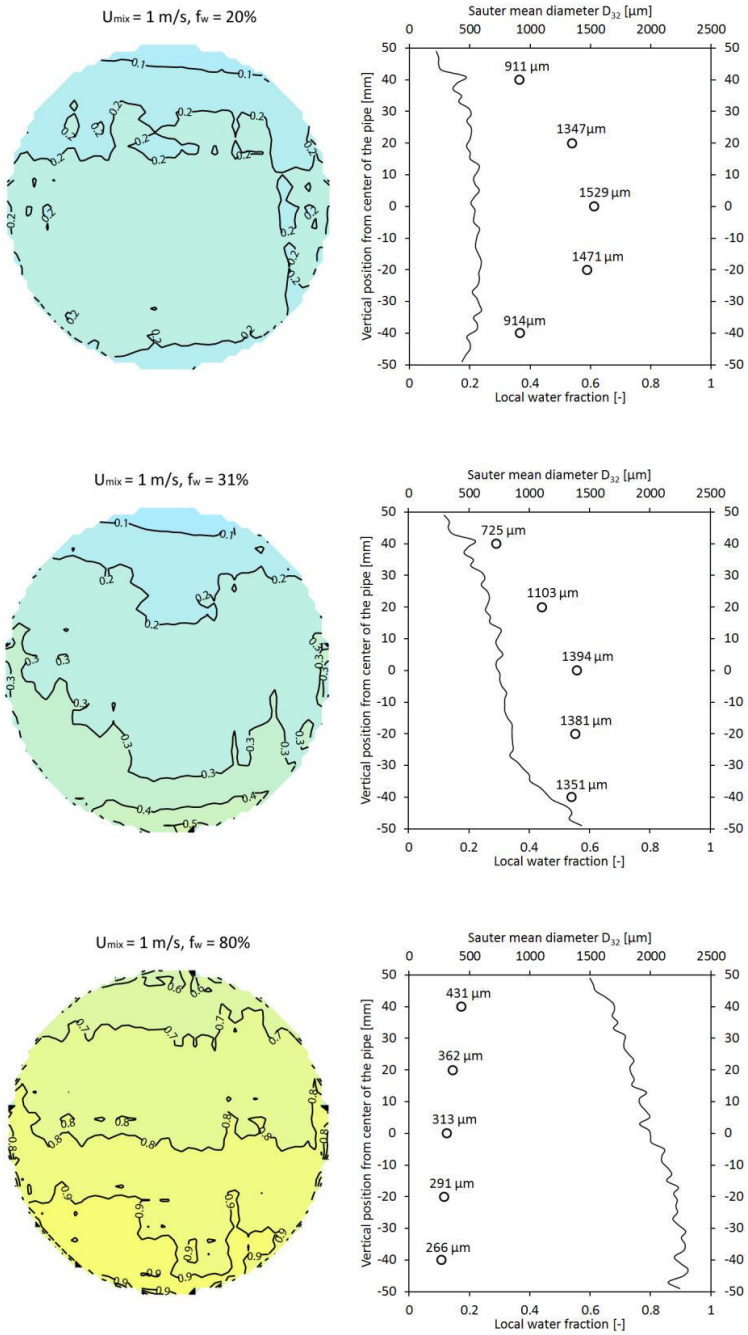

Figure 6: Selected measurements for U_{mix} = 1 m/s. Left column: Cross sectional water distribution. Contour lines show the local water fraction with an increment of 0.1. Right column: Water line fraction measurements and droplet sizes vs. the position in the pipe. The uncertainty of the droplet sizes is approximately 50%. The respective flow patterns are, from top to bottom: oil continuous dispersion; dual continuous flow (dispersion of water in oil & dispersion of oil in water); water continuous dispersion.

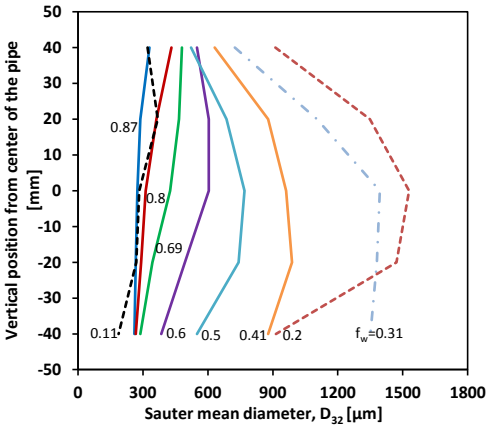

Figure 7: Droplet size profiles at different water-cuts at U_{mix}=1m/s. Data are taken by the FBRM 3 which was in the end of the test section. Continuous lines show water continuous flow, broken lines show oil continuous flow, dotted-broken line shows dual continuous flow. Note that the inversion point is at f_w of approximately 30%.

3.2 Influence of the phase fractions

Figure 7 shows the droplet size change across the pipe at different input water fractions. At each input water fraction we computed the average droplet size over the cross section. To do so, the chord length distributions obtained at each probe position were weighted according to the representative area of the cross section and the respective average dispersed phase fraction in this area. This is illustrated in Figure 8. The dispersed phase fraction was found from the vertical line fraction measurements. Consequently the weighted chord length distributions were averaged and converted to droplet sizes to obtain D_{32}. (Note that phase fraction differences in the horizontal direction were assumed to be negligible in this approach.)

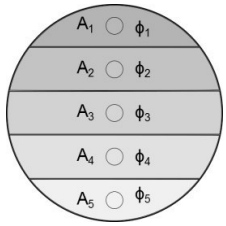

Figure 8: Cross sectional averaging A_i and ϕ_i. denote cross-sectional area of the probed segment, and the phase fraction in that area, respectively. i =1,…N, where N is the maximum number of mesurement positions where the FBRM is operated to collect data.

The result for the most downstream (and hence, most developed) measurement position at $U_{mix} = 1\ m/s$ is shown in Figure 9 for both oil A, B and C. The smallest droplets were found for the lowest dispersed phase fractions. The Sauter mean diameter, D_{32}, increases exponentially towards a peak value at phase inversion. The trend is similar to that of the pressure gradient as a function of input water fraction. Measurements performed using oil C reveal that the droplet size in a oil continuous flow increases dramatically shortly before the inversion. This distinct increase in the Sauter mean diameter right before phase inversion was also observed by others, cf. (Ioannou, 2006).

The oil viscosity herein plays a minor role. Droplets, however, seems to be slightly larger in the water continuous side. An increase in the droplet diameter with increasing dispersed phase viscosity was also observed by Ward and Knudsen (1967), and Middleman (1974) who state that "a high viscosity in the dispersed phase retards disruption of the drop". This is attributed to higher viscosity which leads to a higher energy dissipation during droplet deformation leaving less energy for the break-up process (van der Zande and van den Broek, 1998).

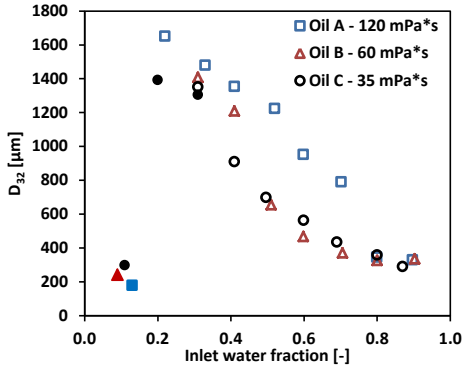

Figure 9: Sauter mean diameter, D_{32}, averaged over the cross section vs. inlet water fraction. U_{mix}=1m/s. Filled symbols show oil continuous flow, open symbols show water continuous flow.

The D_{32} close to the phase inversion point were of similar size for oil and water continuous flow, but as mentioned earlier the droplet size decreases faster with a decreasing dispersed phase fraction on the oil continuous side. Figure 10 shows the Sauter mean diameter as function of the real local dispersed phase fraction normalized by the dispersed phase fraction at the phase inversion. Best fitting curve using the least-squares method take the following form:

$$D_{32} = 2.5 \cdot 10^{-4} + 1.3 \cdot 10^{-3} \left(\phi / \phi_{inv} \right)^{2.7} \qquad (4)$$

Beside measurement uncertainties, the large spread of the data is due to the fact that a gradient of flow velocity inside the pipe creates different shear intensities across the cross section. In addition, the turbulence intensity profile in relation to the DSD variations is of importance (Simmons and Azzopardi, 2001).

Figure 10 further shows that the influence of the phase fraction is rather small when $\Phi / \Phi_{inv} < 0.2$. Also Angeli and

Hewitt (2000) report no influence of the dispersed phase fraction for dilute dispersions, e.g., the coalescence is insignificant for such cases. In their measurements the dispersed phase fraction was as high as 9%.

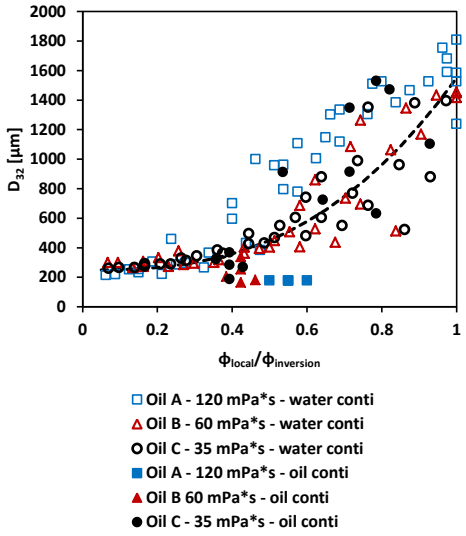

Figure 10: Local droplet size as a function of the local dispersed phase fraction for U_{mix}=1 m/s.

The rapid change of the DSD at phase inversion was measured in a separate experiment. Starting with oil continuous flow at $f_w = 10\%$, the input water fraction was slowly increased until the phase inversion was reached. Following the phase inversion, the water continuous flow regime stabilized at approximately $f_w = 30\%$. Then, the input water fraction was reduced again until the flow inverted back to oil continuity. Figure 11 shows the converted DSDs of the alternating oil/water continuous flow. Corresponding Sauter mean diameters are shown in Figure 12. The DSD and thus the D_{32} change considerably as the volumetric fraction of the dispersed phase are due to a change of the phase continuity at inversion.

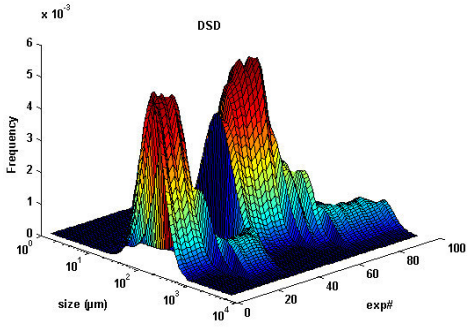

Figure 11: DSDs at phase inversion. The sampling time was 10 sec for each distribution.

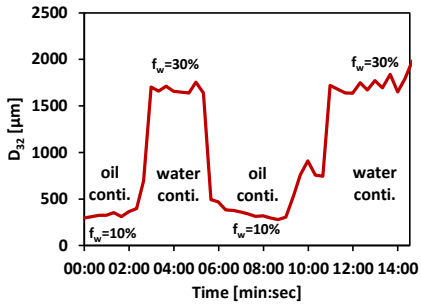

Figure 12: Sauter mean diameter in time through phase inversions.

3.3 Droplet growth

Flow development was obtained by pressure difference measurements along the pipe (Schümann et al.). This could be contributed to an in-flow separation behavior downstream of the static mixer. The flow was assumed to be well mixed when it leaves the static mixer at the pipe inlet. Settling of droplets is expected due to the buoyancy. This will produce the vertical gradient in the local dispersed phase fraction. When the flow is water continuous, larger oil droplets experience a stronger buoyancy force which leads to accumulation of these large droplets in the upper part of the pipe. Our cross sectional measurements as presented in section 3.1 indicate this as well. When the flow is, however, oil continuous the high viscosity of the oil presumably restricts a vertical drift of the water droplets.

The second mechanism is coalescence and break up of droplets as a result of the dynamics of the flow. If coalescence is dominating the droplet size will increase, while break up will lead to smaller droplet sizes. These affect the viscosity of the emulsion tremendously and can also impact to the state of flow (Pal, 1993; Pal, 1996).

These two mentioned mechanisms will influence each other as well. A higher dispersed phase fraction as a result of stratification will lead to higher coalescence rates. Larger droplets as a result of coalescence will lead to a faster stratification. Only at sufficiently high flow rates the mixing of the flow will overcome this separation behavior and break up can dominate.

In Figure 13 and Figure 14 the difference in the averaged Sauter mean diameter was compared between FBRM 1 and 2 and FBRM 2 and 3 respectively for $U_{mix} = 1m/s$. The change was expressed as a percentage growth rate per meter pipe section. Between FBRM 1 and 2 the growth rates are always positive. Oil C seems to grow slowest. However, the growth rates are very similar for oil A, B and C. At $f_w = 20\%$ oil C shows a peak, which might be due to partly inversion of the flow. A similar droplet growth downstream of a static mixer was also observed by (El-Hamouz and Stewart, 6-9 October 1996).

Between FBRM 2 and 3 the trend is less obvious. While oil droplets continue to grow for oil A, negative growth rates were measured for oil C. Oil B shows both.

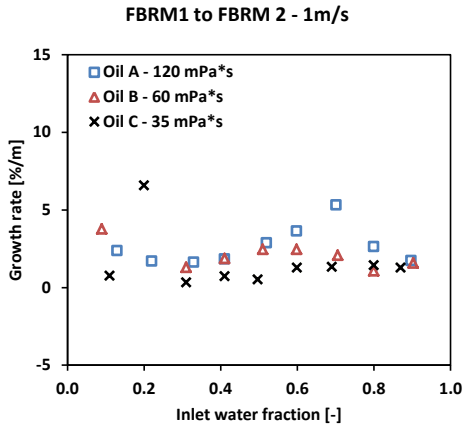

Figure 13: Relative droplet growth rate based on D_{32} between FBRM 1 and FBRM 2.

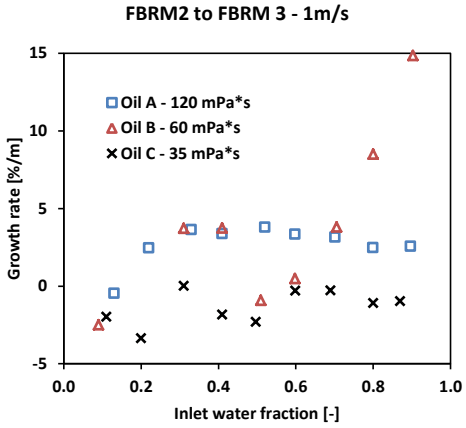

Figure 14: Relative droplet growth rate based on D32 between FBRM 2 and FBRM 3.

4. Comparison with droplet size models

The present data was compared with three models for the maximum droplet size. Results for oil C are shown in Figure 15. Models were tested for water continuous (long lines) and oil continuous (short lines) flow. The measured friction factors, f, were used in the models.

The classical model by (Hinze, 1955):

$$D_{\max}\left(\rho_c/\sigma\right)^{3/5}\varepsilon^{2/5}=0.725 \tag{5}$$

with ε set equal to the mean energy dissipation rate per unit mass (Kubie and Gardner, 1977):

$$\varepsilon_M = 2fU^3/D \tag{6}$$

overpredicted droplet sizes for the lowest dispersed phase fractions by a factor of four. An overprediction was expected as the DSD was initially produced by the inlet mixer. The large difference indicates that the flow cannot be characterized as fully developed yet. Considering the effect of the dispersed phase fraction, the Hinze model, originally developed for non-coalescing systems, is unable to predict the trend of increasing droplet sizes with higher dispersed phase fractions. Instead, the predicted D_{max} decreases due to an increasing friction factor, f.

Another model by Sleicher Jr. (1962) assumed droplet break-up taking place in the wall region mainly instead of isotropic turbulence as it was assumed by Hinze. Furthermore, both the viscosity of the continuous phase, μ_c, and dispersed phase, μ_d, were considered in the model:

$$\frac{D_{\max}\rho_c U_c}{\sigma}\sqrt{\frac{\mu_c U_c}{\sigma}}=38\left[1+0.7\left(\frac{\mu_c U_c}{\sigma}\right)^{0.7}\right] \tag{7}$$

The Sleicher model better predicted D_{max} for the oil continuous case with the lowest dispersed phase fraction. For the water continuous experiments considerably larger droplets were predicted. Again the effect of the dispersed phase fraction could not be reproduced.

Only a model by Brauner (2001), as in equation (8), predicted the effect of the dispersed phase fraction for the water continuous flow well. This model was also the only one considering the dispersed phase fraction directly.

$$\frac{D_{\max}}{D}=2.22C_H^{3/5}\left(\frac{\rho_c U_c^{\,2} D}{\sigma}\right)^{-0.6}\left[\frac{\rho_m}{\rho_c(1-\phi)}f\right]^{-0.4}\left(\frac{\phi}{1-\phi}\right)^{0.6} \tag{8}$$

With the constant $C_H = 0.7$ the predicted D_{max} was in agreement with the Hinze model for the lowest dispersed phase fractions. By substituting the dispersed phase fraction, Φ, with the normalized dispersed phase fraction, Φ/Φ_{inv}, (shown as Brauner_rel in Figure 15) a steeper increase of the droplet size towards the phase inversion point was achieved.

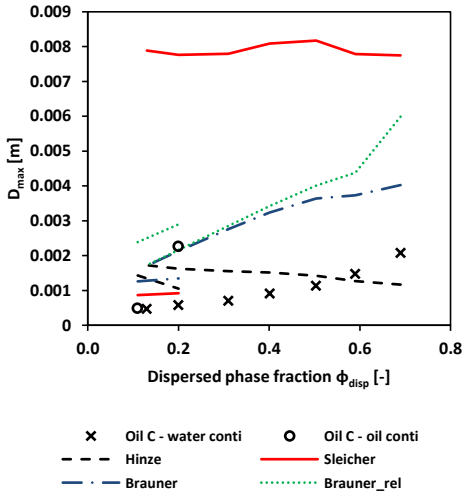

Figure 15: Comparison with droplet size models.

Comparing with the literature it was obvious that in experiments where the test section inlet prevented mixing and droplets arose as a result of the dynamics of the flow (Al-Wahaibi and Angeli, 2008; Angeli and Hewitt, 2000; Lovick and Angeli, 2004; Simmons and Azzopardi, 2001) droplets were larger than predicted by the Hinze, Sleicher or Brauner model. In this work droplets were smaller than predicted by these models.

5. Conclusion

Droplet size measurements in semi and fully dispersed horizontal oil-water pipe flow were presented. An FBRM instrument was used and the chord length data converted to droplet sizes using the calibration technique documented in Schümann et al. (2015). The FBRM instrument provided good stream of data in all tested situations. Cross sectional mean droplet size profiles, obtained from measurements at five different vertical positions, could be correlated with observed flow regimes. Its robustness, unrestricted range of use and the potential to indicate the flow pattern could make the FBRM to a useful tool not only for experimentation but also as control and optimization tool for oil production systems.

Dispersions were produced in a static mixer at the test section inlet. With FBRM measurements at three different positions along the pipe droplet growth downstream of the mixer could be shown. The Sauter mean diameter averaged over the cross section increased with the dispersed phase fraction. This dependency was also achieved when local measurements over the cross section were compared. Only a maximum droplet size model by Brauner (2001) was able to predict such a behavior.

Droplet size profiles over the cross-section show a stratification of droplet sizes, which was more distinct for water continuous flow. Also, for certain measurements of higher dispersed phase fractions smaller droplet sizes were measured close to the wall compared to the pipe center. This could indicate regions of high shear close to the wall leading to stronger break-up.

Droplet growth downstream of the mixer was shown comparing measurements of succeeding FBRM probes. Further downstream the pipe the behavior was less obvious. Also decreasing droplet sizes were observed. The viscosity of the oil seems to play a role as well. Further study is needed to better understand this phenomenon.

6. Acknowledgements

The authors acknowledge the financial support from The Multiphase Flow Assurance Innovation Centre (FACE). FACE is a research cooperation between IFE, NTNU and SINTEF. The centre is funded by The Research Council of Norway and by the following industrial partners: Statoil ASA, GE Oil & Gas, SPT Group - A Schlumberger Company, FMC Technologies, CD-adapco, Shell Technology Norway.

The authors further acknowledge Statoil ASA for the provision of the FBRM instruments used in this study.

7. References

Al-Wahaibi, T., Angeli, P., 2008. Droplet size and velocity in dual continuous horizontal oil-water flows. Chemical Engineering Research and Design 86, 83-93. http://dx.doi.org/10.1016/j.cherd.2007.10.012

Angeli, P., Hewitt, G.F., 1999. Pressure gradient in horizontal liquid-liquid flows. Int J Multiphas Flow 24, 1183-1203. http://dx.doi.org/10.1016/S0301-9322(98)00006-8

Angeli, P., Hewitt, G.F., 2000. Drop size distributions in horizontal oil-water dispersed flows. Chemical Engineering Science 55, 3133-3143.

Brauner, N., 2001. The prediction of dispersed flows boundaries in liquid-liquid and gas-liquid systems. Int J Multiphas Flow 27, 885-910. DOI: 10.1016/S0301-9322(00)00056-2

Brown, D.E., Pitt, L., 1972. Drop size distribution of stirred non-coalescing liquid-liquid system. Chemical Engineering Science 27, 577-583.

Cabellos, E.M., Carvalho, M.S., Ponce, R.V., 2009. Oil-in-water emulsion formation in laminar flow through capillaries. 20th International Congress of Mechanical Engineering, Gramado.

Calabrese, R.V., Chang, T.P.K., Dang, P.T., 1986. Drop Breakup in Turbulent Stirred-Tank Contactors, Part1: Effect of Dispersed-Phase Viscosity. AIChE Journal 32, 657-666.

Coulaloglou, C.A., Tavlarides, L.L., 1976. Drop Size Distribution and Coalescence Frequencies of Liquid-Liquid Dispersions in Flow Vessels. AIChE Journal 22, 289-297.

El-Hamouz, A.M., Stewart, A.C., 6-9 October 1996. On-line measurement of oil-water dispersion using a Par-Tec M300

laser backscatter instrument. SPE Annual Technical Conference, Denver.

Giapos, A., Pachatouridis, C., Stamatoudis, M., 2005. Effect of the number of impeller blades on the drop sizes in agitated dispersions. Chemical Engineering Research and Design 83, 1425-1430.

Hesketh, R.P., Russel, T.W.F., Etchells, A.W., 1987. Bubble size in horizontal pipelines. AIChE Journal 33, 663-667.

Hinze, J., 1955. Fundamentals of the hydrodynamic mechanism of splitting in dispersion processes. AIChE Journal 1, 289-295.

Ioannou, K., 2006. Phase Inversion Phenomenon in Horizontal Dispersed Oil/Water Pipeline Flows. PhD Thesis. University College London,

Kubie, J., Gardner, G.C., 1977. Drop sizes and drop dispersion in straight horizontal tubes and in helical coils. Chemical Engineering Science 32, 195-202. http://dx.doi.org/10.1016/0009-2509(77)80105-X

Lim, J.S., Wong, S.F., Law, M.C., Samyudia, Y., Dol, S.S., 2015. A review on the effects of emulsions on flow behaviours and common factors affecting the stability of emulsions. Journal of Applied Sciences 15, 167-172. 10.3923/jas.2015.167.172

Lovick, J., Angeli, P., 2004. Droplet size and velocity profiles in liquid-liquid horizontal flows. Chemical Engineering Science 59, 3105-3115. DOI:10.1016/j.ces.2004.04.035

Middleman, S., 1974. Drop Size Distributions Produced by Turbulent Pipe Flow of Immiscible Fluids through a Static Mixer. Ind. Eng. Chem. Process Des. Dev. 13, 78-83. DOI: 10.1021/i260049a015

Morales, R., Pereyra, E., Wang, S., Shoham, O., 2013. Droplet formation through centrifugal pumps for oil-in-water dispersions. SPE Journal 18, 172-178. http://dx.doi.org/10.2118/163055-PA

Noïk, C., Dalmazzone, C., Galinat, S., Masbernat, O., Guiraud, P., 2005. Flow of concentrated oil-water dispersion through a restriction. 12th International Conference on Multiphase Production Technology, Barcelona.

Pal, R., 1993. Pipeline Flow of Unstable and Surfactant-Stabilized Emulsions. AIChE Journal 39, 1754-1764. DOI: 10.1002/aic.690391103

Pal, R., 1996. Effect of Droplet Size on Rheology of Emulsions. AIChE Journal 42, 3181-3190. DOI: 10.1002/aic.690421119

Schümann, H., Khatibi, M., Tutkun, M., Pettersen, B.H., Yang, Z., Nydal, O.J., 2015. Droplet Size Measurements in Oil-Water Dispersions: A Comparison Study Using FBRM and PVM. Journal of Dispersion Science and Technology 36, 1432-1443. http://dx.doi.org/10.1080/01932691.2014.989569

Schümann, H., Tutkun, M., Yang, Z., Nydal, O.J., Experimental study of dispersed oil-water flow in a horizontal pipe with enhanced inlet mixing, Part 1: Flow paterns, phase distributions and pressure gradients. Submitted to the Journal of Petroleum Science and Engineering.

Simmons, M.J.H., Azzopardi, B.J., 2001. Drop size distributions in dispersed liquid-liquid pipe flow. Int J Multiphas Flow 27, 843-859. Doi 10.1016/S0301-9322(00)00055-0

Sleicher Jr., C.A., 1962. Maximum Stable Drop Size in Turbulent Flow. AIChE Journal 8, 471-477. DOI: 10.1002/aic.690080410

Sprow, F.B., 1967. Distribution of drop sizes produced in turbulent liquid-liquid dispersion. Chemical Engineering Science 22, 435-442.

van der Zande, M.J., van den Broek, W.M.G.T., 1998. Break-up of oil droplets in the production system. Proceedings of ASME Energy Sources Technology Conference and Exhibition, Housten.

Ward, J.P., Knudsen, J.G., 1967. Turbulent Flow of Unstable Liquid-Liquid Dispersions: Drop Sizes and Velocity Distributions. AIChE Journal 13, 356-365. DOI: 10.1002/aic.690130229

Zhou, G., Kresta, S.M., 1998. Correlation of mean drop size and minimum drop size with the turbulence energy dissipation and the flow in an agiated tank. Chemical Engineering Science 53, 2063-2079.

Paper 4

Modeling the pressure gradient in dense packed layer flow

Heiner Schümann, Murat Tutkun and Ole Jørgen Nydal

To be submitted.

Modeling the pressure gradient in dense packed layer flow

Heiner Schümann[1,2]*, Murat Tutkun[3,4], Ole Jørgen Nydal[1]

[1]Department of Energy and Process Engineering, Norwegian University of Science and Technology, NTNU, Trondheim, Norway
[2]Multiphase Flow Laboratory, SINTEF Petroleum AS, Trondheim, Norway
[3]Department of Fluid Flow Technology, Institute for Energy Technology, Kjeller, Norway
[4]Department of Mathematics, University of Oslo, Oslo, Norway

*Corresponding author, Email: heiner.schumann@ntnu.no

Abstract

Formation of dense packed layer flow was observed in a former experimental campaign. The dense packed layer led to a considerable increase in the pressure drop that could neither be predicted by the stratified two-fluid model nor by the homogeneous flow assumption. A simple model to predict the pressure gradient in semi dispersed flow is presented. The model is based on an extension of the stratified two-fluid model. Comparison with experimental data resulted in good agreement. This work shows the need for also considering the dispersed fluid in order to capture the physics of semi dispersed flow. A drawback of the presented approach is that it relies on the knowledge about the local entrainment. This work motivates to develop an entrainment model in order to fully solve the dense packed layer problem.

1. Introduction

In oil-water transport systems the formation of dispersions of either oil droplets in water or water droplets in oil is common. The dispersion process is often generated or intensified by the application of pumps and valves or instabilities in the flow itself. Also, a dispersion might already evolve in the reservoir.(Cabellos et al., 2009)

Practical consequences can be problems as increased frictional pressure loss and difficulties during post-transport separation, but also advantages as for instance drag reduction effects. The effect of dispersion on the horizontal pressure drop has been studied by for instance Angeli and Hewitt (1999), Arirachakaran et al. (1989), Nädler and Mewes (1997) or (Pal, 1993).

In previously performed experiments (Schümann et al.) droplet settling and a partly separation of dispersed flow created in an inlet mixer in a horizontal test section was observed. The resulting semi dispersed flow forming a characteristic dense packed layer led to a distinct pressure loss exceeding that of both stratified and fully dispersed flow.

The object of this paper is to investigate a possibility of modeling the pressure drop in such dense packed layer flows. A complete multiphase flow model consists of several parts determining the flow pattern, in-situ phase fractions and finally pressure gradient. In this work, only the last part, computation of the pressure gradient, should be considered. Therefore, we take knowledge about the correct flow regime and in-situ phase fractions as granted.

In a study by (Smith et al., 2015) semi dispersed oil-water flow was modeled by considering two layers: a continuous oil layer and a continuous water layer. The emulsion layer was considered as of type oil droplets in water only and hence mixture properties were used for the water continuous layer.

Our approach, in contrast, is to check if a simple extension of the traditional stratified two-fluid model including a third, dense packed layer will improve predictions. The extended two-fluid model will be described in section 2. Model development. In section 3. Model verification the performance of the new model is verified by comparison with experimental data and the classical stratified two-fluid model and homogeneous flow model.

2. Model development

The stratified two-fluid flow model, consisting of an oil layer on top of a water layer, is taken as starting point. This geometry is extended by a third layer, representing the dense packed droplet section, as shown by Figure 1. Even if a curved interface is indicated in some literature (Lovick and Angeli, 2004; Valle and Kvandal, 1995), for simplicity, we assume straight horizontal interfaces. A curved interface is considered by for instance (Brauner, 2003).

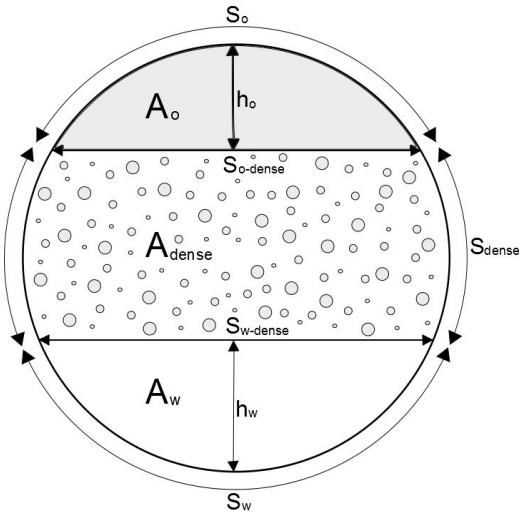

Figure 1: Geometry of the dense packed layer model.

A further simplification is the assumption that the dispersed phase fraction, Φ, is constant within the dense packed layer. This would be justified for low flow rates when the gravitational force dominates, but at the same time the coalescence frequency is rather small keeping the droplets dispersed. The local phase fractions for oil, ε_o, and water, ε_w, in the dense packed layer are then set equal to those required for phase inversion. Similar, this assumption was made by (Smith et al., 2015) for the dispersed region close to the oil-water interface. By this assumption in our model the problem becomes independent of the kind of dispersion. The ratio of oil to water at phase inversion, which is a characteristic of the system, is constant and independent of the previous continuity of the flow. It is therefore insignificant if the dense packed layer is of oil continuous, water continuous or dual continuous type. The oil to water ratio required for phase inversion has to be known for the system. Correlations exist but are rather uncertain (Arirachakaran et al., 1989; Brauner, 2003).

As the phase fraction also the effective viscosity, μ_{mix}, of the dense packed layer is assumed to be constant. A widely-used model by (Pal and Rhodes, 1989) is used here:

$$\mu_{mix} = \mu_c \left[1 + \frac{0.8415\Phi / \Phi_{\mu_r=100}}{1 - 0.8415\Phi / \Phi_{\mu_r=100}} \right]^{2.5} \quad (1)$$

In equation (1) μ_c is the viscosity of the continuous phase. $\Phi_{\mu_r=100}$ is the dispersed phase fraction when the mixture viscosity exceeds hundred times that of the continuous phase. $\Phi_{\mu_r=100} = 0.765$ was proposed by (Søntvedt and Valle, 1994). Here a water-continuous phase was considered. This was in good agreement with the observations from the experiments and is also mentioned by (Smith et al., 2015). It is known that the frictional pressure gradient and hence the effective viscosity reaches a peak value at phase inversion ((Angeli and Hewitt, 1999; Arirachakaran et al., 1989; Nädler and Mewes, 1997; Pal, 1993)). Therefore, the correct prediction of this peak by the chosen effective viscosity model is essential.

The mixture density can be calculated from:

$$\rho_{dense} = \varepsilon_{o\_dense}\rho_o + \varepsilon_{w\_dense}\rho_w \quad (2)$$

where ϵ_{w_dense} and ϵ_{o_dense} are water and oil fractions in the dense packed layer respectively and $\varepsilon_{o\_dense} + \varepsilon_{w\_dense} = 1$.

The amount of entrained liquid has to be known in order to define the position of the interfaces. An entrainment model would be required for this purpose and has to be studied separately. The entrainment model used in the point model by (Smith et al., 2015) did not perform well for their experiments. As oil-water flow can have considerably long developing lengths an entrainment model should probably consider the state of the development and the upstream history (mixing as a result of the dynamics of the flow or enhanced mixing by valves and pumps) of the flow. In this study the interface positions were known from line fraction measurements and video recordings available for the experimental data used for comparison. This allows computing the perimeters (S_o, S_{dense} and S_w) and areas occupied by each layer in the cross section (A_o, A_{dense} and A_w) as shown in Figure 1. The dense packed layer can now be handled as separate phase with individual fluid properties (see Figure 2). The total local phase fractions obtained by this method agreed well with those obtained experimentally. The absolute deviations were within ± 0.03.

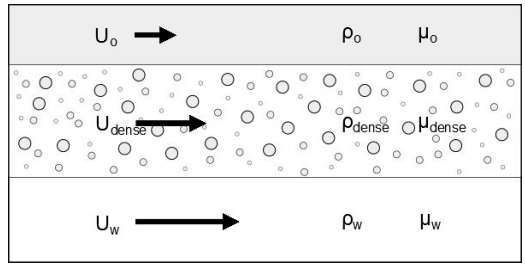

Figure 2: Model considerations, the dense packed layer is handled as separate phase.

From continuity of the phases equation (3) and (4) are given for the bulk velocities of each layer:

$$U_w = \frac{Q_w - U_{dense}A_{dense}\varepsilon_{w\_dense}}{A_w} \quad (3)$$

$$U_o = \frac{Q_o - U_{dense}A_{dense}\varepsilon_{o\_dense}}{A_o} \quad (4)$$

By assuming equation (5):

$$U_{dense} = \frac{U_o + U_w}{2} \quad (5)$$

the bulk velocities can be computed directly. This assumption is based on visual observations from our experiments with medium viscosity oil showing that $U_o < U_{dense} < U_w$. However, if the oil viscosity is low and the perimeter of the dense packed layer, S_{dense}, is large, it is possible that the oil bulk velocity exceeds U_{dense}.

The problem can now be solved for the pressure loss. We applied a relatively simple method as described by Arirachakaran et al. (1989). The partial pressure loss for each phase is computed as if the phase would occupy the entire cross section. The total frictional pressure gradient is then computed as the sum of the single phase pressure gradients for each phase multiplied with the perimeter fractions wetted by the respective phase:

$$\left(\frac{dp}{dz}\right)_{total} = \frac{S_o}{S}\left(\frac{dp}{dz}\right)_o + \frac{S_{dense}}{S}\left(\frac{dp}{dz}\right)_{dense} + \frac{S_w}{S}\left(\frac{dp}{dz}\right)_w \quad (6)$$

Here, the single phase pressure gradients are given by:

$$\left(\frac{dp}{dz}\right)_i = \frac{f_i \rho_i U_i^2}{2D} \quad (7)$$

In equation (7) the friction factor f is obtained by solving the Hagen-Poiseuille equation for laminar flow or the Colebrook equation if the flow is turbulent, with the Reynolds number given by equation (8).

$$\mathrm{Re}_i = \frac{\rho_i U_i D}{\mu_i} \quad (8)$$

In the computation above the pipe inner diameter D was used. Also a computation with a hydraulic diameter, D_h, as suggested by (Brauner, 2003) was tested. The results were, however, not improved by this approach.

3. Model verification

3.1 Experiments

The model was compared with experimental results presented earlier by Schümann et al. (). A static mixer installed at the inlet of a transparent horizontal test section premixed the phases. Depending on the mixture velocity the flow separated with varying intensity downstream of the mixer, which resulted in various flow regimes. Dense packed layer flow was typically observed for mixture velocities of $0.3\ m/s \leq U_{mix} \leq 0.6\ m/s$. Example pictures are shown in Figure 3.

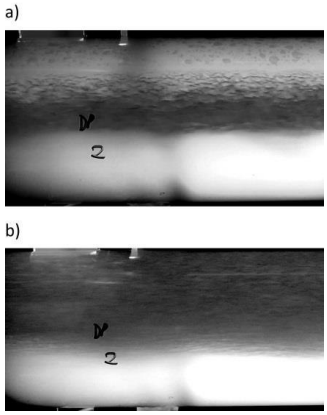

Figure 3: Dense packed layer flow: a) oil - dense packed layer - water, b) dense packed layer - water.

Clear boundaries dividing the dense packed layer and droplet free layers can be observed. The test section had an inner diameter of $D = 10\ cm$. Oil viscosities of $\mu_o = 35\ mPa*s$, $60\ mPa*s$ and $120\ mPa*s$ were tested. Pressure and local phase fraction measurements compared in this paper were taken approximately $20\ m$ $(L/D = 200)$ downstream of the inlet.

3.2 Comparison models

Beside the presented model the data is also compared with the classical stratified two-fluid model and the homogenous flow model.

The two-fluid model was solved analogue as described above. In this case the dense packed layer disappears. With given local phase fractions the velocities U_o and U_w are explicitly known. The dense packed layer flow model is consistent with the two-fluid model in the case of stratified flow when no flow dispersion occurs. The stratified two-fluid model predicted well stratified flow. All predicted values were within the measurement uncertainty.

The homogeneous flow model assumes fully dispersed, well mixed flow. The pressure gradient is computed as for single phase flow considering the mixture density, mixture velocity and an effective viscosity, that we, again, model regarding to (Pal and Rhodes, 1989). Also this model performed well when compared with fully dispersed data at high mixture velocities. Only for input water fractions in the phase inversion region the agreement became worse. It is most likely the performance of the Pal model for the effective viscosity leading to higher deviations. But here it has to be mentioned that the experiments showed a slight gradient in the phase fractions measured over the cross-section, thus, the flow was not completely homogeneous.

3.3 Comparison results

Figure 4 shows pressure gradient measurements together with predictions from the tested models versus the input

water fraction at constant mixture velocity $U_{mix} = 0.5\ m/s$. The oil viscosity was $\mu_o = 60\ mPa*s$ in this case. The example well reflects the general behavior of the three tested models when dense packed layer flow was predicted. The flow patterns observed during the experiments are indicated in the figure. In the shown example a dense packed layer was present at input water fractions $f_w > 0.3$. At high input water fractions the free oil layer disappeared and the dense packed layer wetted the complete upper pipe wall. At this transition, the measurements reach a peak value.

The stratified two-fluid model predicts a pressure gradient smoothly decreasing with increasing input water fraction. As soon as a dense packed layer develops the pressure gradient is under-predicted, because the increasing effective viscosity in this emerging layer is not considered. The homogeneous flow model under-predicts the pressure gradient even more at dense packed layer flow. At an input water fraction, $f_w = 0.2$ the for phase inversion typical peak is shown. Only the dense packed layer model is able to predict a higher pressure gradient as a dense packed layer evolves. Also the peak when the oil layer disappears is predicted. The model over-predicted pressure gradients when the effective viscosity model by Pal was implemented (which gives $\mu_{dense} = 200\ mPa*s$ at $f_w = 0.2$). The experimental data could be matched by assuming a constant viscosity of $\mu_{dense} = 140\ mPa*s$. (Smith et al., 2015) used Brinkman's correlation (Brinkman, 1952):

$$\mu_{mix} = \mu_c \left(1-\Phi\right)^{-2.5} \tag{9}$$

This, however, would result in a too low effective viscosity. Another reason could be a slightly wrong dispersed phase fraction assumed in the dense packed layer. The viscosity correlation by Pal predicts a steep increase for high dispersed phase fractions. An effective viscosity of $\mu_{dense} = 140\ mPa*s$ can be matched by changing the dispersed phase fraction by just 2% ($\Phi = 0.78$ instead of 0.8).

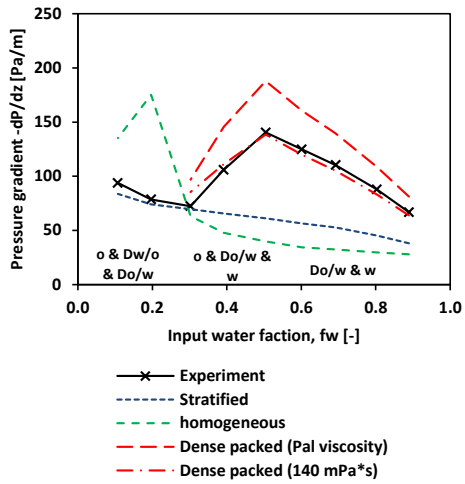

Figure 4: Pressure gradient versus input water fraction for U_{mix} = 0.5 m/s and an oil viscosity of 60 mPa*s.

A comparison of predicted and measured pressure gradients for all experimental casees where a dense packed layer was present is shown in Figure 5 for the three tested models. The matched viscosity was used for the dense packed layer model. We see that the under-prediction by the stratified two-fluid model is more serious for oil with lower viscosity. In these cases the influence of the dense packed layer becomes more significant. The correctness of the homogeneous flow model instead appears to be independent of the oil viscosity. This is because the model, applying the effective viscosity model by Pal, considers the continuous phase viscosity only, which is the one of water for most of the cases. The dense packed layer model in general predicts the pressure gradient well. 78% of the predictions are within $\pm 20\%$ error margins and 90% within $\pm 30\%$. The highest absolute deviations were obtained for cases with mixture velocities $U_{mix} > 0.5$. Here the droplets are wider spread over the cross-section and the assumption of a dense packed layer probably does not apply anymore.

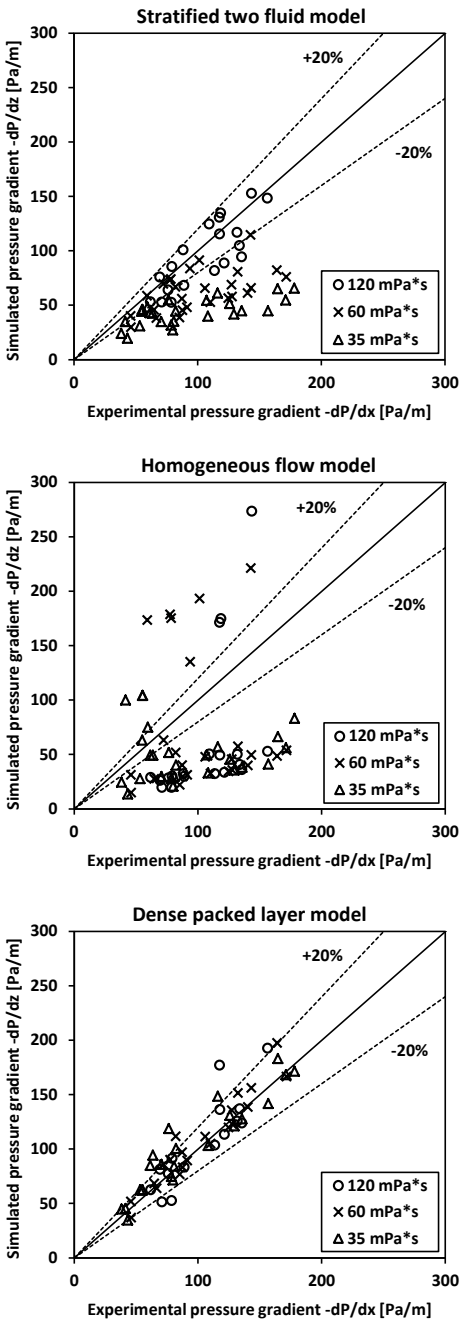

Figure 5: Model versus experiment for experimental cases where a dense packed layer was present.

4. Conclusion

The stratified two-fluid model has been extended by adding a third layer which represents a dense packed layer. A constant phase fraction distribution within the dense packed layer was assumed. The phase fractions were similar to that needed for phase inversion. With this simplified model a higher pressure gradient was predicted as it would be the case for the classical two-fluid model. The model was able to well predict the effect of the higher effective viscosity within the dense packed layer, and thus increased friction losses at the pipe wall wetted by this layer. From comparison with experimental data it was found that the effective viscosity model by Pal and Rhodes (1989) over-predicts the effective viscosity within the dense packed layer. By fitting the data an effective viscosity of $\mu_{dense} = 140\ mPa * s$ is proposed which gave good results for the most cases.

The proposed model only predicts the computation of the pressure gradient assuming the amount of dispersion is known. An entrainment model considering the development of the flow would be needed in order to completely model dense packed layer flow.

5. Nomenclature

A	cross sectional area
D	pipe inner diameter
f	friction factor
f_w	input water fraction
h	vertical height of a layer
L	length
P	pressure
Q	volumetric flow rate
S	interface/perimeter
U	bulk velocity
Re	Reynolds number
ϵ	local phase fraction
μ	viscosity
ρ	density
Φ	dispersed phase fraction

Subscripts

c	continuous
$dense$	dense packed layer
h	hydraulic
mix	mixture
o	oil
w	water

6. Acknowledgements

The authors acknowledge the financial support from The Multiphase Flow Assurance Innovation Centre (FACE). FACE is a research cooperation between IFE, NTNU and SINTEF. The center is funded by The Research Council of Norway and by the following industrial partners: Statoil ASA, GE Oil & Gas, SPT Group - A Schlumberger Company, FMC Technologies, CD-adapco, Shell Technology Norway.

7. References

Angeli, P., Hewitt, G.F., 1999. Pressure gradient in horizontal liquid-liquid flows. Int J Multiphas Flow 24, 1183-1203. http://dx.doi.org/10.1016/S0301-9322(98)00006-8

Arirachakaran, S., Oglesby, K.D., Malinowsky, M.S., Shoham, O., Brill, J.P., 1989. An Analysis of Oil/Water Flow Phenomena in Horizontal Pipes. SPE Production Operations Symposium, Oklahoma City. Society of Petroleum Engineers. http://dx.doi.org/10.2118/18836-MS

Brauner, N., 2003. Liquid-Liquid Two-Phase Flow Systems, Modelling and Experimentation in Two-Phase Flow. Springer Vienna, pp. 221-279.

Brinkman, H.C., 1952. The viscosity of concentrated suspensions and solutions. J. Chem. Phys. 20, 571-581.

Cabellos, E.M., Carvalho, M.S., Ponce, R.V., 2009. Oil-in-water emulsion formation in laminar flow through capillaries. 20th International Congress of Mechanical Engineering, Gramado.

Lovick, J., Angeli, P., 2004. Experimental studies on the dual continuous flow pattern in oil-water flows. Int J Multiphas Flow 30, 139-157. http://dx.doi.org/10.1016/j.ijmultiphaseflow.2003.11.011

Nädler, M., Mewes, D., 1997. Flow induced emulsification in the flow of two immiscible liquids in horizontal pipes. Int J Multiphas Flow 23, 55-68. http://dx.doi.org/10.1016/S0301-9322(96)00055-9

Pal, R., 1993. Pipeline Flow of Unstable and Surfactant-Stabilized Emulsions. AIChE Journal 39, 1754-1764. DOI: 10.1002/aic.690391103

Pal, R., Rhodes, E., 1989. Viscosity/Concentration Relationships for Emulsions. Journal of Rheology 33, 1021-1045. http://dx.doi.org/10.1122/1.550044

Schümann, H., Tutkun, M., Yang, Z., Nydal, O.J., Experimental study of dispersed oil-water flow in a horizontal pipe with enhanced inlet mixing, Part 1: Flow paterns, phase distributions and pressure gradients. Submitted to the Journal of Petroleum Science and Engineering.

Smith, I.E., Nossen, J., Kjølaas, J., Lund, B., 2015. Development of a Steady-State Model for Prediction of Gas/Oil and Water/Oil Pipe Flow. Journal of Dispersion Science and Technology 36, 1394-1406. http://dx.doi.org/10.1080/01932691.2014.989568

Søntvedt, T., Valle, A., 1994. Capacities of Troll Oil Flow Lines wit High Water Cuts. Predictions based upon Recorded Pipe Flow Friction Factors for Stable Troll Oil Dispersions, Report no. R-068557, Norsk Hydro ASA, Norway.

Valle, A., Kvandal, H.K., 1995. Pressure drop and dispersion characteristics of separated oil-water flow. International Symposium on Two-Phase Flow Modelling and Experimentation, Rome.

Paper 5

Oil-water pipe flow development after a valve

Heiner Schümann, Pankaj Chandra and Ole Jørgen Nydal

Accepted for presentation at the
9th International Conference on Multiphase Flow
May 22nd – 27th, 2016, Firenze, Italy

Is not included due to copyright

Paper 6

Oil-Water Flushing Experiments with Complex Pipe Geometry

Heiner Schümann, Milad Kazemihatami and Ole Jørgen Nydal

Proceedings of the
8th International Conference on Multiphase Flow
May 26th – 31th, 2013, Jeju, Korea

Is not included due to copyright

Paper 7

Liquid-liquid displacement in a horizontal and inclined pipe section

---

Heiner Schümann, Milad Kazemihatami, Zhilin Yang, Mariana Diaz
and Ole Jørgen Nydal

Proceedings of the
9th North American Conference on Multiphase Technology,
11-13 June, Banff, Canada
One Petro: BHR-2014-A1

Liquid-liquid displacement in a horizontal and inclined pipe section

H Schümann[1], M Kazemihatemi[1], Z Yang[1,2], M Diaz[1], O J Nydal[1]
[1] *Department of Energy and Process Engineering, Norwegian University of Science and Technology, Norway*
[2] *Research, Development and Innovation, Statoil ASA, Norway*

ABSTRACT

In this paper experimental results from liquid-liquid displacement experiments are presented. Four scenarios, flushing oil with water and flushing water with oil, in a horizontal and downward inclined test section, respectively, were tested at different flow rates. The transparent test section of 15 m length and 60 mm ID allowed for visualization of the flushing front. The flushing front propagation velocity was measured by conductivity ring probes. The liquids were tap water and a mineral oil with a viscosity of 60 cP. The experimental results are compared with the commercial flow simulator OLGA.

1 INTRODUCTION

In a liquid dominant production flow line, one of the phases, either oil or water can accumulate due to uneven topology of the flow line and low production rate. The extreme scenario is a production stop. An accumulation of one phase can either increase the risk of hydrate formation (water phase accumulation), or make the production restart difficult (viscous oil phase accumulation).

Only a few cases of liquid-liquid displacement experiments are reported in literature. Displacement of trapped water by oil in low spots of pipelines was experimentally investigated by Xu et al. [1]. A critical minimal flow rate for the onset of water displacement, depending on the pipe diameter, was identified. Furthermore, a model based on the mechanism of plug formation was developed. Twerda et al. [2] investigated cool down and cold restart behaviour of high viscosity oil in a 2" test section. Experiments were compared with the CFD code Fluent and the flow simulator OLGA. Both codes predicted the cool down behaviour after shut down well. However, predicting the transient behaviour during restart was found to be more difficult. While OLGA predicted the arrival of the flushing fluid delayed, Fluent showed an under-prediction of the arrival time. The plug flow assumption was mentioned to be the main reason for this over-prediction of restart time by the OLGA code [3].

Flushing experiments in complex geometries with horizontal and vertical flow sections (subsea jumper) with the background in hydrate inhibition were presented by Cagney et al. [4] and Dellecase et al. [5].

In a previews study [6] displacement experiments with low viscosity oil and water in a jumper pipe geometry have shown the complexity of the flow. Comparison with simulations showed the largest discrepancy for low flow rates. Therefore, the present study focuses on displacement experiments with low flow rates (U_S < 0.5 m/s). For a better understanding of the influence of individual flow parameters the pipe geometry was kept simple and the test cases were well defined. The flushing front propagation in a straight pipe was investigated. The flushing liquid, flow rate and the inclination of the pipe were varied.

2 EXPERIMENTAL SETUP

2.1 Facility

The experiments were performed in the Multiphase Flow Laboratory at the Norwegian University of Science and Technology, NTNU. The facility provides test sections with different ID and shapes. An inclinable, straight test section of 15m length and 60 mm ID was used. The test section ended in a slug catcher before entering a liquid-gas separator and the final liquid-liquid separator in the basement of the building. The liquids were pumped separately by centrifugal pumps, available in different sizes depending on the flow rate, before they were mixed in a V-shape mixer at the test section inlet. For the reported experiments an inlet section of approximately 2 m length was installed to provide the possibility of initial conditions as described in 2.3. The inlet section was connected to the V-shape mixer and the test section by flexible hoses of the same ID. That allowed inclining the inlet section by any angle. Figure 1 shows a sketch of the flow loop. Not shown in the sketch is a short up-and-down section at the end of the test section preventing gas entrainment from the slug catcher.

The flow rate was controlled by setting the pump frequency as well as by pneumatic valves. Coriolis and electromagnetic flow meters in different ranges were used to measure the flow rate. The specifications of the pumps and flow meters are given in Appendix A. Conductivity ring probes were installed at several positions along the test section. These probes can reliably measure the local water fraction for stratified flow, which was the case for the reported experiments. The accuracy of the local water fraction measurements with conductivity ring probes depends on several factors. The main factors are the fluctuation of the electronics due to environmental conditions and the saturation of the signal which results in a small signal drift. Furthermore the precision of the manually performed calibration, noise of the signal and the assumption that the flow is perfectly or close to stratified play a role. A calibration curve and error calculation are given in Appendix B. The absolute upper limit of uncertainty was estimated to be less than 5% for the local water fraction measurements.

2.2 Liquids

Tap water and a mineral oil were the two test liquids. Fluorescence powder was added to the water in order to better distinguish between the two liquids. Viscosity measurements of the water confirmed that the fluorescence powder did not change the rheology. Also the powder does not react with the oil. The medium viscous mineral oil was a mixture of Exxsol D60 and Nexbase 3080 with a measured density of 840 kg/m^3 and a viscosity of 60 cP measured at room temperature (22 °C) by an AR-G2 rheometer by TA Instruments.

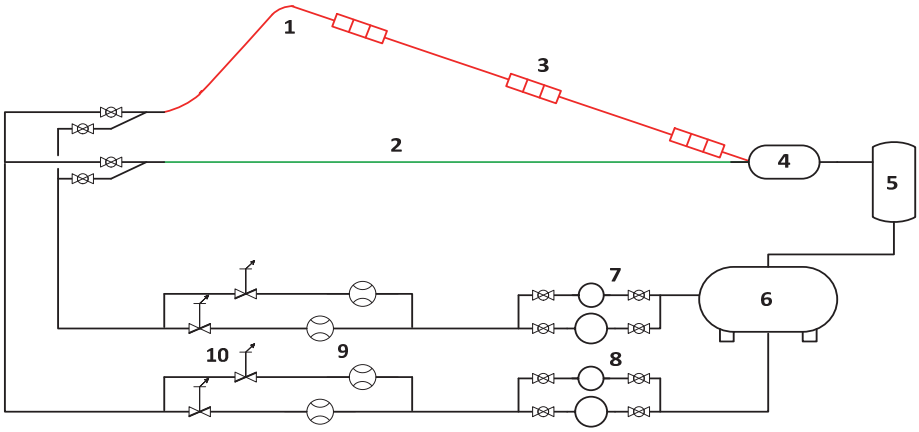

1. Test section
2. Bypass section
3. Conductance probe
4. Slug catcher
5. Liquid-gas separator
6. Separator tank
7. Centrifugal oil pumps
8. Centrifugal water pumps
9. Flow meters
10. Remote controlled flow valves

Figure 1: Flow loop facility.

2.3 Procedure

Every experiment was started from a specific initial condition that was the test section filled with liquid A and a short standing column of liquid B in the inclined inlet section. This condition was achieved by flushing the test section with liquid A at a high flow rate. The flow was then stopped and liquid B was carefully injected at a very low flow rate until the desired position in the inclined test section was reached. Depending on the scenario, flushing with oil or flushing with water, the inlet section was upward or downward inclined. The inlet section was added to ensure that the flow rate had enough time to accelerate and stabilize before the flushing front reached the test section. Furthermore the relatively steep inclination (26°) ensured that the flushing front was sharp when reaching the test section. This was due to gravitational forces predominating in the steeply inclined pipe at low flow rates.

When the initial condition was reached liquid B was bypassed as shown in Figure 1 and the flow rate was adjusted. When the desired flow rate was reached, the flow was abruptly routed to the test section by manually operated valves. An experiment was stopped when the test section was completely flushed or the local water fraction measurements from the conductivity ring probes did not show a significant change anymore.

3 RESULTS

Four scenarios were tested. For the first two scenarios the test section was in horizontal alignment and the pipe, initially filled with liquid A, was flushed by liquid B. We will call these scenarios HW for the case flushing with water and HO for the case flushing with oil. In scenario three and four the test section was slightly downward inclined by 2.8°. Again, in scenario three, IW, the pipe initially filled with oil was flushed by water. However, scenario four was slightly different. Due to the setup and the operational conditions of the flow loop in this scenario an oil plug standing in the elbow of the apart from that water filled pipe was flushed by water. In this case, the scenario will be called

IO followed by the initial length of the oil plug while the fluid was in rest. Figure 2 is showing a sketch of the initial condition for each scenario.

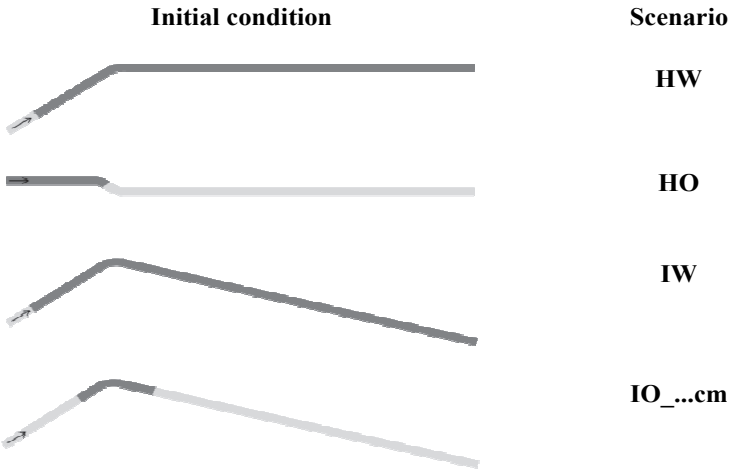

Figure 2: Initial conditions for each scenario.

From the local water fraction time series by the conductivity ring probes averaged flushing front propagation velocities were computed by:

$$U_F = \frac{s_{12}}{t_{5\%\_C2} - t_{5\%\_C1}}$$

with:

U_F	Flushing front propagation velocity
$t_{5\%\_C1\,/C2}$	Time when the normalized signal of the first/second probe exceeds 5% (95% in the case flushing with oil)
s_{12}	Separation distance between the first and the second probe.

For scenario HW the conductivity ring probes were placed 2.15 m, 4.70 m and 7.25 m downstream of the beginning of the test section. For scenario HO, IW and IO the conductivity ring probes were placed 2.15 m, 6.70 m and 13.78 m downstream of the beginning of the test section. An experimental overview including the averaged front propagation velocities is given in Appendix C.

Figure 3 shows a picture of a typical flushing front. The flow can be considered as stratified.

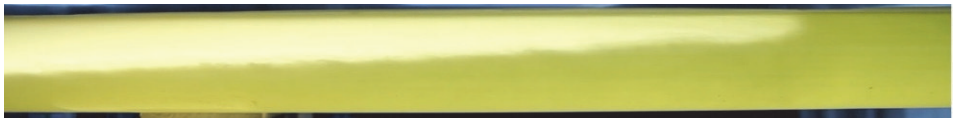

Figure 3: Flushing front experiment IO_190cm, U_S = 0.421 m/s.

Figure 4 (left) shows the normalized flushing front propagation velocity vs. superficial velocity for each scenario. For each superficial velocity two front propagation velocities, averaged between the first and second and between the second and third conductance

ring probe respectively, are given. Figure 4 (right) shows a sample time series of the local water fraction measurements for each scenario.

3.1 Scenario HW – oil flushed by water in a horizontal test section

Except of the lowest flow rate the two averaged propagation velocities are very similar. Therefore, the flushing front can be expected to propagate at constant velocity. A clear trend of decreasing ratio U_F/U_S with increasing superficial velocity was found. This indicates that the flushing front becomes steeper with increasing flow rate of the flushing liquid. This trend is expected to continue approaching a constant ratio for higher flow rates. A ratio of unity would indicate that the flushing front is moving with the same velocity as the superficial velocity of the flushing liquid. In this case, the flushing front could simply be modelled as plug flow. However, for all the flow rates tested, this was not the case. Even if only displaying the oil-water interface passing a fixed location, the time series of the local water fraction give an impression of the shape of the flushing front. The first water arrives in a steep front followed by a slow increase in water fraction. Even after 150 sec the water fraction has just reached 0.6. Since the pipe section is not fully filled with water the ratio U_F/U_S has to be larger unity which was the case for all experiments of this scenario.

3.2 Scenario HO – water flushed by oil in a horizontal test section

Two experiments in the horizontal test section with oil as flushing liquid and water as the initial liquid were performed. Already at the low superficial velocities tested the ratio is close to unity. The flushing front can be considered as plug flow. The viscous oil replaces the water immediately in contrast to scenario HW where water creeps along the bottom of the pipe and slowly removes the oil. Also from the local water fraction time series one can identify the steep front. The water is replaced after only a few seconds.

3.3 Scenario IW – oil flushed by water in a 2.8 ° downward inclined test section

Two flow rates were tested for scenario IW. The first and the second front propagation velocity are almost identical for each experiment respectively. The front propagates with constant velocity. Comparing experiment 3.1, U_S = 0.1 m/s, with the scenario HW, experiment 1.2, the inclination of the test section was the only difference. The ratio U_F/U_S matches well for both experiments. One could expect that the small inclination angle has no effect on the flushing behaviour. However, comparing the time series for the local water fraction the inclined pipe experiment gives a much steeper flushing front that suddenly flattens out while the water fraction for the horizontal pipe increases continuously. In the inclined case buoyancy forces become important acting on the oil phase against the flow direction which leads to an oil layer of constant thickness on top of the water layer.

3.4 Scenario IO – oil plug flushed by water in a 2.8 ° downward inclined test section

Scenario IO was different compared to the other experiments in the way that a short plug of oil surrounded by water was flushed through the test section. Now, the oil plug was free to develop at both ends. Experiments with various superficial velocities and different lengths of the initial oil plug were performed.

The results for this scenario in Figure 4 show a wide spread of the data. However, the ratio U_F/U_S is clearly increasing with increasing superficial velocity. The first flushing front propagation velocity was in general larger than the second propagation velocity measured further downstream. Comparing experiments with constant superficial velocity but different initial oil plug length shows that a larger plug length results in a larger ratio U_F/U_S.

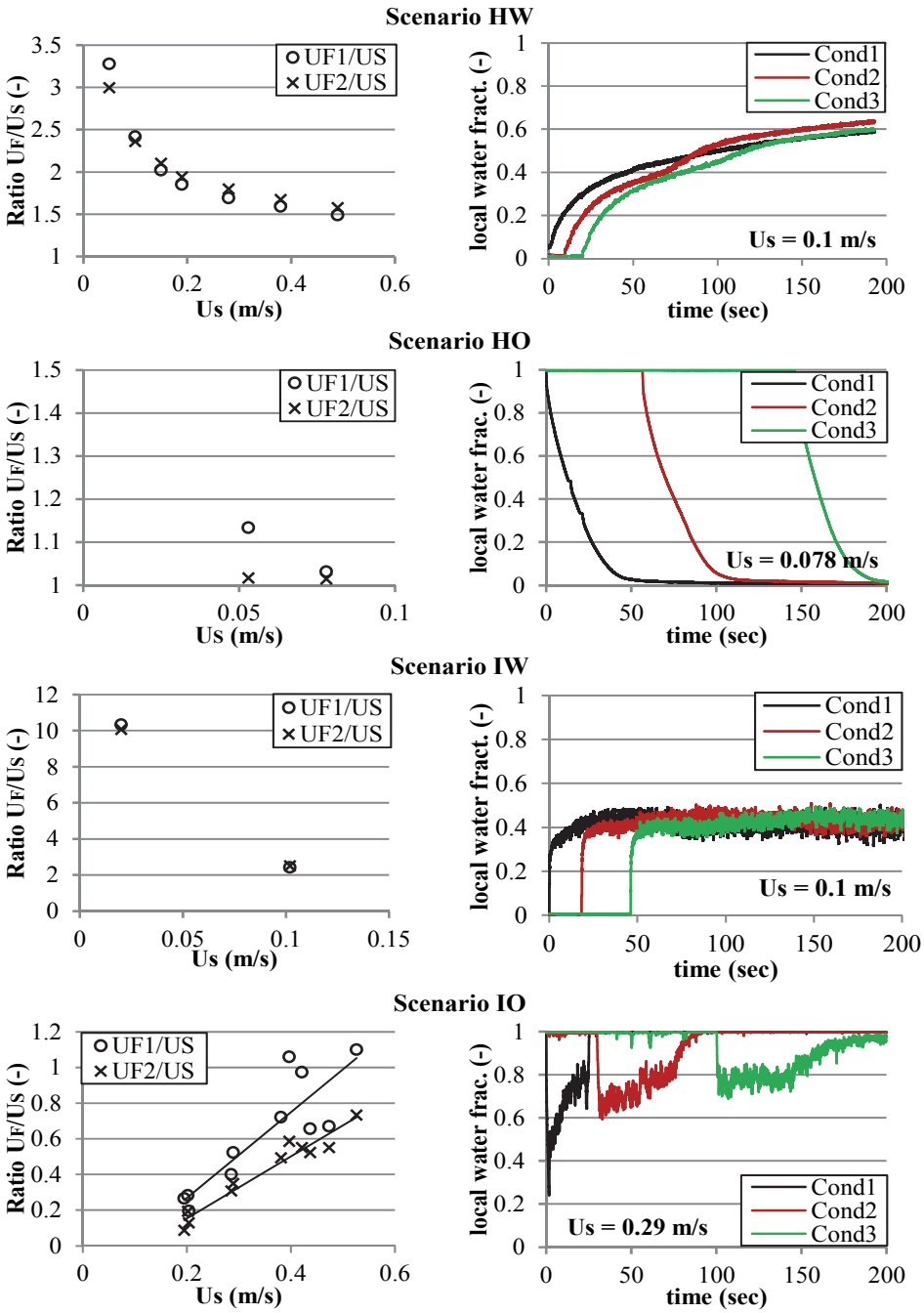

Figure 4: Experimental results sorted by scenario; (left side) Ratio U_F/U_S vs. U_S, (right side) selected time series for the local water fraction.

From the time series for the local water fraction, shown for experiment 4.6, one can observe the development of the flushing front and the plug in general. As soon as the flushing operation is initiated the bulk of the oil is moving with superficial flushing velocity or slightly faster since the oil plug becomes stretched. At a certain point of time the water will break through the plug and the oil phase is not filling the whole cross section anymore. Water will pass the plug at the bottom of the pipe. The oil phase will be driven downstream by slip while buoyancy forces are acting in opposite direction. This explains a ratio U_F/U_S smaller than unity except of two measurements. For these two measurements the plug was certainly still filling the whole cross section. This is supported by the fact that a positive ratio was only observed for the two longest plugs.

4 COMPARISON WITH THE SIMULATION TOOL OLGA

The experiments were compared with the commercial flow simulator OLGA 7.1. Both the standard OLGA and the OLGA HD flow model were tested. The flushing front propagation velocities predicted by OLGA compared with the experiments for all four scenarios are shown in Figure 5. Only the flushing front further downstream was compared.

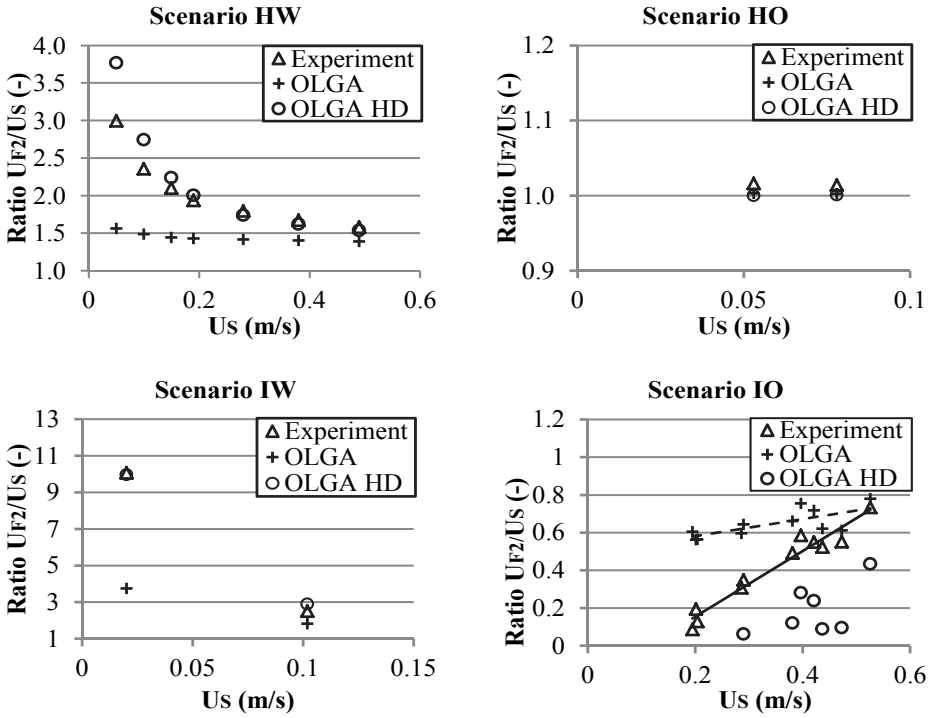

Figure 5: Experimental results compared with OLGA.

For the scenarios HW, HO and IW the standard OLGA model predicted a lower flushing front propagation velocity than measured in the experiments. While the error is rather small for scenario HO where water is flushed by oil with a higher viscosity, the error is large for the scenarios where water is flushing the oil. A low superficial velocity resulted in a large deviation, while the prediction improved with increasing flow rate. For

scenario IO where the flushing front propagation velocity was smaller than the superficial velocity, OLGA predicted a faster front propagation than measured in the experiments. In general it was found that the flushing front propagation velocity predicted by OLGA was closer to the superficial velocity than measured in the experiments in all cases. Comparing experiments with the OLGA HD model good agreement was achieved for the scenarios HW, HO and IW. Larger deviations were only found for the lowest superficial velocities in scenario HW. Here, the flushing front propagation velocity was overestimated. For scenario IO the flushing front propagation velocity was underestimated. Also, in case of the lowest superficial velocities the OLGA HD model predicted a standing oil bubble and flushing was not achieved at all.

An explanation for the large deviation of standard OLGA results can be found comparing the shape of the flushing fronts predicted and observed in the experiments, Figure 6. The standard OLGA model tends to predict a flushing front much steeper than the experiment, hence a flushing behaviour close to plug flow. That means that the arrival time of the flushing front is over-predicted (except of scenario IO), while the total replacement time is under-predicted. This is in agreement with the results of [2] and explains the better agreement of the results for scenario HO and for higher flow rates where the flushing behaviour was closer to plug flow.

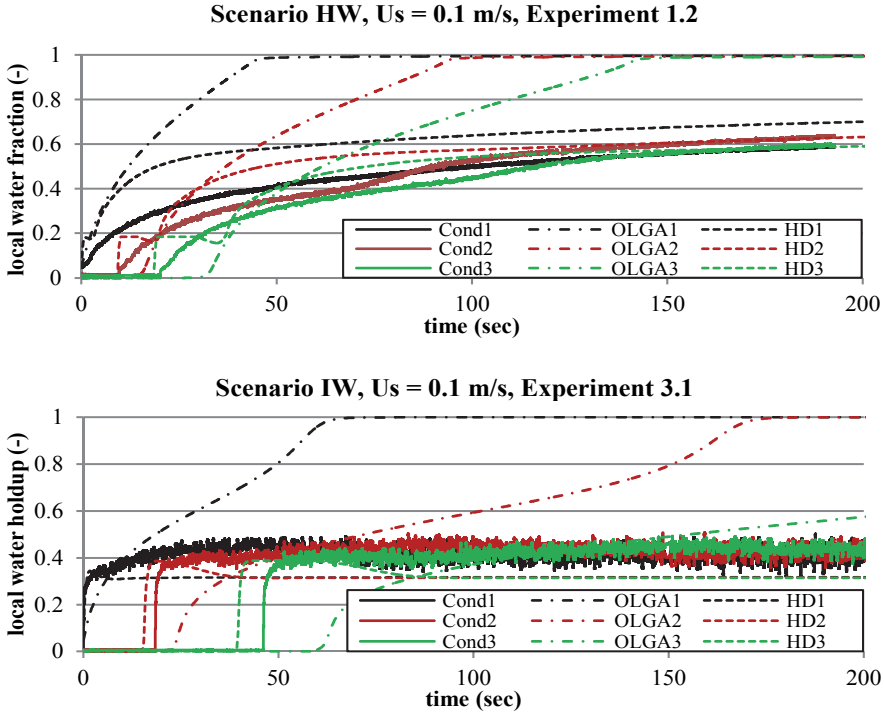

Figure 6: Comparison of local water fraction time series.

In contrast, the shape of the flushing front predicted by the OLGA HD model is very close to the experiments. OLGA HD is able to much better predict details like the final local water fraction and therewith an incomplete flushing behaviour. The one-dimensional equations of the standard OLGA model apply bulk balances over the phases, which lead to a loss of information. Dimensionless correlations based on experimental data, as used in these models, are often difficult to extrapolate [7]. The OLGA HD model

introduces friction and velocity shape factors considering a velocity distribution over the cross section which agrees with the log law at the wall and a generalized log law at an interface [8]. It seems that this model much better predicts the slip between the phases which leads to considerable improvement of the predicted flushing behaviour.

5 CONCLUSION

Liquid-liquid displacement experiments in a horizontal and slightly downward inclined test section were performed. Both scenarios, water displacement by medium viscosity oil and oil displacement by water, were tested. Clear trends were observed:

- Displacement of a low viscosity liquid by a higher viscosity liquid is more effective than the opposite scenario.
- The flushing front becomes steeper with increasing flow rate. In contrast, the flushing front propagation velocity normalized by the superficial velocity decreases with increasing flow rate.
- Buoyancy/gravitational forces acting in the direction of the flow in inclined pipes will influence the flushing behaviour.
- Displacement of an oil plug is a complex behaviour. The development of the liquid interfaces at both ends will lead to a stretching of the plug.

All scenarios were simulated with the standard OLGA model as well as the OLGA HD model. Comparison of the predictions with the experiments showed that OLGA is able to predict the correct trends. However partially large deviations were observed. The predictions were considerably improved when the OLGA HD model was applied.

- Standard OLGA was able to very well predict water displacement by oil, where the oil has a higher viscosity than the water.
- Displacement of oil by water showed a prediction of a too steep flushing front and too slow flushing front propagation velocities for the standard OLGA model. This equals an over-prediction of the total displacement behaviour.
- Results by OLGA improve as the flow rate increases and the displacement behaviour can be considered as plug flow.
- The OLGA HD model agrees very well with the experiments for most of the cases. The approach of considering a velocity profile over the cross section seems to be better suited for this kind of problem, where the slip between the phases is of particular importance.

6 ACKNOWLEDGEMENTS

The authors acknowledge Statoil ASA for the partial financial support. H. Schümann also acknowledges the partial financial support from The Multiphase Flow Assurance Innovation Centre (FACE). FACE is a research cooperation between IFE, NTNU and SINTEF. The centre is funded by The Research Council of Norway and by the following industrial partners: Statoil ASA, GE Oil & Gas, SPT Group - A Schlumberger Company, FMC Technologies, CD-adapco, Shell Technology Norway.

7 REFERENCES

[1] Xu, G.-l., et al., *Trapped water displacement from low sections of oil pipelines.* International Journal of Multiphase Flow, 2011. 37(1): p. 1-11.

[2] Twerda, A., et al., *Experimental and numerical assessment of cold restart process of viscous oil pipeline*, in *World Heavy Oil Congress* 2012: Aberdeen.

[3] Yang, Z., et al., *Cold restart of viscous multiphase flowline by hot water flushing*, in *16th International Conference on Multiphase Production Technology* 2013, BHR Group: Cannes.

[4] Cagney, T.L., S.C. Hare, and S.J. Svedman, *Hydrate Inhibition of Subsea Jumpers During Shut-in*, in *SPE Annual Technical Conference and Exhibition* 2006, Society of Petroleum Engineers: San Antonio.

[5] Dellecase, E., et al., *Hydrate Inhibitor Displacement Experiments in Jumper-Like Pipe Configurations* in *16th International Conference on Multiphase Production Technology* 2013, BHR Group: Cannes.

[6] Schümann, H., M. Kazemihatemi, and O.J. Nydal, *Oil-Water Flushing Experiments with Complex Pipe Geometry*, in *8th International Conference on Multiphase Flow* 2013: Jeju.

[7] Biberg, D., et al., *Basic flow modelling for long distance transport of wellstream fluids*, in *Multiphase Production Technology 14,* 2009, BHR Group: Cannes.

[8] Biberg, D. *The HD Stratified Flow Model*. in *Design og drift av flerfasesystemer for olje og gass*. 2012. Oslo: TEKNA.

8 APPENDIX

8.1 Appendix A

Table 1: Specifications of pumps and flow meters.

Assembly	Name	Principle	range
Water pump (large)	ATB Antriebstechnik G. Bauknecht AG	Centrifugal	-
Water pump (small)	ASEA MT 80A 19F100-2	Centrifugal	-
Oil pump (large)	Grundfos CR 64	Centrifugal	-
Oil pump (small)	Grundfos CR 8	Centrifugal	-
Water flow meter (large)	Fischer Porter Magnetic Flowmeter 10 DX 3311 A	Electromagnetic	0.83 – 15 l/s
Water flow meter (small)	Endress + Hauser Promag 33A	Electromagnetic	0.053 - 0.987 l/s
Oil flow meter (large)	Micro Motion T150T R 68151Z	Coriolis	1000 – 36000 kg/h
Oil flow meter (small)	Micro Motion F0255	Coriolis	0 – 1000 kg/h

8.2 Appendix B

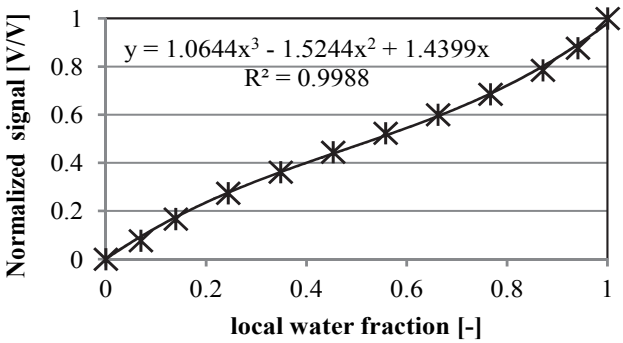

Figure 7: Sample calibration curve for a conductivity ring probe.

In this chapter a total error of the local water fraction measurements is estimated based on main elemental errors, Table 2. The elemental error e_{strat}, which results from potential droplet generation at the liquid-liquid interface, could not be measured but is expected to be small. To account for this error, the total error is multiplied with a factor of two. The equation for the final total error, R, reads then:

$$R = 2\sqrt{\sum_n {e_n}^2}$$

Table 2: Error estimation for the conductivity ring probes.

Error	Explanation	% (abs)
e_{env}	The fluctuation of the electronics due to environmental conditions was corrected for previous to a measurement. For this the offset and maximum of the signal was measured at a local water fraction H=0 and H=1 respectively. For that reason it is neglected.	-
e_{drift}	A small signal drift due to saturation of the electronics was maximum for a local water fraction of H=1.	0.89
e_{nonlin}	The behaviour of the probes is nonlinear and was modelled by a 4^{th} order polynomial function. The largest deviation of the function from the calibration data is stated.	2.15
e_{noise}	The error due to noise by the electronics + potential air bubbles in the system is expressed by the standard deviation of a steady state measurement at H=1.	0.16
e_{strat}	Error due to not perfectly stratified flow. The interface can somehow be disturbed (droplet entrainment) which will slightly change the behaviour of the probe. This can unfortunately not be corrected for.	-
R	Total error.	4.66

8.3 Appendix C

Table 3: Experimental overview.

Experiment	Scenario	U_S (m/s)	U_{f1} (m/s)	U_{f2} (m/s)
1.1	HW	0.05	0.164	0.150
1.2	HW	0.10	0.241	0.236
1.3	HW	0.15	0.303	0.315
1.4	HW	0.19	0.351	0.368
1.5	HW	0.28	0.473	0.503
1.6	HW	0.38	0.604	0.635
1.7	HW	0.49	0.729	0.773
2.1	HO	0.053	0.060	0.054
2.3	HO	0.078	0.080	0.079
3.1	IW	0.102	0.247	0.256
3.2	IW	0.020	0.209	0.203
4.1	IO_184cm	0.179	0.041	
4.2	IO_142cm	0.195	0.051	0.017
4.3	IO_69cm	0.202	0.057	0.039
4.4	IO_91cm	0.204	0.040	0.026
4.5	IO_87cm	0.286	0.114	0.088
4.6	IO_130cm	0.290	0.151	0.101
4.7	IO_133cm	0.381	0.274	0.187
4.8	IO_230cm	0.397	0.420	0.233
4.9	IO_190cm	0.421	0.409	0.232
4.10	IO_83cm	0.437	0.286	0.229
4.11	IO_69cm	0.473	0.317	0.261
4.12	IO_231cm	0.526	0.577	0.386